University of Thessaly
Department of Mechanical Engineering

Numerical simulation of oil steel tank structural behavior under fire conditions

Daphne Pantousa
Dr. Ing. Civil Engineer

Master thesis

Submitted to
the Department of Mechanical Engineering
in Fulfillment of the Requirements
of Master of Science in
"State-of-the-Art Design and Analysis Methods in Industry"

Supervisor: Professor Spyros A. Karamanos

Institutional Repository - Library & Information Centre - University of Thessaly
02/06/2024 20:36:34 EEST - 18.222.76.217

Institutional Repository - Library & Information Centre - University of Thessaly
02/06/2024 20:36:34 EEST - 18.222.76.217

University of Thessaly
Department of Mechanical Engineering

Numerical simulation of oil steel tank structural behavior under fire conditions

Daphne Pantousa
Dr. Ing. Civil Engineer

Master thesis

Submitted to
the Department of Mechanical Engineering
in Fulfillment of the Requirements
of Master of Science in
"State-of-the-Art Design and Analysis Methods in Industry"

Examination Committee:

Spyridon Karamanos, Professor at University of Thessaly, (Supervisor)
Euripidis Mistakidis, Professor at University of Thessaly (advisor committee)
Alexis Kermanidis, Assistant Professor at University of Thessaly (advisor committee)

Volos 2015

Institutional Repository - Library & Information Centre - University of Thessaly
02/06/2024 20:36:34 EEST - 18.222.76.217

Institutional Repository - Library & Information Centre - University of Thessaly
02/06/2024 20:36:34 EEST - 18.222.76.217

Institutional Repository - Library & Information Centre - University of Thessaly
02/06/2024 20:36:34 EEST - 18.222.76.217

Acknowledgments

Institutional Repository - Library & Information Centre - University of Thessaly
02/06/2024 20:36:34 EEST - 18.222.76.217

Abstract

Tank fire incidents take place mainly in petroleum refineries, oil terminals or storage tanks and they can prove to be catastrophic. During the last years, engineering societies (American petroleum institute, National Fire Protection Association etc) have published strict engineering guidelines and standards for the construction, material selection, design and safe management of storage tanks. Nevertheless, tank fire incidents are increasing in the last decades. The problem addressed in this thesis is the thermal buckling behavior of steel oil-storage cylindrical tanks under fire loading induced by an adjacent tank. The interest is focused on the case of fixed-roof tanks. The study is conducted numerically through the Finite Element method. The general purpose Finite Element code MSC Marc, which is optimized for non-linear problems, is used for the simulation. Three-dimensional models are developed using shell elements. A simplified approach of a conical roof is adopted for the simulation. Moreover, a thermal load pattern is used for the simulation of the fire-induced load. The pattern considers square cosine temperature variation around the circumference of the heated tank and uniform temperature distribution along the height of the cylindrical shell. The problem is solved through non-linear transient thermal/structural numerical analysis considering large displacements in the formulation of the mathematical model. The basic objective is the evaluation of the deflection field of thin-walled steel cylindrical shells under non-uniform temperature distribution around the circumference of the tank, taking into account the restraints (axial and rotational) that are induced at the upper and lower base of the cylinder due to the base-support and the fixed-roof conditions respectively and the degradation of material mechanical properties at elevated temperatures. Furthermore, the critical buckling temperatures for oil-storage tanks are calculated. Initially the problem is solved through non-linear geometric analysis, considering linear elastic material law and the corresponding results are given. A more realistic approach follows and the thermal buckling behavior of the steel storage tank is evaluated taking into account the material's non-linearity at elevated temperatures. In both cases, the effect of the roof stiffness in the critical buckling temperature is studied. Parametric numerical analyses are conducted in order to reveal the main factors that affect the thermal buckling behavior of oil-storage fixed-roof tanks. The parameters that are considered are the initial geometric imperfections, the level of the stored liquid and the circumferential range of the heated zone of the tank. It is found that the behavior of the tank depends strongly to the aforementioned parameters. The results of the analyses indicate that the empty tanks buckle for low temperature levels with respect to the tanks that are partially filled. Moreover, the effect of the roof stiffness is revealed and is shown that tanks that use stiff roofs buckle earlier with respect to the tanks of slender roofs. It is concluded that the effect of initial geometric imperfections and plasticity of steel should be included in the numerical simulation.

Institutional Repository - Library & Information Centre - University of Thessaly
02/06/2024 20:36:34 EEST - 18.222.76.217

Institutional Repository - Library & Information Centre - University of Thessaly
02/06/2024 20:36:34 EEST - 18.222.76.217

Contents

List of figures

Institutional Repository - Library & Information Centre - University of Thessaly
02/06/2024 20:36:34 EEST - 18.222.76.217

Institutional Repository - Library & Information Centre - University of Thessaly
02/06/2024 20:36:34 EEST - 18.222.76.217

Institutional Repository - Library & Information Centre - University of Thessaly
02/06/2024 20:36:34 EEST - 18.222.76.217

Institutional Repository - Library & Information Centre - University of Thessaly
02/06/2024 20:36:34 EEST - 18.222.76.217

Chapter 1. Introduction

1.1 Motivation

Although tank fires are rare, the number of the identified tank fire incidents is increasing during the last decades, as indicated in the detailed review of Brandforsk Project (Persson and Lönnermark, 2004). Most of the accidents occur in petroleum refineries, oil terminals or storage tanks and they are related to fire and explosions. According to Chang and Lin (2006) 30% of the tank fires were caused mainly due to lightning and human errors, including poor operations and maintenance. Other causes were equipment failure, sabotage, crack and rupture, leak and line rupture, static electricity, open flames etc.

Storage tanks contain large volume of flammable and hazardous liquids and a fire accident may result in socio-economical losses, injuries, deaths, stock devaluation or company bankruptcy and environmental disasters. During the last years engineering societies such as the American petroleum institute (API), the American institute of chemical engineers (AIChE), the American society of mechanical engineers (ASME), and the National Fire Protection Association (NFPA) have published strict engineering guidelines and standards for the construction, material selection, design and safe management of storage tanks. Although most companies are following the instructions, oil tank fire accidents are still happening.

Recently, a massive fire and explosions incident of oil tanks in a storage facility near Kiev (Figure 1-1) killed five firefighters and various Ukrainian officials gave contradicting reports indicating the environmental situation in Kiev after the blaze. On December 11, 2005 a catastrophic tank fire took place at the Buncefield Oil Storage Depot in the north of London (Figure 1-2). International attention was given in the specific fire event since it was the largest fire in Europe and significant alert was placed on the serious risks that may arise. The fire event motivated the scientific research in order to better understand the major cause of tank explosions and fire spread (Johnson 2010, Atkinson et al. 2015, Mishra 2013). In Mishra (2013) it is indicated that the accidents may occur due to different reasons ranging from malfunctioning of an installed mechanical device to mistakes committed by members of the personnel. The consequence of such failure results in abrupt release of stored fuels that allow collecting and forming a vapor cloud around. Depending on the flammability and the availability of a potential source of ignition as a vapor cloud may lead to a severe explosion which is referred in the literature as Vapor Cloud Explosion (VCE).

In all these cases the understanding of the sequence of the events that took place involving the explosions, the fire spread and the thermal/structural behavior of oil tanks is demanding. Some research studies are focused on domino effect that is responsible for severe accidents

Institutional Repository - Library & Information Centre - University of Thessaly
02/06/2024 20:36:34 EEST - 18.222.76.217

that took place in the chemical and process industry (Landucci, 2009, Khan and Abbasi, 1999; Lees, 1996) and on the safety and security distance of flammable liquid storages tanks (Lin, 2011). Another aspect that arises is the possibility that the thermal induced deformations of heated tanks (Figure 1-2c,d) to have a triggering effect for the leakage or the spill of the stored oil (Liu, 2011). This means that the deflected tank configuration may actually accelerate a possible explosion and thus contribute to the catastrophic failure. Thus, it becomes important to study the thermal/structural behavior of oil steel tanks and the failure modes in order to discover their role in the sequence of the devastating events and to proceed to fire safety assessment.

Figure 1-1 Kiev oil tank fire event.

(a) (b)

(c) (d)

Figure 1-2. Buncefield Oil Storage Depot fire event.

Institutional Repository - Library & Information Centre - University of Thessaly
02/06/2024 20:36:34 EEST - 18.222.76.217

1.2 Overview –Aim

The main hazards associated with tanks containing flammable fluids are the explosions and the fire attack. Explosions are the major cause of structural damage in most of the fire events identified until now. On the other hand the tank failure due to fire load seems to be of similar importance.

In the case of a fire engulfed tank, that contains flammable liquids such as oil, it can be easily foreseen that the tank will collapse due to the material degradation at elevated temperatures. The temperature rise in these cases is high enough and come up to 1200°C which is the melting point of steel. If the fire does not spread, the fire engulfed tank is actually the heat generator for the adjacent tanks. The heat is transferred mainly through radiation and becomes the thermal load for the neighbor tanks. In this case in the adjacent tank the temperature distribution is non-uniform in both the circumferential and the axial direction and depends on the position of the fire engulfed tank. Thus, there exists an important temperature difference between the hotter and the colder part of the heated tank and significant compressive stress may arise due to restrained thermal expansion. The reduction of mechanical properties of steel in conjunction with the thermal induced stresses may lead to thermal buckling and failure of the tank.

In order to minimize the risk, several organizations (e.g. APO, NFPA, EPA etc) propose guidelines regarding the tank layout in the oil depot. The suggested layout takes into account the accessibility of fire-fighting vehicles and the safe distances between the process plant and residential infrastructures. The minimum distance between the tanks is calculated through the heat flux between the fire engulfed tank and the adjacent tank and obviously this varies as the distance between them changes. The distance at which the heat flux becomes equal to 4.732 kW/m^2 is considered to be the safe inter-tank distance since no material is expected to ignite with a heat flux lower than this value (Sengupta et al. 2010). Nevertheless, questions arise if these limits are assuring the structural integrity of the heated adjacent tanks. This heat flux is equal to the energy radiated from a black body with a temperature of 260°C. In another research a critical temperature of 540°C is deemed to be a threshold for the safety of steel tanks (Liu, 2011, Beyler 2004b) in determining safe separations. Recent research activity in this area (Silva Santos and Landesmann 2014, Fontenelle 2012) demonstrated that the temperature variation on the target tank can be up to 800°C depending on the type of stored fuel (gasoline or ethanol), the structural tank side wall material (steel or concrete) and the incidence of wind. Specifically, in the study of Silva Santos and Landesmann (2014) it is indicated that the minimum safety distances are changing rapidly with the wind and that the presentNFPA30:2012 design recommendations need to be modified, in order to achieve a satisfactory failure prediction for different storage fuels (e.g. ethanol). The previous indicate that the minimum safety distances do not take into account all the involved factors that may

Institutional Repository - Library & Information Centre - University of Thessaly
02/06/2024 20:36:34 EEST - 18.222.76.217

affect the behavior of the heated tanks during the burning stage of the fire-engulfed tank. Further research should be conducted in order to study the behavior of the heated tanks which can be affected by both material degradation at elevated temperatures and thermal induced stresses.

The basic objective of this thesis is to study the fire behavior of steel fixed-roof oil storage tanks heated by an adjacent tank. *The problem actually is the evaluation of the deflection field of thin-walled steel cylindrical shells under non-uniform temperature distribution around the circumference of the tank taking into account the restraints (axial and rotational) that are induced at the upper and lower base of the cylinder due to the support and the fixed-roof conditions respectively and the degradation of material mechanical properties at elevated temperatures*. The problem is solved numerically using the Finite Element method. Three dimensional models are developed for the simulation of the fire behavior of the storage tank. A thermal pattern, available in the literature, is used to simulate the thermal load induced in the heated tank by the adjacent fire-engulfed tank. Parametric analyses are conducted in order to reveal the key factors that mainly affect the behavior of the heated tank.

1.3 Organization

The thesis is organized in seven Chapters. The second Chapter presents a detailed literature overview concerning the older and the most recent published research studies related to the objectives of this thesis. Specifically, the literature overview is focused on three different issues. First, the most relevant analytical/numerical/experimental scientific studies concerning the thermal buckling of shells are presented. Next, the available models for the simulation of pool fires that are proposed ion the literature are referred. Finally, the most relevant studies concerning the basic objective of this thesis are described in detail.

Chapter 3 focuses on the basic principles of heat transfer theory and on the basic concepts concerning the modeling in the context of fire engineering. First, the basic mechanisms of heat transfer, convection, conduction and radiation are discussed. In the sequel, the basic elements for the application of the theory to the numerical simulation of heat transfer are presented. This Chapter contains also the solutions that are suggested by EN 1991-1-2 in order to find analytical solutions for the heat transfer problem in the case of steel sections.

The fourth Chapter deals with the material properties of steel at elevated temperatures. Both the mechanical and the thermal properties are discussed. The first aspect is the mathematical model used in order to describe the non-linear temperature dependent stress-strain relationship at elevated temperatures, according to guidelines of EN 1993-1-2. Finally, the thermal properties, including the thermal conductivity and the specific heat are provided.

Chapter 5 presents the steel oil-storage tank that is studied in thesis and defines the problem that is solved. Details about the numerical modelling are given. Specifically, first the three-

Institutional Repository - Library & Information Centre - University of Thessaly
02/06/2024 20:36:34 EEST - 18.222.76.217

dimensional shell finite element is presented and details about the thermal load pattern that is used in the study for the simulation of the fire-induced load are given. Moreover, the problem is solved through Linear Buckling analysis (LBA) in order to take some primary results for the thermal buckling behavior of the heated tank.

The thermal buckling behavior of the heated cylindrical tank is studied in detail in Chapter 6. The numerical analysis techniques that are used for the simulation and the solution of the problem are presented. First the problem is solved through geometric non-linear analysis, taking into account linear elastic material law and the corresponding results are given. Specifically, the results are given mainly in terms of critical buckling temperature which indicates the occurrence of the instability and the buckling takes place in the tank. A more realistic approach follows and the thermal buckling behavior of the steel storage tank is solved taking into account the material non-linearity at elevated temperatures. In both cases, the effect of the roof stiffness in the critical buckling temperature is studied.

Finally, in the last Chapter (Chapter 7), parametric numerical analyses are conducted in order to reveal the main factors that affect the thermal buckling behavior of oil-storage fixed-roof tanks. The parameters that are considered are the geometric initial imperfections, the level of the stored liquid and the circumferential range of the heated zone of the tank. It is found that the behavior of tank depends strongly to the aforementioned parameters.

Institutional Repository - Library & Information Centre - University of Thessaly
02/06/2024 20:36:34 EEST - 18.222.76.217

Chapter 2. State of the art/Literature Review

This Chapter presents a state of the art report on the main scientific areas of this thesis which is the thermal buckling of cylindrical oil tanks heated by an adjacent tank. Although the impact of this problem is important, limited studies are devoted to the investigation of the behavior of heated tanks during a fire event. This review covers the most relevant scientific studies for the thermal buckling of shells that are included in the literature. Next, a brief review concerning the pool fire models available in the literature is presented and finally, the most related studies concerning the fire behavior of cylindrical tanks are reviewed.

2.1 Thermal Buckling of shells

Thin shells as structural elements are broadly used in civil, mechanical, architectural, aeronautical, and marine engineering. In mechanical engineering, shell forms are used in piping systems and pressure vessels. Aircrafts, missiles, rockets, ships, and submarines are examples of the use of shells in aeronautical and marine engineering. Accurate structural analysis of composite cylindrical shells is of great importance in aerospace industry as it closely relates to aircraft fuselage design. Since the load-carrying capability of thin shells is mostly determined by the buckling load, it is very important to determine a reliable and accurate value of this load for design purposes, especially in the case of thin-walled structures subjected to mechanical and thermal loadings.

Thornton (1993) has conducted a detailed review of the research on thermal buckling of plates and shells. A brief review of this study is presented here. Initially cylindrical shells were investigated to determine the potential thermal buckling of frame-reinforced fuselages in aircrafts in high speed flights. In these studies it was derived that because of the aerodynamic heating, thin cylindrical shells experience higher temperatures than the heavier reinforcing frames. The shells subjected to higher temperatures tend to expand in a radial way more significantly than the restraining frame, thus inducing compressive circumferential membrane stresses $N_\theta(x)$, Figure 2-1.

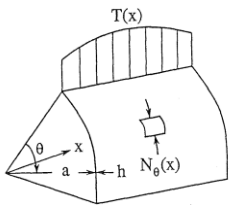

Figure 2-1: Circumferential Membrane Force induced by Temperature Distribution in T(x) in Cylindrical Shells (Thornton, 1993)

Institutional Repository - Library & Information Centre - University of Thessaly
02/06/2024 20:36:34 EEST - 18.222.76.217

At early stages the research was focused in determining the critical skin temperature levels for buckling due to compressive membrane stresses, leading to the solution of the linear Donnell stability equations in uncoupled form for thermal buckling of cylindrical shells.

Zuk (1957) described a solution method by assuming N_x, $N_{x\theta}$ are equal to zero and N_θ is proportional to $E\alpha\Delta T$, following the assumption that the temperature rise ΔT of the shell is achieved uniformly. In this case the $N\theta$ membrane force varies trigonometrically with x and is compressive over the length of the shell. Assuming a shape for w that satisfied zero deflection and slope at each end of the shell, he used Galerkin's method to satisfy the above equation approximately. This resulted in an expression that allowed the determination of the critical buckling temperature of a clamped cylindrical shell although no numerical results were presented.

In a later study, Johns (1959, 1962) indicated that the circumferential stresses that appear at the frame's junction and thin shell are localized and decrease rapidly away from the support. For that reason, he proposed a function for the circumferential stress that decreased exponentially with *x*. Hoff (1957b) presented an analysis for the buckling of a simply supported cylindrical shell where the circumferential stresses are determined from a pre-buckling analysis. The displacement components u, v, w were assumed as infinite series of trigonometric functions that satisfied simply-supported boundary conditions. At the two ends of the shell (x = 0, L), the radial and circumferential displacements as well as the axial membrane stress and the axial bending moment were assumed to vanish. This approach led to an infinite determinant for the critical buckling stress. The pre-buckling circumferential membrane force is obtained by first solving for the displacement w from the linear equilibrium equation, assuming a uniform rise ΔT in the shell temperature. As a conclusion it was pointed out that circumferential thermal stresses due to a uniform temperature rise are not likely to cause elastic buckling. In a similar study, Anderson (1962a) developed a similar theory to calculate the buckling temperature of a uniformly heated, ring-stiffened shell including axial compression, by using a shell theory by Batdorf and considering both simply supported and clamped shell end conditions. As in Hoff's study, the paper concluded that buckling of a ring-stiffened cylinder due to uniform temperature alone will not occur for small values of a/h. Nevertheless, the paper noted that for large values of a/h (e.g. a/h = 2000), such buckling can occur. Sunakawa (1962) also investigated the deformation and buckling of cylindrical shells due to aerodynamic heating. The book by Johns (1965) gives a simple formula for the critical temperature for buckling by circumferential membrane stresses,

$$T_{cr} = -k\frac{h}{\alpha a} \tag{2.1}$$

where k depends on the boundary conditions. This work on cylinders with uniform temperatures was used as a basis on applications to fuselages with the assumption of

Institutional Repository - Library & Information Centre - University of Thessaly
02/06/2024 20:36:34 EEST - 18.222.76.217

axisymmetric heating. At a later stage, investigation began on cylinders that were not uniformly heated around their circumference.

Gossard and Seide (1952) on a previous research on flat plates with spatial temperature gradients had established that for relatively small spatial temperature gradients, thermal buckling could occur. Moreover, Abir and Nardo (1959) investigated thermal buckling of circular cylindrical shells with circumferential temperature gradients. For a simply supported shell, they investigated buckling due to the variation of the axial membrane force N around the shell circumference (Figure 2-2).

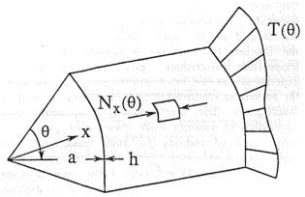

Figure 2-2: Longitudinal Membrane Force N_x induced by Temperature Distribution T(θ) in Cylindrical Shell (Thornton, 1993).

The study concluded that the critical value of the axial thermal stress distribution occurs at a value equal to the critical stress in uniform axial compression. For a fully restrained cylinder the axial compression stress for a temperature increase ΔT , the critical buckling temperature for uniform compression is:

$$\Delta T_{cr} = -\frac{h}{\alpha a}\frac{1}{[3(1-\nu^2]^{0.5}} \tag{2.1}$$

The elastic instability of a cylindrical shell under an arbitrary circumferential variation of axial stress was also studied by Bijlaard and Gallagher (1960) and their conclusions were consistent with Abir and Nardo. In a similar study, Hill (1959) studied buckling of circular cylindrical shells heated along an axial strip in a more analytically and experimentally manner. More precisely, they used the Donnell shell equations and attempted a solution using a Ritz method, and that by assuming that a simplified axial thermal stress distribution occurs where the stress is constant in x but varies around the circumference. Aluminium and steel cylinders were experimentally locally heated by infrared lamps, and 2 types of cylinder-end conditions were employed. Thermocouples were used to measure the temperatures and Linear Variable Differential Transformers (LVDTs) were used to measure the displacements.

Thermal buckling analyses of perfect cylindrical shells of isotropic and homogeneous materials and cylindrical shells of composite materials based on Donnell and improved Donnell stability equations (Donnell 1950, 1965 and 1958) are studied by Eslami et al. (1996 and 1999). A number of thermal buckling problems of practical importance, such as uniform temperature rise, radial, and axial temperature differences are discussed in the papers. It is

Institutional Repository - Library & Information Centre - University of Thessaly
02/06/2024 20:36:34 EEST - 18.222.76.217

emphasized here that while the Donnell equilibrium equation is basically developed on the Love-Kirchhoff hypothesis and the Sander's nonlinear strain-displacement relations. It is shown by Eslami that resulting buckling loads predicted for long cylindrical shells are improved when the improved stability equations are used. Supplementary, in Eslami (1998), analytical solutions for the critical temperature of imperfect shells submitted to gradient temperature are given. The thermal loads which are studied are the uniform temperature rise, the linear radial and axial temperature differences.

Buckling of the cylinders appeared where the buckling deformations were strongly dependant on the end conditions of the experiment. For aluminium cylinders with a/h = 430, critical buckling temperatures were relatively low) depending on end conditions. These experimental results for the critical buckling temperature were considered to be in reasonable agreement with the theoretical calculations. However, the study showed the difficulty and complexity of performing analytical predictions for the thermal buckling stresses due to localized temperature distributions and demonstrated the practical problems of creating experimental end conditions consistent with a mathematical model.

Anderson and Card (1962) in their study described the case where several stainless steel ring-stiffened cylinders were subjected to a pure bending moment and heated rapidly until buckling occurred. For most of the cylinders the heating was non-uniform around the circumference. Temperature and deflections were measured at several locations, and in some tests strains were measured. Strains were successfully measured below 175°F, but the rest of the data were unreliable for higher temperatures. An elementary thermal stress theory was found to be inadequate for the prediction of the thermal stresses.

In a related paper, Anderson (1962b) reviews theoretical and experimental investigations on buckling of cylinders due to both circumferential and axial thermal stresses. The paper indicates that the severity of the circumferential thermal stress is strongly dependent on the boundary conditions and suggested the need for additional experimental results. For cylinders that are heated non-uniformly, the paper discusses the difficulty of predicting axial thermal stresses and identified the need for research in thermal buckling of longitudinally stiffened cylindrical shells for launch vehicles.

In the mid-1960s, the Stanford University group of NJ Hoff continued to investigate thermal buckling of cylinders. Three papers describe further research on buckling of thin circular cylinders heated along an axial strip. Hoff, Chao and Madsen (1964) analytically study the problem assuming uniform compressive axial stress to occur in a narrow strip while the rest of the shell is stress free. The shell is assumed very long, and Donnell's equations are used. The results of the analysis support the earlier conclusion of Abir and Nardo (1959) that the critical stress of the heated strip is the same as the critical stress of a complete cylindrical shell subjected to uniform compression unless the heated strip is very small. With very narrow

Institutional Repository - Library & Information Centre - University of Thessaly
02/06/2024 20:36:34 EEST - 18.222.76.217

heated strips, the critical stress rises rapidly as the strip width decreases.

Ross *et al*.(1965) continued and extended the experimental studies initiated by Hill. A series of stainless steel and cold-rolled steel cylinders were heated along an axial strip by infrared heat lamps. End supports were designed to simulate fully-fixed conditions. The instruments used included thermocouples as well as a microphone to provide an audio signal at the occurrence of buckling. The heated width varied (from 1.5% to 18%) of the total shell circumference. Tests were conducted by subjecting the cylinders instantaneously to maximum heating from the infrared lamps and axial and circumferential temperature distributions were then recorded until the shell buckled. Computations were performed with the Donnell theory using measured circumferential temperature distributions. As a result, some agreement of analysis with experiment was fair, but it was judged good enough for the authors to confirm previous conclusions of several investigators that the buckling temperature corresponding to uniform axial compression provides a lower limit of stability for thin cylindrical shells subjected to highly non-uniform circumferential healing.

Hoff and Ross (1967) performed further analysis of the problem using the experimental temperature distributions and obtained reasonable agreement with the experimental data. The consistent trend demonstrated by these analyses was that experimental critical buckling temperatures were consistently higher than values predicted by analyses. This trend was in direct contradiction to the well-established trend that for mechanical loads experimental critical buckling values are consistently *lower* than predicted values.

Ross, Hoff, and Horton (1966) conducted additional experiments to address the thermal buckling anomaly. Six stainless-steel cylinders (a/h = 344) and five cold rolled steel cylinders (a/h = 291) were heated axi-symmetrically by an array of twelve infrared heat lamps. The cylinder’s ends were longitudinally restrained and clamped. The test procedure was essentially the same as used by Ross et al (1965). Upon heating, a test cylinder experienced thermal expansion in the radial direction, and the thin cylindrical shell became barrel-shaped. Ultimately, the shell buckled near the clamped end supports. However, after comparing the experimental results with the predictions of available shell-buckling theories, there was poor agreement. It was finally concluded that because the cylinder "barrels out" during heating, the axial compressive stress is reduced resulting in higher critical temperatures than is predicted by linear buckling theory.

Hoff (1965) and Ross (1966) also investigated the use of simple models to explain thermal buckling of shells. Hoff used a two-bar mechanism with a nonlinear spring, and Ross used a beam-column with a nonlinear spring. Gellatly, Bijlaard, and Gallagher (1965) investigated thermal buckling of sandwich cylindrical shells for simply and clamped supports. Using the approach of Hoff (1957b), critical buckling temperatures were determined for circumferential stresses varying with x. Numerical results were presented for isotropic and sandwich

Institutional Repository - Library & Information Centre - University of Thessaly
02/06/2024 20:36:34 EEST - 18.222.76.217

cylinders.

Chang and Card (1970,1971) at NASA Langley developed programs for analyzing thermal buckling of orthotropic, multi-layered, cylindrical shells stiffened by uniform, equally spaced rings and stringers. Thermal effects are taken into account by specifying axi-symmetric temperature distributions in the shell and stiffeners. The theory was developed from strain energy expressions corresponding to nonlinear Donnell-von Karman displacements, and equilibrium equations were derived by the principle of minimum potential energy. These equations were separated into equations governing axi-symmetric pre-buckling behaviour and equations governing behaviour at buckling. The ends of the stiffened cylinder were assumed to be free to expand longitudinally. In the analyses thermal buckling occurs as a consequence of circumferential compressive stresses introduced by radial restraint at the boundaries and/or from restraints resulting from differences in expansion between the stiffeners and shell. Thermal buckling behaviour of un-stiffened, ring-stiffened, stringer-stiffened and ring/stringer-stiffened shells was investigated. For un-stiffened cylinders the numerical solutions were validated by comparisons with the analytical solutions of Hoff (1957b) and Sunakawa (1962). Recall that the Hoff analysis (1957b) of a simply supported cylinder under hoop stresses varying in the x direction predicted buckling at a very high temperature.

Chang and Card's computer analysis of the same cylinder was unable to determine this critical buckling temperature, as no buckling temperature could be found within a practical temperature range. The difference between the two analyses was determined to lie in the assumptions made in the linearized Donnell pre-buckling equations employed by Hoff where rotations and derivatives of rotations are neglected. These pre-buckling rotations were included in the Chang and Card formulation, but when these terms were suppressed the Chang and Card predictions were in agreement with Hoff. The conclusion was that the pre-buckling rotations are required, and for simple supports the buckling temperature is beyond the elastic range. Chang and Card's predictions were in good agreement with Sunakawa's analysis for a clamped cylinder since Sunakawa's shell theory included pre-buckling rotations.

For ring-stiffened cylinders the comparisons made were successfully with Anderson's analysis (1962b). Thermal buckling studies of an aluminium large diameter, longitudinally stiffened cylinder and a titanium ring- and stringer-stiffened cylinder were also conducted. At about the same time, Bushnell of the Lockheed Palo Alto Research Laboratory was developing a computer program called BOSOR for the general analysis of shells of revolution. Applications of BOSOR to thermal buckling are described in a book (1989) and several papers (1971a, b, 1973). The BOSOR program is based on an energy formulation with the method of finite differences. Axi-symmetric ring-stiffened shells are assumed. The program has been used to solve several of the thermal buckling problems mentioned previously and also other, more complex, thermal buckling problems. Bushnell (1971a) solves the Hoff

Institutional Repository - Library & Information Centre - University of Thessaly
02/06/2024 20:36:34 EEST - 18.222.76.217

(1957b) problem of the simply supported cylinder subjected to a uniform temperature rise. Buckling of a ring-stiffened aluminium cylinder subjected to axial compression, external pressure and various temperature distributions is also studied in detail. The effect of ring-out-of-plane bending stiffness on thermal buckling of ring-stiffened cylinders is discussed by Bushnell (1971b) and demonstrated to be important.

Bushnell and Smith (1971) describe calculations of thermal stresses and buckling of non-uniformly heated cylinders and cones. The BOSOR program was used to analyze several cylinder tests including the studies of Hill (1959), Anderson and Card (1962), Ross, Mayers and Jaworski (1965), as well as Ross, Hoff, and Horton (1966). These analyses are valuable because they represent the first systematic comparison of computational results with experimental data.

In addition, the computational approach permitted issues to be addressed that previously had been intractable because of limitations of analytical methods. Particular attention was given to the effect of boundary conditions on predicted stress and critical temperatures. For example, the anomaly raised in the experimental study of Ross et al (1966) is attributed to undesired flexibility in the experimental boundary condition. The paper also concluded that for shells which are long compared to a boundary layer, critical temperatures of uniformly heated monocoque cylinders and cones are as sensitive to initial imperfections as are critical axial loads.

In a later paper, Bushnell (1973) used BOSOR to study thermal buckling of cylinders with axi-symmetric thermal discontinuities. The first problem considered was buckling of a cylinder heated halfway along its length. The problem was considered because of questions raised by the Hoff (1957b) problem of thermal buckling due to circumferential stresses. Bushnell reached the same conclusions that Chang and Card: pre-buckling rotations should be included in the analysis, and elastic buckling will not occur for the simply supported cylinder with uniform temperature. The second problem considered was a clamped cylindrical shell (a/h = 2540) analyzed and tested by Johns (1962). A BOSOR analysis (with pre-buckling rotations) of the Johns' cylinder predicted a critical temperature of 150°C whereas the experimental value was 324°C.

Subsequent investigation showed that the large difference between computational results and tests could be explained by the presence of temperature gradients near the boundaries of the cylinder. The study concluded that critical buckling temperature calculations are sensitive and dependant to the shape of the temperature distribution. In order to obtain better correlation between predictions and tests, temperature distributions had to be measured carefully and the spatial variations included in the analysis.

Two papers in the mid-1970s analyzed thermal buckling of orthotropic cylindrical shells. Gupta and Wang (1973) used a Rayleigh-Ritz approach to analyze a simply-supported

Institutional Repository - Library & Information Centre - University of Thessaly
02/06/2024 20:36:34 EEST - 18.222.76.217

orthotropic shell with uniform temperature. Pre-buckling rotations were not considered. Parametric studies illustrated the effects of the axial and circumferential coefficients of thermal expansion. Radhamohan and Venkataramana (1975) analyzed an orthotropic clamped cylindrical shell using an approach based on Sanders' nonlinear shell theory. Effects of pre-buckling rotations, different forms of clamped boundary conditions and other parameters were studied. A brief paper by Belov (1978) described an experimental study of stability of cylindrical shells partially filled with liquid. The study was motivated by aerodynamic heating of fuel tanks. In the experimental program, cylindrical shells were subjected to heating and were loaded by axial compression and internal pressure. Although good agreement between calculations and experiment data was stated, details of the analysis and tests were not given.

In the late 1970s, two test programs on buckling of cylinders with combined mechanical and thermal loads were conducted at the Technion in Israel. Frum and Baruch (1976) describe buckling of cylindrical shells heated along two opposite generators. A series of 46 tests of aluminium cylinders with a/h = 301 were conducted. The end supports were designed to be fully restrained and axial loads were applied by a hydraulic jack. There were also two infrared line heaters installed above and below the shell. The temperature distribution was measured with thermocouples, and displacements were measured with LVDTs. The instant of buckling was detected with a microphone. The effects of the u displacement boundary conditions were studied, and the authors concluded that previous investigators had not treated the condition with enough care. They also concluded that the u displacement has a dominant influence on the buckling results. Comparisons of experimental data with computations are only fair. The experimental data was used to construct an axial load-temperature interaction curve.

Ari-Gur, Baruch and Singer (1979) described buckling of cylindrical shells under combined axial preload, non-uniform heating and torque. Similar test cylinders and the test rig employed in the previous study were used after modifications to allow torsion. A series of 35 tests were conducted. A temperature-torque interaction curve was developed from the experimental data. Studies of thermal buckling of laminated composite circular cylinders began in the 1980s and continue to the present time. So far, the studies have been analytical. However experimental studies have not yet been conducted.

Wilcox and Ma (1989) used an energy approach to derive a set of equilibrium equations based on classical thin shell theory with Donnell's assumptions. Galerkin's method with an assumed trigonometric variation for w for a simply-supported cylinder leads to a matrix eigen-value problem. For critical buckling temperatures for various composite parameters such as lamination angle, numerical results were presented.

Finally, Thangaratnam et al (1990) used the finite element method to conduct parameter studies of a simply supported cylinder with uniform temperature. Birman (1990) studied the thermally induced dynamic response of reinforced composite cylinders. The study was based

Institutional Repository - Library & Information Centre - University of Thessaly
02/06/2024 20:36:34 EEST - 18.222.76.217

upon Donnell's theory of geometrically nonlinear shells and includes axial and ring stiffeners. Solutions were developed for a simply supported cylinder subjected to a uniform rise in temperature. The paper concludes that if a shell is subject to an instantaneous rise in temperature it exhibits stable steady-state oscillations. However, if the temperature exceeds a critical buckling level, the character of the response changes and the deflections can increase dramatically.

2.2 Pool Fires

A pool fire is defined as a buoyant diffusion flame in which the fuel is configured horizontally (Hamins et al., 1995). The fuel can be liquid gas or solid. The fuel bed may be of arbitrary geometry but for simplicity reasons most studies consider a circular shape and the single geometrical parameter that is used is the pool diameter. The main characteristics of the fire hazard are the total heat release rate, the flame spread rate and the power radiated to the surroundings. Fire hazard can be modified by ambient conditions such as the absence or presence of an enclosure, wind, currents or ventilation.

Depending on the fuel and the size of the fire, up to 20 % of the fuel mass is converted to smoke particulate in the combustion process (SFPE, 1999). This smoke shields much of the luminous flame region from the viewer, and it is this luminous flame region that is the source of most of the thermal radiation. This shielding effect is most pronounced for fires that are tens or hundreds of meters in diameter because of the decreased efficiency of combustion at these scales (McGrattan et al. 2000). Figure 2-3 illustrates a large liquid fuel fire.

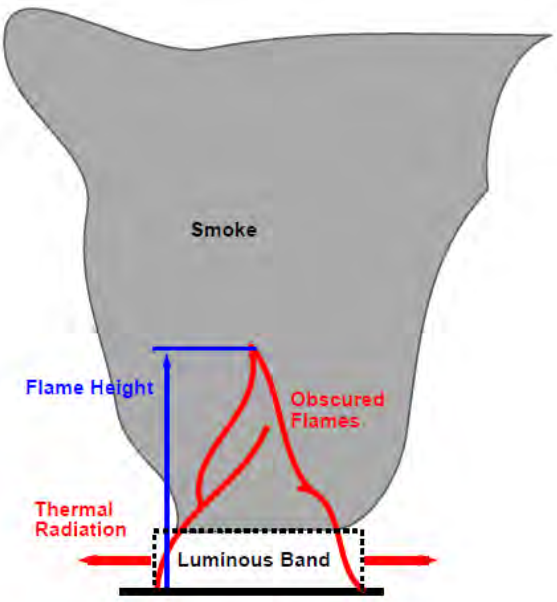

Figure 2-3: Large liquid fuel fire scheme (McGrattan et al. 2000)

There are many mathematical predictive tools that are used to assess the consequences of hydrocarbon pool fires and these vary from empirical models to more complicated

Institutional Repository - Library & Information Centre - University of Thessaly
02/06/2024 20:36:34 EEST - 18.222.76.217

Computational Fluid Dynamics (CFD) calculations. Empirical models characterize the geometry of the pool fire, using correlations based on dimensionless modelling and the results of appropriate experiments. These models are divided into two types: point source models and solid flame models (Figure 2-4).

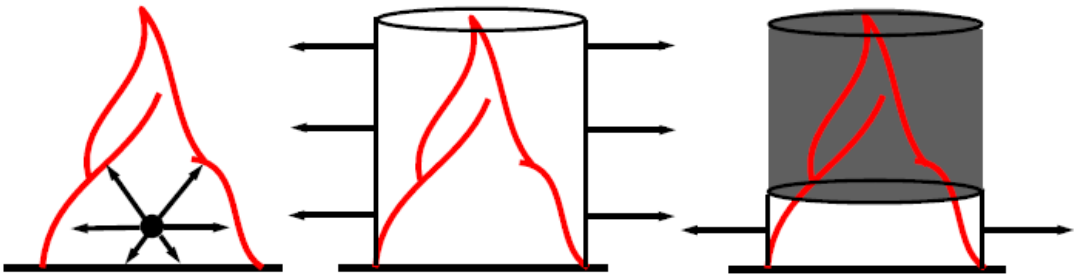

(a) Point source model (b) Solid flame model (convectional) (c) Solid flame model (modified)

Figure 2-4: Thermal radiation models

Point source models are the simplest type of empirical models and can be used to predict the radiant heat flux around a fire. Cowley and Johnson (1992) asserted that the point source model can be used, fairly reliably, to predict radiant heat flux beyond approximately five pool diameters from the flame.

Solid flame models apply correlations based on appropriate experiments to derive a flame shape, which is dependent on factors such as fuel type and wind-speed.

Generally, a well-defined geometrical shape, such as a cylinder or a cone, is used to represent the flame shape. Further correlations are used to estimate the emissive power of the flame. The radiant heat flux at the target is obtained by calculating the view factor of the flame from the position and orientation of the target. CFD models solve the partial differential equations (Navier-Stokes equations) that describe fluid flow across a vast grid of cells, known as a mesh. In order for them to predict fire behaviour, they must incorporate sub-models that describe the chemical and physical processes that occur in the fire. Radiant heat transfer is solved by means of an enthalpy conservation term that arises within the Navier-Stokes equations (Cox and Kumar, 2002), while, as stated by Cowley and Johnson (1992),

CFD models provide a rigorous framework for solving combustion problems but, at present, they are essentially research tools. The CFD sub-models pertaining to combustion, smoke production and radiative heat transfer do not yield as good a prediction of radiant heat from a pool fire to external objects as those offered by the available empirical models.

Although CFD models are capable of predicting a wide range of fire scenarios, providing that the input is correctly specified, there are distinct disadvantages associated with these models: they require a great deal of time and effort, in terms of both human effort (i.e., input) and computational effort (in solving the Navier-Stokes equations).

Institutional Repository - Library & Information Centre - University of Thessaly
02/06/2024 20:36:34 EEST - 18.222.76.217

2.3 Tanks heated by fire

The most relevant study concerning the thermal buckling behavior of steel tanks is the PhD dissertation conducted by Liu (2012). This thesis presents a systematic exploration of the potential thermal and structural behaviours of an oil tank when one of its neighbour tanks is on fire. The main objectives of this thesis were to reveal the thermal distribution patterns developed in an oil tank under the heating from an adjacent tank fire, to understand the underlying mechanism responsible for the buckling of tank structure, and to explore the influences of various thermal and geometrical parameters on the buckling temperature of the tanks. The study began with analytical solutions for stresses and deformations in a partially filled roofless cylindrical tank under an idealized axisymmetrical heating regime involving thermal discontinuity at the liquid level. The results demonstrate that large compressive circumferential membrane stresses occur near the bottom boundary for an empty tank and near the liquid level for a partially-filled tank. Heat transfer analysis was conducted to explore the temperature distribution developed in the tank when the fire reaches a steady state. Parameters and assumptions used in the adopted pool fire model were carefully examined. The results show that a rather non-uniform distribution of temperature is developed in the tank especially around the tank circumference. A simple model was then proposed to describe the temperature distribution based on the numerical heat transfer analysis. The accuracy of the proposed temperature distribution model for predicting the structure behaviour was evaluated by comparing its predictions with those using directly the temperature distribution obtained from the numerical heat transfer analysis. Extensive geometric and material nonlinear analyses were carried out to capture the buckling behaviour of the tank using both the proposed temperature distribution and that from heat transfer analysis. It was found large vertical compressive membrane stresses are induced in the tank, causing buckling. The influence of fire diameter, location, liquid filling level and tank geometry were investigated.

A recent paper (Godoy and Batista, 2012), presents computational modeling and results of steel storage tanks under heat induced by an adjacent fire. In this research, modeling is restricted to the structural behavior of the tank, with emphasis on thermal buckling of the shell. Two tanks that buckled under a huge fire in Bayamo´ n, Puerto Rico in 2009, are investigated in detail: a small tank with a self-supported conical roof, and a large tank in which the conical roof is supported by a set of rafters and columns. For a tank that is empty, the results show that a relatively low temperature is enough to produce static buckling of the shell. In pre-buckling states, the cylindrical shell has thermal expansion; at the critical state the displacements reverse and inwards displacements are observed at advanced post-buckling states. Parametric studies are performed to understand the influence of the shell thickness, the level of fluid stored in the tank, the area affected by fire in the circumferential direction, and the temperature gradient through the thickness. The buckling modes are compared with real deflection of tanks that were affected by fire.

Institutional Repository - Library & Information Centre - University of Thessaly
02/06/2024 20:36:34 EEST - 18.222.76.217

The study of Batista and Godoy (2013) reports the computational results of an investigation of oil storage tanks with the shape of an open cylindrical shell under thermal loads induced by fire. Interest in this problem has arisen as a consequence of a catastrophic fire that affected an oil storage facility in Puerto Rico in 2009 that caused the failure of 21 large tanks. To identify patterns of deformations that could be expected under various fire conditions, computer modeling has been carried out for one tank geometry. It is assumed that fire occurs outside the tank and induces an increasing temperature field affecting part of the external surface in the circumferential direction. The nonlinear shell response is modeled using finite elements under thermal loads and self-weight. The nonlinear behavior is computed to identify thermal buckling of the shell as a limit point. The response is initially computed for empty tanks, and the influence of various factors is investigated, including the liquid stored, a temperature gradient across the thickness, the circumferential zone affected by fire, and the shell thickness. The results for open tanks show that the location of large out-of-plane displacements attributable to thermal buckling coincides with the heated zone. The importance of thermal gradients in the thickness to the buckling load and mode are shown.

It is concluded that there is limited research till now on thermal buckling under fire loading since only three studies exist in this area. The present thesis aims to reconsider the same problem that is covered by the aforementioned studies and to look thoroughly to the mechanisms of thermal buckling of fixed-roof steel tanks.

Institutional Repository - Library & Information Centre - University of Thessaly
02/06/2024 20:36:34 EEST - 18.222.76.217

Chapter 3. Elements of heat transfer theory

This Chapter focuses on the heat transfer theory, applied in fire-engineering problems, for the determination of the temperature-profile of the structural members. Since, the problem of the fire development in the enclosure is solved; the gas-temperature time-history is obtained. The heat transfer from the hot-gases to the surfaces of the structural members takes place through convection and radiation. Then, the heat is transferred through the conduction mechanism. The differential equation that describes the problem of heat conduction is solved by the application of the appropriate solid-fluid boundary conditions that describe radiation and the convection mechanisms. It is noted that the governing equations of the problem are non-linear and the problem should be solved numerically, using the finite element method. The last part of the Chapter presents analytical, simplified solutions that are suggested in EN 1993-1-2 for the determination of the temperature profile of steel sections.

3.1 Convection

Convection is the heat transfer at the interface between a fluid and a solid element. The distinction between the forced and natural convection depends on the motion of the fluid. Free or natural convection takes place when the heat is transferred by the circulation of fluids (in this case the hot air) due to buoyancy from the density changes induced by the heating itself. On the other hand, in the case where the fluid flows on the solid surface at speed, the convection is called forced. Heat transfer through convection takes place only when a fluid comes in contact with a solid surface.

3.2 Radiation

Thermal radiation is the exchange of energy by means of electromagnetic waves that are emitted from a surface or an object. As in the case of light, these electromagnetic waves can be absorbed, transmitted or reflected on a surface. Heat transfer through radiation always takes place when the temperature of a fluid or a solid increases, regardless it comes in contact with another body.

3.3 Heat conduction

The one-dimensional heat conduction is governed by the well-known law of Fourier which is written in the form

$$\dot{Q} = -k \frac{dT}{dx} \tag{3.1}$$

Institutional Repository - Library & Information Centre - University of Thessaly
02/06/2024 20:36:34 EEST - 18.222.76.217

where dx is an infinitesimal thickness of a specific material, $\dot{Q}$ (resp. dT) is the heat flux (resp. the temperature difference) across this thickness and k is the thermal conductivity of the material. The thermal conductivity is normally dependent on the material temperature and this fact makes the solution of even the simplest problems nonlinear, requiring a numerical method for their treatment. Values for the thermal conductivity for different structural materials can be found in many sources. EN 1993-1-2 has incorporated the thermal conductivity properties for the various structural materials. Details for steel and concrete will be given in the sequel.

In civil engineering structures, heat transfer occurs usually in three dimensions. In this case, an infinitesimal material volume $dx \times dy \times dz$ is considered. The application of the energy conservation principle in this case implies that for stationary heat transfer the heat inflow in the element should be equal to the heat outflow from it and leads to the partial differential equation:

$$k_x \frac{\partial^2 T}{\partial x^2} + k_y \frac{\partial^2 T}{\partial y^2} + k_z \frac{\partial^2 T}{\partial z^2} = 0 \tag{3.2}$$

where k_x, k_y, k_z are the thermal conductivities of the material in each one of the three spatial directions. In transient state heat transfer, the temperature on a material volume increases or decreases over time. The transient state heat conduction partial differential equation is written in the form:

$$k_x \frac{\partial^2 T}{\partial x^2} + k_y \frac{\partial^2 T}{\partial y^2} + k_z \frac{\partial^2 T}{\partial z^2} = \rho C \frac{\partial T}{\partial t} \tag{3.3}$$

where ρ is the density of the material and C is its specific heat. As in the case of the thermal conductivity coefficient, the specific heat is normally dependent on the temperature of the material. In cases that phase changes occur, the function that describes the specific heat may not be continuous. Moreover, in the case of porous materials, as e.g. the concrete, the specific heat is affected by the evaporation phenomena that occur over a range of temperatures. Details for the materials treated here will be given in Chapter 6.

3.4 Boundary conditions

Boundary conditions should be applied in order to find a solution to equation 5.3. In heat transfer, the boundary conditions are of three general types.

Adiabatic boundary conditions

Adiabatic boundaries can be treated as a special case of the general fixed flux boundary conditions. No heat exchange takes place across such a boundary and the adiabatic boundary condition is written in the form:

Institutional Repository - Library & Information Centre - University of Thessaly
02/06/2024 20:36:34 EEST - 18.222.76.217

$$-k_n \frac{\partial T}{\partial n} = 0 \tag{3.4}$$

Adiabatic boundaries are used in order to simulate symmetry conditions (no heat exchange takes place along the symmetry axis or surface) or boundaries which are almost completely insulated.

Fixed temperature boundary conditions

This is the simplest form of boundary conditions, where in specific points of the material, or along edges or surfaces the temperature is assumed known:

$$T = T_0 \tag{3.5}$$

Fixed flux boundary conditions

In this case, the heat flux in a direction normal to a boundary surface is assumed known. This boundary condition is written in the form

$$-k_n \frac{\partial T}{\partial n} = \dot{q}_0 \tag{3.6}$$

where k_n is the thermal conductivity measured in the direction normal to the boundary surface and $\dot{q}_0$ is the known heat flux. A special case of this boundary condition is that of an adiabatic boundary. Across such a boundary no heat exchange takes place, therefore the heat flux is equal to zero. The adiabatic boundary condition is therefore written in the form:

$$-k_n \frac{\partial T}{\partial n} = 0 \tag{5.7}$$

Adiabatic boundary conditions are used in order to simulate symmetry conditions (no heat exchange takes place along the symmetry axis or surface) or boundaries which are almost completely insulated.

Boundary conditions at solid-fluid boundaries

In the case that solid boundaries are in contact with moving fluids, the following boundary condition can be written:

$$-k_n \frac{\partial T}{\partial n} = h_f (T_f - T_s) = h_f \Delta T \tag{3.8}$$

where h_f is the heat transfer coefficient and ΔT is the temperature difference between the fluid and the solid boundary surface. In this case T_f is the fluid ambient temperature (assumed as known) and T_s is the temperature of the solid surface, which is not a priori known, but is calculated as a result of the solution process. For cases which are of interest in structural analysis problems, both convective and radiation heat exchange takes place and

Institutional Repository - Library & Information Centre - University of Thessaly
02/06/2024 20:36:34 EEST - 18.222.76.217

Equation 5.8 can be written in the form

$$-k_n \frac{\partial T}{\partial n} = a(T_f - T_s)^{\beta} + \Phi \varepsilon_r \sigma (T_f^4 - T_s^4) \qquad (3.9)$$

where

a and β are coefficients that depend on the side of the structural elements (fire side or ambient temperature air side)

Φ is the configuration or view factor,

ε_r is the resultant emissivity (which depends on the fluid and solid emissivities) and

σ is the Stefan-Boltzmann constant.

The first part of the r.h.s. of Equation 5.9 is known as the convective term whereas the second one is known as the radiative term.

The term ε_r can be evaluated by the simple formula

$$\varepsilon_r = \varepsilon_f \times \varepsilon_s \qquad (5.10)$$

where ε_f is the emissivity of fire (usually taken equal to 1.0) and ε_s is the emissivity of the structural material.

Institutional Repository - Library & Information Centre - University of Thessaly
02/06/2024 20:36:34 EEST - 18.222.76.217

Chapter 4. Material properties at elevated temperatures

The properties of steel at elevated temperatures are very important for the analysis of structures subjected to fire. Taking into account the conclusions of studies that have been conducted in the past from various researchers, it is obvious that it is of great importance to simulate numerically the dependence of material properties to temperature, in order to study the response of structures in fire conditions. The dependence of all mechanical-thermal properties of materials to temperature contributes to a more complex numerical analysis. The following section describes the mechanical and thermal properties of steel, which are adopted in the present study, complied with the mathematical models as are proposed in EN 1993-1-2.

For heating rates between 2 and 50 K/min, the strength and deformation properties of steel at elevated temperatures are obtained by the stress-strain curve of Figure 4-1. The stress-strain curve of structural steel at high temperatures is quite different from that at ambient temperature as it is illustrated in Figure 4-2. The elastic range is followed by an elliptic branch, occurring until the suggested strain limit of $\varepsilon_{y,\theta}$=2%. A yield plateau appears in the last part of the curve until strain is up to $\varepsilon_{t,\theta}$=15%. The variation of the stress-strain relationship, for structural steel S275, as the temperature increases is presented in Figure 4-2. Structural steel begins to lose strength at temperatures above 400°C. The reduction is immediate and at the temperature of 800°C the yield stress is equal to 11% of its initial value. In the present study, it is assumed that steel melts at the temperature of 1200°C where its strength is becoming zero.

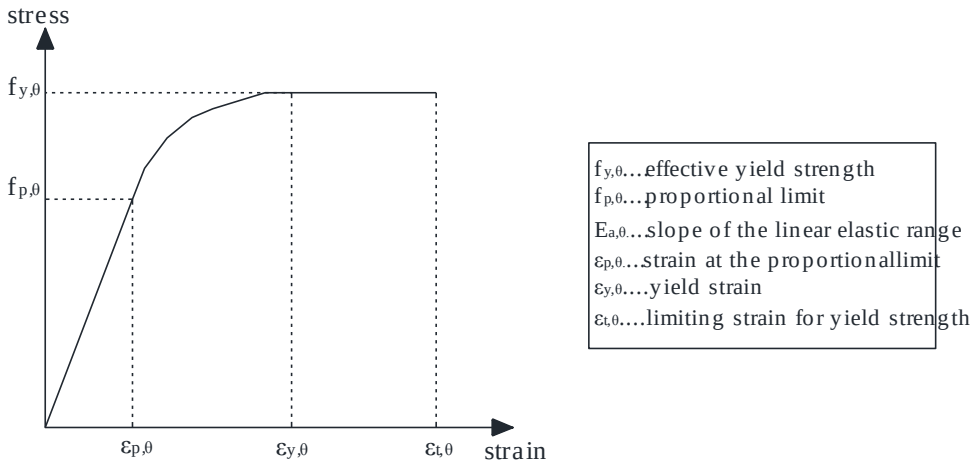

Figure 4-1: Stress-strain relationships of structural steel at elevated temperatures.

Institutional Repository - Library & Information Centre - University of Thessaly
02/06/2024 20:36:34 EEST - 18.222.76.217

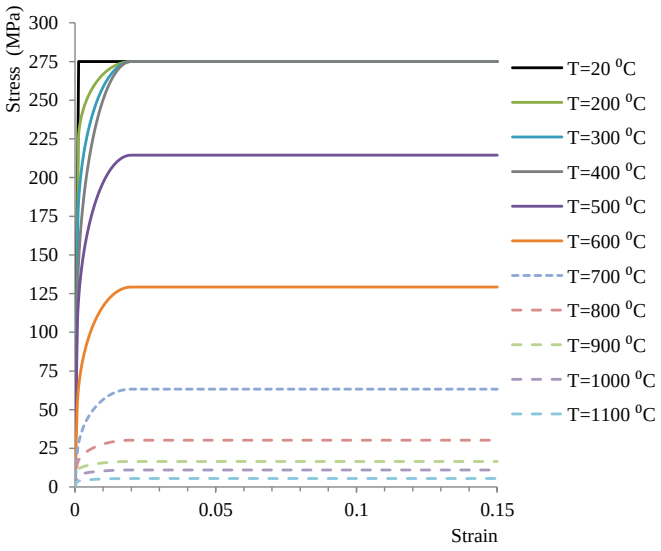

Figure 4-2: Stress-strain relationships of structural steel S275 at elevated temperatures.

At elevated temperatures, effective yield strength, proportionality limit and slope of linear elastic range are reduced according to factors specified on Table 3.1 EN 1993-1-2 for structural steel.

An important issue that determines the behaviour of steel during fire exposure is the temperature induced strains. These strains include the thermal expansion and the creep strain. The thermal expansion coefficient of steel α has a great importance in modeling composite structures under fire conditions. The dependence of the coefficient α on temperature is illustrated in Figure 4-3. Additionally, it is well known that the creep strain appears during the heating of metals. In fire-engineering only the primary and the secondary creep strains are considered, due to the short time of fire-exposure. Various models have been proposed in the literature (Plen model, Dorn-Harmathy model etc.). The incorporation of the creep strain models in the calculations is a demanding task. For simplicity, the effect of creep is implicitly taken into account to the stress-strain relationship, according to EN 1993-1-2.

The temperature dependent thermal properties are thermal conductivity and specific heat. It is obvious from equation (2) that the thermal conductivity k and the specific heat C are the basic thermal properties defining the temperature distribution in a structural member. The thermal conductivity of structural steel reduces as the temperature increases as it is shown in Figure 4-4.

The specific heat is increasing slightly at elevated temperatures until 600°C. In the range between 600°C and 900°C the specific heat increases rapidly until the value of 5000 J/kg K at 735°C (Figure 4-5). This occurs due to the phase transition of steel at this temperature. The thermal properties of reinforcing steel and structural steel are identical.

Institutional Repository - Library & Information Centre - University of Thessaly
02/06/2024 20:36:34 EEST - 18.222.76.217

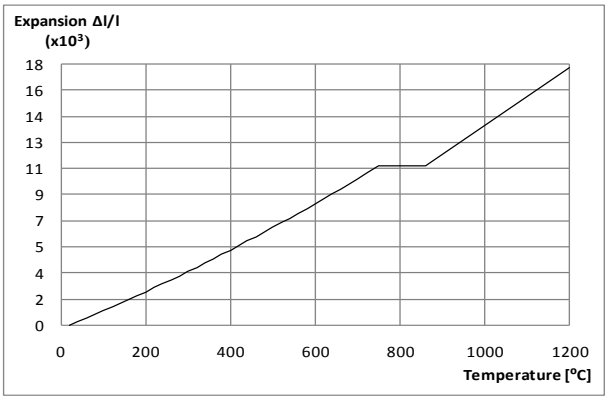

Figure 4-3: Thermal expansion of steel.

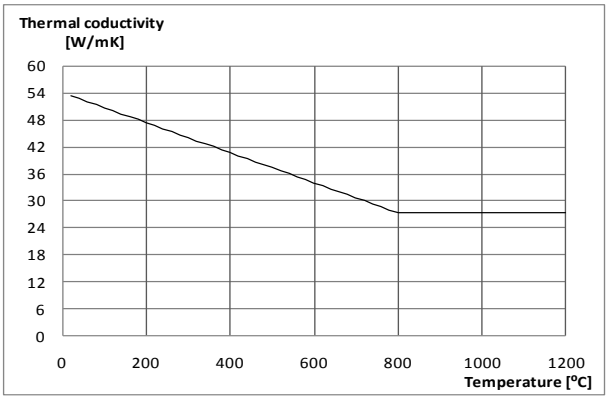

Figure 4-4: Thermal conductivity of steel.

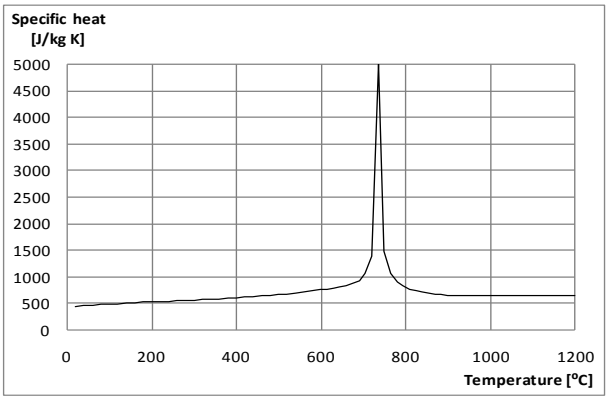

Figure 4-5: Specific heat of steel.

Institutional Repository - Library & Information Centre - University of Thessaly
02/06/2024 20:36:34 EEST - 18.222.76.217

Chapter 5. The case study – Primary results

This Chapter initially presents the cylindrical fixed-roof tank that is studied in this thesis and defines the problem that is solved. Next, the problem is solved through Linear Buckling analysis (LBA) in order to take some primary results for the thermal buckling behavior of the heated tank.

5.1 Case Study

The typical cylindrical thin-walled tank which is considered in this study has uniform wall thickness of 10mm, is 20m high and the diameter equal to 20m (Figure 5-1). The tank is used for oil storage with density equal to 0.74tn/m^3. The roof is considered conical with slope equal to 10°. Actually, it is more realistic to use internal trusses to support the roof in order to enhance the roof stiffness. In this study the roof it is chosen to be simulated through the conical shell roof approach in order to simplify the calculations. It would be more accurate to include the details of the roof structure but this would not have any profit to this study, since as it would be proved in the following the roof is not a key parameter and that the main problems occur in the heated zone of the tank and the roof remains intact. This is realistic in most cases but it depends on the roof stiffness. To this end, parametric studies are conducted in order to discover the effect of the roof stiffness to the fire-behavior of the heated tank and to the final failure modes. The roof stiffness is modified using different shell thickness. Two extreme cases are considered and the thickness of the roof shell (t_r) is taken equal to the thickness of the cylindrical tank (t_c) and on the other side it is considered 100 times thicker. Parametric study is performed for intermediate values i.e. $1 \le t_r \le 100$.

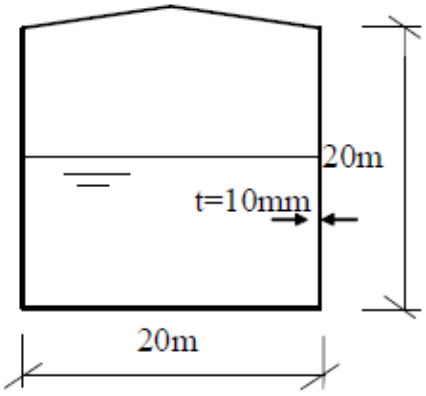

Figure 5-1: Geometry of the cylindrical tank.

Institutional Repository - Library & Information Centre - University of Thessaly
02/06/2024 20:36:34 EEST - 18.222.76.217

5.2 Thermal loading

In the problem that is considered in this study, the thermal loading of the heated tank is generated from the fire-engulfed adjacent tank and the dominant mechanism of heat transfer is radiation. In this case, it is expected that the temperature distribution will be non-uniform. The side of the tank which is on the face of the source tank will be hot comparing with the opposite face which may be not affected by the fire. The higher temperature of the heated tank will be detected to the meridian of incidence of fire and the temperature will be decreased at medians that are further away in the circumferential direction. Moreover, it is logical to assume that the level of the stored liquid can affect the temperature pattern in the vertical direction. I particular the upper part of the tank which is not in contact with the stored liquid will be heated more than the lower part due to the fact that the heat transfer coefficient of air is low (in the upper part) and the thermal inertia of the stored liquid is high (in the lower part).

Pool-fire semi-empirical models available in the literature can be used in order to determine the temperature distribution of the heated tank. Alternatively, the temperature field can be determined numerically through Computational Fluid Dynamics analysis or through the Finite Element method. This problem is rather complicated and the evaluation of the temperature field of the heated tank is out of the scope of this thesis. The findings of the study of Liu (2012) are found to be reasonable and to describe adequately the complicated phenomenon and they are adopted for the simulation of the thermal loading of the heated tank.

Specifically, it is considered that when the source tank is of the same diameter, only half of the heated tank is submitted to temperature rise (Figure 5-2). As the diameter of the burning tank is increased it produces wider spread of heated zone in the target tank. On contrary the heated zone of the target tank is eliminated. Two different circumferential temperature patterns are adopted and they are illustrated in Figure 5-2 for the case of the half heated tank ($\theta_0 = 90^o$). The square cosine function

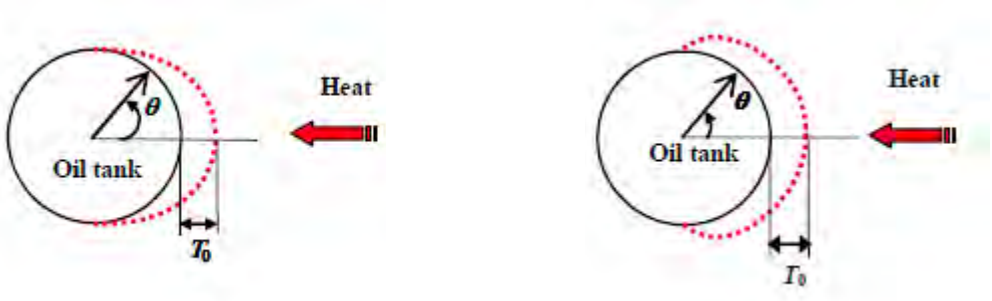

(a) Square cosine pattern (b) Cosine pattern

Figure 5-2: Temperature pattern of the heated tank.

Institutional Repository - Library & Information Centre - University of Thessaly
02/06/2024 20:36:34 EEST - 18.222.76.217

The square cosine pattern is given by the expression:

$$T_\theta = \begin{cases} (T_{0m} - T_{0a}) \cos^2\left(\frac{\theta}{\theta_0}\frac{\pi}{2}\right) & if\ |\theta| \le \theta_0 \\ 0 & if\ |\theta| > \theta_0 \end{cases} \quad (5.1)$$

While the equation that describes the cosine pattern is:

$$T_\theta = \begin{cases} (T_{0m} - T_{0a}) \cos\left(\frac{\theta}{\theta_0}\right) & if\ |\theta| \le \theta_0 \\ 0 & if\ |\theta| > \theta_0 \end{cases} \quad (5.2)$$

where θ is the circumferential coordinate, θ_0 is the critical angle that defines the heated zone, T_{0m} is the temperature of the most heated meridian and T_{0a} is the ambient temperature.

The different circumferential temperature patterns are used in order to study the sensitivity of the structural fire behavior of the heated tank to the temperature distribution.

Regarding the vertical direction two different cases are considered. In the case of the empty tank the temperature is considered constant along the vertical direction. In the case where the tank is partially filled a trilinear distribution is taken into account (Figure 5-3). In the upper part the temperature pattern already described is used. In the lower zone where the tank is in contact with the stored liquid, the temperature is considered to be equal to the temperature of the liquid i.e. the ambient temperature. Between the upper and the lower zone, a transition zone is introduced in order to simulate the heat conduction from the upper hot zone to the lower cold zone. The length of the transition zone is equal to 0.20m and the temperature decreases linear based on the temperature pattern used for the upper zone.

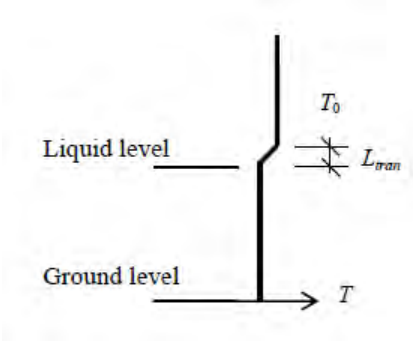

Figure 5-3: Trilinear temperature pattern along the vertical direction

The roof is considered either “hot” or “cool”. These two conditions correspond to the effects due to different flame heights in the adjacent fire-engulfed tank. In the case where the roof is “hot”, the temperature pattern at the circumferential direction is the same with the one that is used for the tank and it is assumed to vary linearly with the radial coordinate.

Institutional Repository - Library & Information Centre - University of Thessaly
02/06/2024 20:36:34 EEST - 18.222.76.217

5.3 Numerical modelling

The problem is solved numerically using the Finite Element (FE) method. The numerical model is developed using the nonlinear finite element code MSC-Marc (2011). The three-dimensional model that is developed for the simulation of the behavior of the thin-walled steel tank uses the element of type 75 of the library of MSC-Marc (2011). This is a four-node, thick-shell element with global displacements and rotations as degrees of freedom. Bilinear interpolation is used for the coordinates, displacements and the rotations. The membrane strains are obtained from the displacement field; the curvatures from the rotation field. The transverse shear strains are calculated at the middle of the edges and interpolated to the integration points. In this way, a very efficient and simple element is obtained which exhibits correct behavior in the limiting case of thin shells.

The steel tank is pinned at the base and the conical roof is connected with the rest of the cylindrical tank using the same nodes. The thermal loading is actually imposed as fixed nodal temperature using the temperature pattern already described in Section 5.2 and no-heat exchange takes place. The material properties are temperature dependent as it is defined in EN 1993-1-2.

The meshing at both circumferential and vertical coordinated should be carefully chosen to capture the possible buckles that may arise. Considering results of the literature (Liu 2012, Godoy and Batista-Abreu 2012) significant compression forces appear at the near the boundaries and at the liquid surface and fine mesh is requires in the specific regions. The discretization should be non-uniform in order to decrease the total number of the finite elements that are used in the simulation in order to avoid excessive computational cost and to capture accurately the local buckling phenomena that may arise due to large compressive forces. Mesh sensitivity study is conducted, using Linear Bucking Analysis, in order to determine the mesh of the cylindrical tank and is presented in the following section.

5.4 Primary Results - Linear Bucking Analysis (LBA)

The first step is to conduct Linear Bucking Analysis (LBA) aiming to evaluate the bucking modes and the critical temperature values. In the specific type of analysis the steel is considered elastic and the modulus of elasticity decrease as the temperature is increased. The coefficient of thermal expansion is also taken into account and for simplicity is assumed to be constant. Although the response of the heated thin-walled tank is non-linear, the results of buckling analysis present a good approximation of the final failure and the possible global/local bucking phenomena.

In the LBA the incremental loading is the temperature pattern presented in Section 5.2 and both the schemes for the “cool” and “hot” roof are adopted. The gravity load is included in the preloading stage and is imposed in the first step of the analysis.

Institutional Repository - Library & Information Centre - University of Thessaly
02/06/2024 20:36:34 EEST - 18.222.76.217

5.4.1 Mesh Sensitivity Study

Since there is no analytical solution for comparison with the numerical results concerning the critical temperature and the buckling mode, mesh sensitivity study is performed. A more dense mesh is adopted near the base, at the liquid surface and at the upper bound of the cylindrical shell as it is illustrated in Figure 5-4.

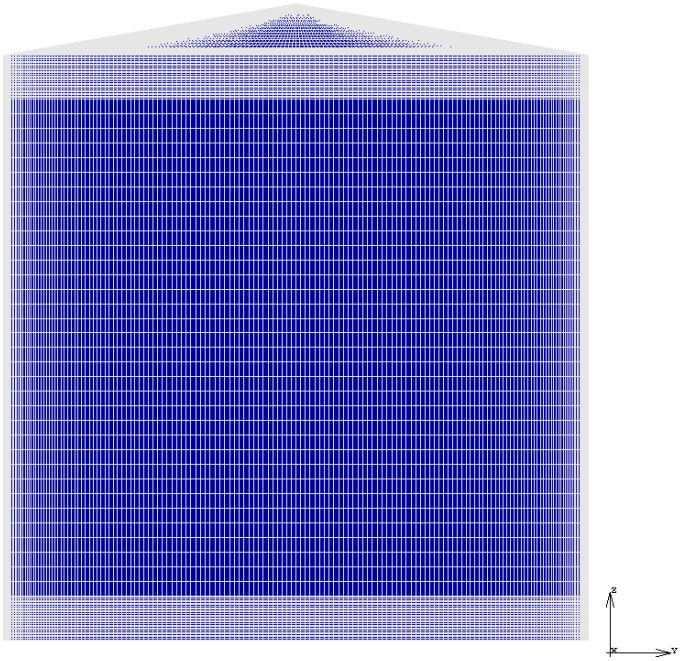

Figure 5-4: Mesh of the tank and the refined zones.

Regarding the circumferential direction, the reference mesh size is considered equal to 1° while in the vertical coordinate the loose mesh is 0.05m and the refined mesh is 0.005m. This mesh scheme is considered to be the reference state. The reference critical buckling temperature that results from the reference LBA and corresponds to the first eigenmode is compared to the respective critical values that result from analysis with different meshing schemes. The results are presented in Table 5-1.

Circumferential mesh	Vertical mesh (coarse zone)	Vertical mesh (fine zone)	Critical temperature
0.5°	0.0025	0.025	133°C
0.5°	0.005	0.05	136°C
1°	0.0025	0.025	138.5 °C
1°	0.005	0.05	143°C
3°	0.0025	0.025	164°C
3°	0.005	0.05	167°C
6°	0.0025	0.025	195°C
6°	0.005	0.05	197°C

Table 5-1: Results of sensitivity study.

It is concluded that the temperature of less dense meshing schemes deviate from the reference critical temperature and the critical values are ascending. On the contrary, as the mesh (in both refined and non-refined regions) becomes dense, the results converge to the reference

Institutional Repository - Library & Information Centre - University of Thessaly
02/06/2024 20:36:34 EEST - 18.222.76.217

case. Thus the meshing scheme of the reference case is adopted in this study.

It is noted that for the mesh sensitivity study the roof thickness t_r is considered to be two times the thickness of the cylindrical shell (t_c) i.e. $t_r = 2t_c$. In the case where the roof shell thickness is less than this value, the roof buckling mode takes place at very low temperature as it will be presented in the next Section.

5.4.2 Results of LBA

The results of LBA analyses indicate the buckling load (temperature) for both temperature patterns (square cosine and cosine patterns) taking into account the "cool" roof scheme and different roof to cylindrical shell thickness ratios, are presented in Table 5-2 for the first 12 buckling modes. The buckling temperature is actually the temperature of the most heated meridian of the tank i.e. the meridian of incidence of fire. The negative eigenvalues correspond to the case where the tank is submitted to decreasing temperature history that follows the specific patterns. These buckling modes are out of interest of this study. It is noticeable that the eigenmodes appear in pairs for the same eigenvalue and the one is symmetric while the other is antisymmetric.

It can be concluded that the fixed-roof tank buckles earlier i.e. in lower temperature in the case of square cosine pattern in comparison with the cosine pattern. Additionally, it is indicated that the results concerning the buckling temperature are almost the same if the roof is considered "hot" or "cool", thus the heating of roof is not a sensitive parameter for this problem. This can be attributed to the fact that the buckling temperature of the cylindrical shell does not exceeds the level of 200°C and the modulus of elasticity of steel is slightly reduced. Thus, the restraint introduced by the fixed roof to the cylindrical cell is almost the same in both cases ("hot" and "cool" roof).

The eigenmodes are illustrated in Figure 5-5, Figure 5-6and Figure 5-7 for the square cosine and the cosine temperature patterns respectively. In both cases, the circumferential wave length is smaller compared with the respective length in the vertical direction and this denotes the sensitivity of the results to the meshing discretization in the circumferential direction. Furthermore, the square cosine temperature pattern inserts stronger circumferential temperature gradient and leads to higher buckling modes and lower buckling temperature in comparison with the cosine pattern.

Actually, the problem can be decomposed in two different problems. The first one involves the differential thermal expansion due to the temperature pattern in the circumferential direction which generated the respective stresses in this direction due to the restrained thermal expansion. In the second problem meridional compression forces arise due to the restrain introduced by the fixed roof. These forces obviously are dependent on the stiffness of the roof.

Institutional Repository - Library & Information Centre - University of Thessaly
02/06/2024 20:36:34 EEST - 18.222.76.217

	Square cosine temperature pattern					Cosine T. P.
eigenmode	$t_r = 2t_c$	$t_r = 3t_c$	$t_r = 5t_c$	$t_r = 10t_c$	$t_r = 100t_c$	$t_r = 2t_c$
1	138.5	133.8	129.2	126.1	146.4	-176
2	138.5	133.8	129.2	126.1	146.4	-176
3	-139.8	-135	-130.3	-127.2	156.4	-188.8
4	-139.8	-135	-130.3	-127.2	157	-188.8
5	-139.9	-135.1	-130.4	-127.3	161.7	-193.2
6	-139.9	-135.1	-130.4	-127.3	-165.2	-193.2
7	140.8	136	-130.4	128	-165.2	-198.3
8	140.8	136	131.3	128	-165.2	-198.3
9	156.2	151.8	147.4	144.2	-165.2	-198.6
10	156.2	151.8	147.4	144.2	165.4	-198.6
11	160.4	154.8	149.5	145.8	169.8	202.5
12	160.4	154.8	149.5	145.8	170.2	202.6

Table 5-2: Critical buckling temperatures for the fixed-roof tank.

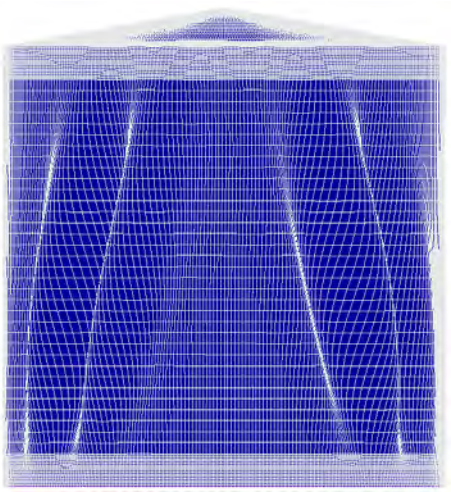

1st eigenmode (elevation view)

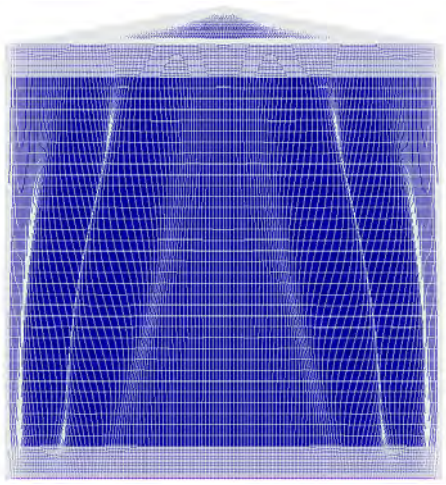

2nd eigenmode(elevation view)

1st eigenmode (plan view)

2nd eigenmode (plan view)

Figure 5-5: 1st and 2nd buckling modes of fixed-roof tank for the square cosine temperature pattern (cool roof)

Institutional Repository - Library & Information Centre - University of Thessaly
02/06/2024 20:36:34 EEST - 18.222.76.217

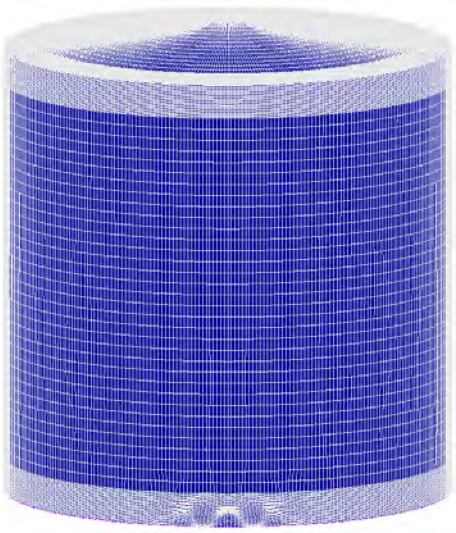

7th eigenomde (elevation view)

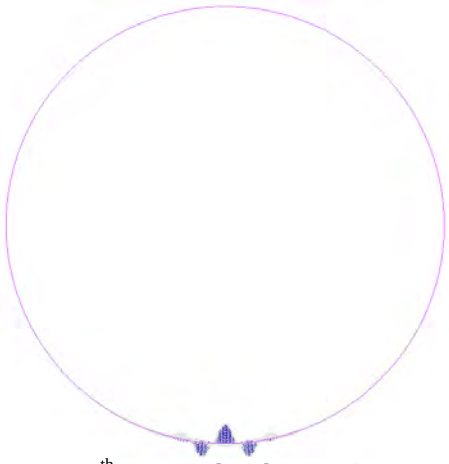

7th eigenmode (plan view)

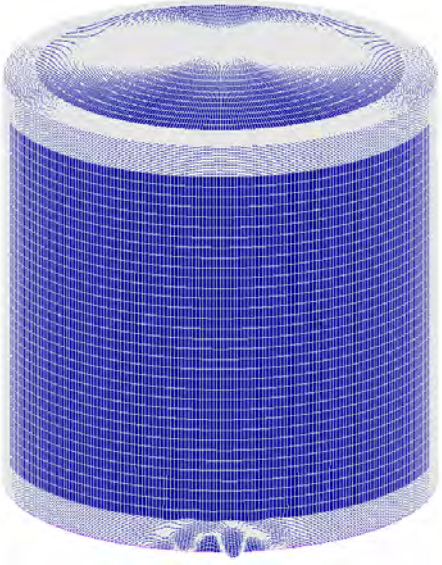

8th eigenomde (elevation view)

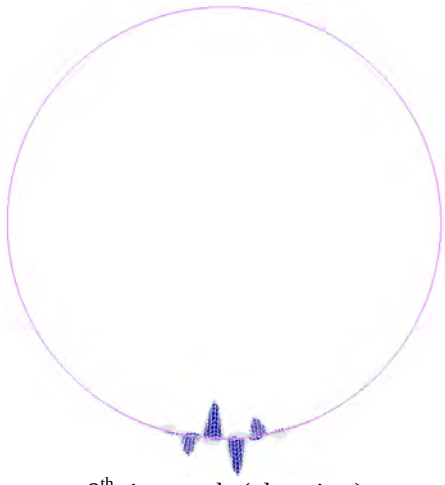

8th eigenmode (plan view)

Figure 5-6: 7th and 8th buckling modes of fixed-roof tank for the square cosine temperature pattern

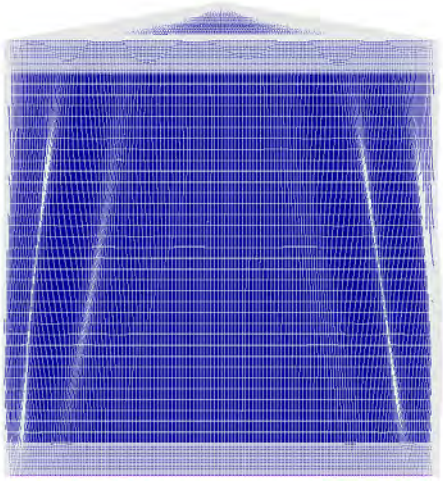

1st eigenmode (elevation view)

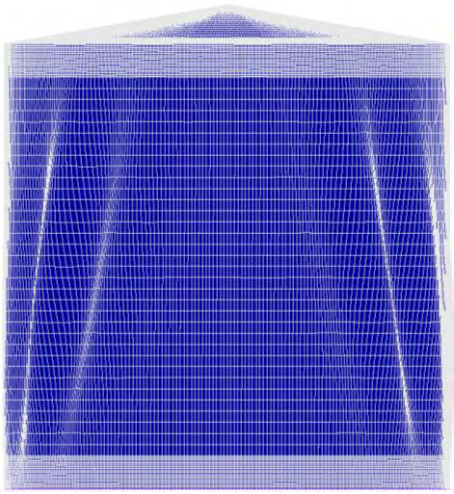

2nd eigenmode(elevation view)

Figure 5-7: Buckling modes of fixed-roof tank for the cosine temperature pattern (cool roof).

Institutional Repository - Library & Information Centre - University of Thessaly
02/06/2024 20:36:34 EEST - 18.222.76.217

Chapter 6. Thermal buckling of fixed-roof heated tanks

The thermal buckling behavior of the heated cylindrical tank is studied in detail in this Chapter. The numerical analysis techniques that are used for the simulation and the solution of the problem are presented. First the problem is solved through Geometric non-linear analysis, taking into account linear elastic material law and the corresponding results are given. Specifically, the results are given mainly in terms of critical buckling temperature which indicates the occurrence of the instability and the buckling takes place in the tank. A more realistic approach follows and the thermal buckling behavior of the steel storage tank is solved taking into account the material non-linearity at elevated temperatures. In both cases, the effect of the roof stiffness in the critical buckling temperature is studied.

6.1 Numerical analysis

The fire behavior of the fixed-roof tank (target), heated by the adjacent (source) tank is simulated using the finite element method and the problem is solved through non-linear transient thermal/structural numerical analysis considering large displacements in the formulation of the mathematical problem. The numerical model, described in the previous Chapter (Chapter 5) is used and the square cosine pattern is adopted in order to simulate the thermal load. During the analysis the temperature is increased linearly through driven table input and the temperature of the most heated generator is the variable that replaces the load in the equilibrium path. For the empty tank the unique concurrent mechanical-static load is the gravity load. In the case where the liquid is present the hydrostatic pressure is also taken into account. It is noted that the temperature profile of the heated tank is prescribed according to the thermal pattern and actually no heat transfer takes place. Specifically, the *fixed temperature* boundary condition is use in order to define the temperature-history foe each need of the numerical model. The non-heated zone is assumed to be at ambient temperature.

The arc-length method is utilized for the evaluation of the equilibrium path of the structural system and the AUTO STEP scheme, available in MSC Marc, is used. In this case, the primary control of the load step is based upon the number of recycles needed to obtain convergence. There are a number of optional user-specified criteria that can be used to additionally control the load step.

Here, the artificial damping energy based time stepping scheme is used. This scheme is appropriate for solving problems where instabilities (local or global) are expected to occur. The basic idea behind this scheme is that *du*M*du/dt* (with *du* the incremental displacement vector, *M* the lumped mass matrix based on a unit density and *dt* the time increment) is used

Institutional Repository - Library & Information Centre - University of Thessaly
02/06/2024 20:36:34 EEST - 18.222.76.217

to define a damping energy rate. Based on the user defined damping ratio (default = 0.0002), the amount of artificial damping energy is related to the actual strain energy. For a linear case, the total amount of damping energy will be equal to the total strain energy times the damping ratio. For cases where instabilities occur, the amount of damping energy is increased to stabilize the solution. The actual amount of damping energy is available on the post file as a global variable. By comparing the estimated (damping) energy with the actual values, the time increment is either increased or decreased. By comparing the estimated (damping) energy with the actual values, the time increment can be increased or decreased.

An illustrative description of the method is included in Simulia (2008) and it is forwarded here. *While the model is stable, the viscous forces and, therefore, the viscous energy dissipated are negligible compared with the strain energy of the system. Thus, the additional artificial damping has no effect on the structural behavior. If a local region becomes unstable, the local velocities increase and, consequently, part of the strain energy released is dissipated by the applied damping. Normally the examined structure is stable at the beginning of the step and that instabilities may develop in the course of the step. Such condition is assumed in the numerical implementation of the damping parameter. The first increment of the step is stable without the need to apply a damping. The damping factor is then determined in such a way that the dissipated energy for a given increment with characteristics similar to the first increment is a small fraction of the extrapolated strain energy. The fraction is called the dissipated energy fraction and has a default small value of 0.0002 but the user is free to assign an even smaller or larger value. The damping factor is controlled by the convergence history and the ratio of the energy dissipated by the viscous damping to the total strain energy. If the convergence behavior is problematic because of instabilities or rigid body modes, the damping factor is automatically increased. On the other hand, damping factor may also be reduced automatically if instabilities and rigid body modes subside*.

Since the phenomenon is mainly dominated by the thermal forces due to the restrained thermal expansion the problem initially is solved through geometric non-linear analysis (GNA) assuming elastic temperature-dependent material law. In the sequel, the elastic-plastic material law is incorporated in the numerical model and geometric/material non-linear analysis is conducted in order to reveal the effect of steel hardening to the behavior of the heated tank. Parametric analyses with respect to the yield stress of steel indicate that in the case of low-yield steel, the elastoplastic material behavior stabilizes the behavior of the heated tank and contributes beneficially since the premature occurrence of elastic thermal buckling is prevented. If high-strength steel is adopted, the structural behavior is dominated by the thermal buckling and the plasticity can be omitted during the numerical analysis.

6.2 Evaluation of the thermal behavior of heated tank through GNA

Figure 6-1 illustrates the deformed shape of the fixed-roof cylindrical empty tank at

Institutional Repository - Library & Information Centre - University of Thessaly
02/06/2024 20:36:34 EEST - 18.222.76.217

characteristic levels of temperature of the most heated generator, in the case where the roof is considered ten times thicker that the cylindrical shell. It is note that in this case the roof of the tank is considered to be at ambient temperature (cool roof). The global buckling takes place at temperature equal to 145°C and the deformed configuration of the heated tank near the buckling (Figure 6-1a) is dominated by the first buckling mode as it is shown in Figure 5-5 and the buckling temperature predicted using GNA is slightly higher comparing with the corresponding value that comes from LBA. During the post-buckling stage (Figure 6-1b) the geometry if the cylindrical shell becomes complicated and large displacements can be detected at the crest of the buckles. It is also observed that the deformed shape of the cylindrical tank (Figure 6-1c) becomes different as temperature increases and successive buckling appear at multiple areas. This can be more obvious in Figure 6-2 where the radial displacement field of the cylindrical tank is captured at representative levels of temperature. It can be noted that the displacement field of the tank changes rapidly during the buckling stage.

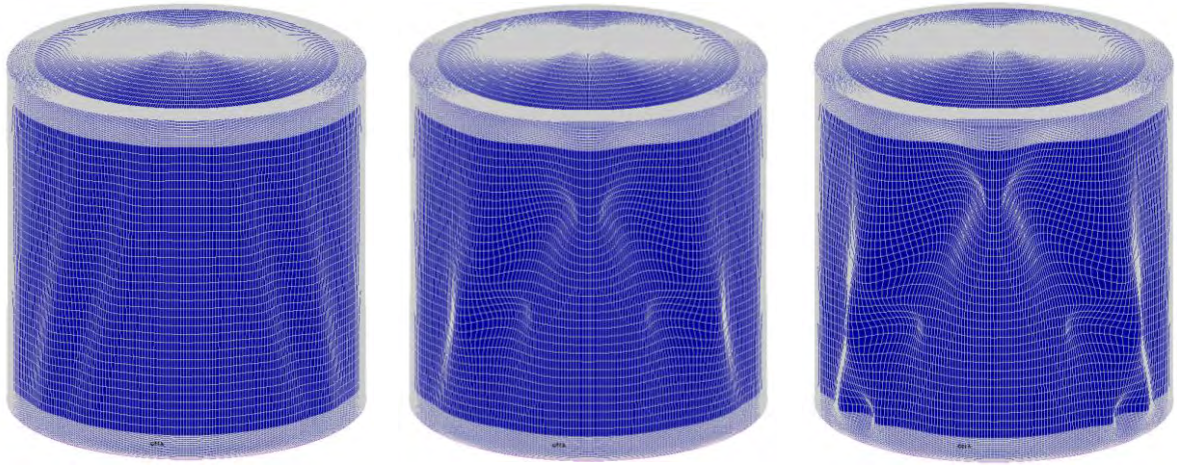

(a) Near buckling (T=145 °C) (b) Post-buckling (T=147°C) (c) Post-buckling (T=190°C)

Figure 6-1: Deformed shape of the cylindrical tank during GNA ($t_r = 10t_c$).

The buckling zones are totally different at the early stages of the buckling (Figure 6-2a) and at the post-buckling stage (T=145°C) where the temperature of the most heated generator is 147°C. Moreover, during the post-buckling stage the buckles are spreading (zone A in Figure 6-3) and multiple buckles take place (zone C in Figure 6-3). Relative large values of the radial displacements are observed during the post buckling stage and they are ten times higher than the corresponding values at the early stage of buckling.

In Figure 6-3, the temperature-radial displacement curves for the nodes at the crest of the buckles in zones A, B and C are presented. It is observed that initial the buckling takes place in region A and almost immediately in zone B. Specially in zone B a sudden jump of the radial displacement from positive to negative values takes place for temperature near 145°C. In zone C the radial displacement of the node at the crest of the buckle increases until the first buckling (in zones B and C) takes place. Next, it is slightly modified until temperature equal

Institutional Repository - Library & Information Centre - University of Thessaly
02/06/2024 20:36:34 EEST - 18.222.76.217

to 190°C, where it jumps to negative values. This identifies a (second) local buckling of the cylindrical shell. The phenomenon is rather complicated due to both the temperature gradient along the circumferential direction and the degradation of modulus of elasticity of steel as temperature increases.

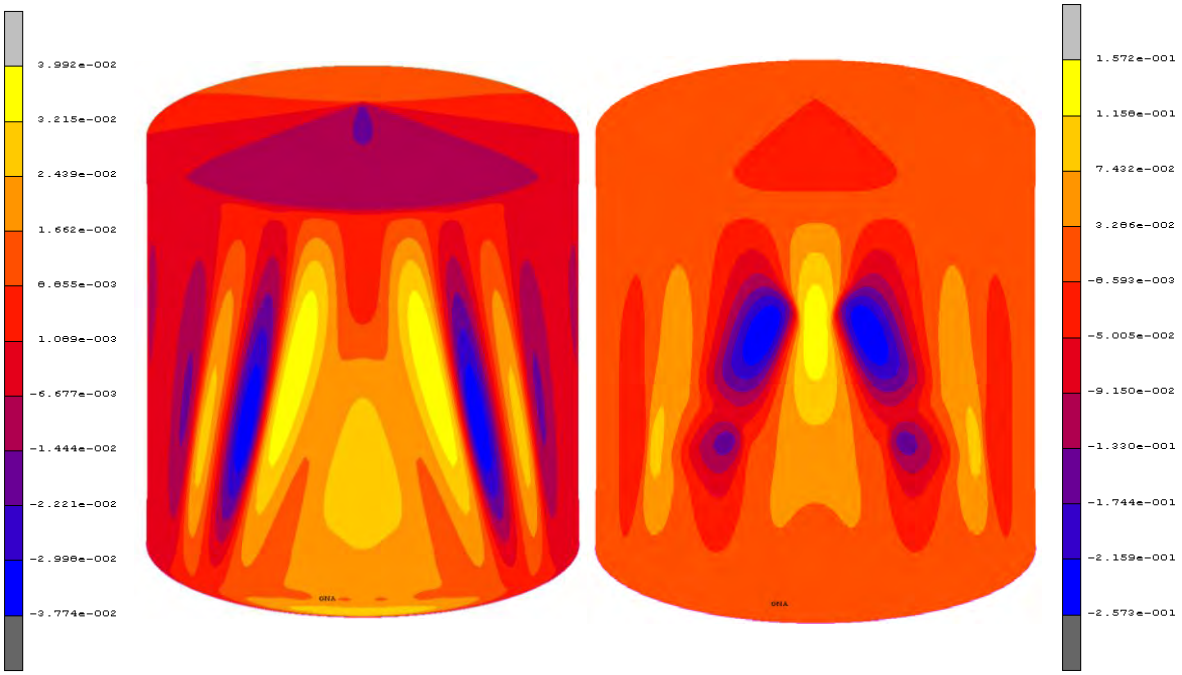

(a) Near buckling (T=145 °C) (b) Post-buckling (T=147°C)

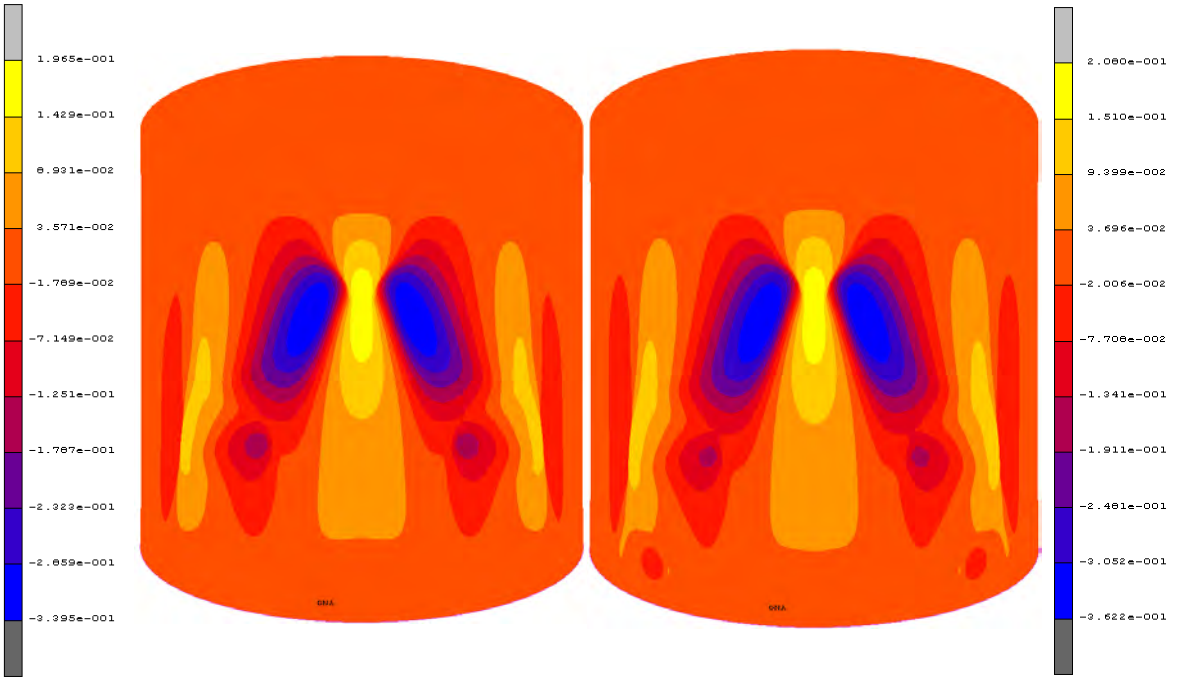

(c) Post-buckling (T=190°C) (d) Post-buckling (T=200°C)

Figure 6-2: Snapshots of radial displacement field of cylindrical tank (heated side) at various at characteristic temperature levels ($t_r = 10t_c$).

Institutional Repository - Library & Information Centre - University of Thessaly
02/06/2024 20:36:34 EEST - 18.222.76.217

In order to explain the complicated phenomena that arise in the heated tank, the tensor of Cauchy stresses are plotted for various paths along the cylindrical shell. Figure 6-4 presents both the circumferential and meridional stresses around the circumference of the cylindrical tank at the mid-height (z=10m) at the pre and post-buckling stage. Specifically, the half of the circumference is plotted since the phenomenon is symmetric with respect to x-axis. The value $\theta = 0^o$ correspond to the most heated generator, while $\theta = 180^o$ identifies the opposite generator that is allocated in the side of the tank that is not heated i.e. the interval $0^o \le \theta \le 90^o$ lies on the heated region while the interval $90^o \le \theta \le 180^o$ is at ambient temperature.

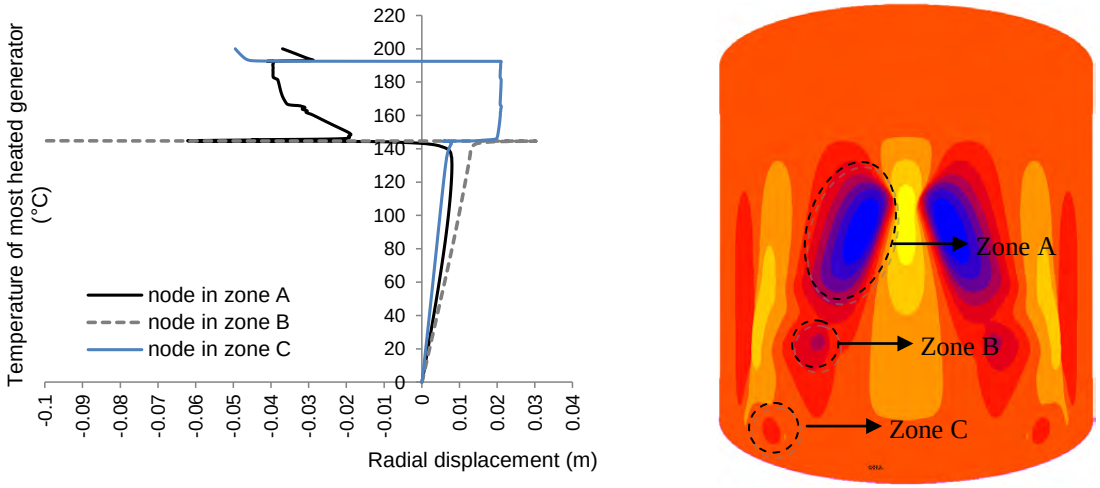

Figure 6-3: Temperature-radial displacement curves at crest of buckles in Zones A. B and C ($t_r = 10t_c$).

During the pre-buckling stage, the pattern around the circumference shows axial compression due to restrained expansion over the heated face ($0^o \le \theta \le 45^o$) with a corresponding axial tension (to satisfy axial equilibrium) in the side zone ($45^o \le \theta \le 90^o$), followed by axial compression again on the cold back face (to satisfy global moment equilibrium). It is noted that the magnitude of the circumferential stresses is smaller with respect to the values of meridional stresses. At the early stage of heating, the heated face is in compression in circumferential direction ($0^o \le \theta \le 45^o$) and in tension in the rest of the hot zone. This pattern becomes more complicated and changes between tension and compression as the temperature increases (T=95°C). The circumferential stresses become insignificant in the cold face of the tank. Buckling occurs on the heated side because of the large compressive stress accompanied with a reduced modulus of the steel there. On the cool side, the compressive stress is slightly smaller and the modulus is not reduced so it is not critical there.

During the post-buckling stage the magnitude of both meridional and circumferential stresses increases significantly and the patterns of the stresses along the circumference change rapidly as the temperature increases. Near the buckling temperature (T=145°C) significant compressive stress arise in the heated zone ($30^o \le \theta \le 45^o$). In the sequel, as the temperature increases (post buckling stage) the most compressed part of the cylindrical shell (taking in to

Institutional Repository - Library & Information Centre - University of Thessaly
02/06/2024 20:36:34 EEST - 18.222.76.217

account both meridional and circumferential stresses) lies between $15^{o} \le \theta \le 30^{o}$.

The radial displacement pattern around the circumference of the cylindrical tank at mid-height (z=10m) for both pre-buckling and post-buckling stage are plotted in Figure 6-5. During the pre-buckling stage positive radial displacements (the positive values indicate displacement vector is oriented out of the surface) arise in the bigger part of the cylindrical shell, both in hot and in cool faces. This pattern changes at all after the buckling, where the magnitude of the radial displacements is considerably increased and negative values are detected for $15^{o} \le \theta \le 30^{o}$ and $50^{o} \le \theta \le 70^{o}$. The previous verify the deformed shape of the cylindrical shell, illustrated in Figure 6-2.

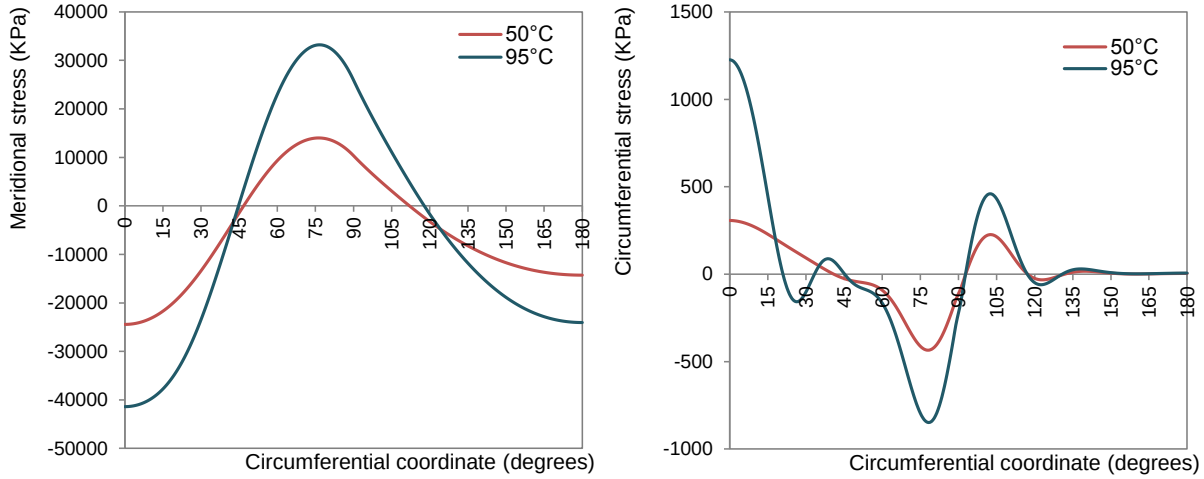

(a) Pre-buckling stage

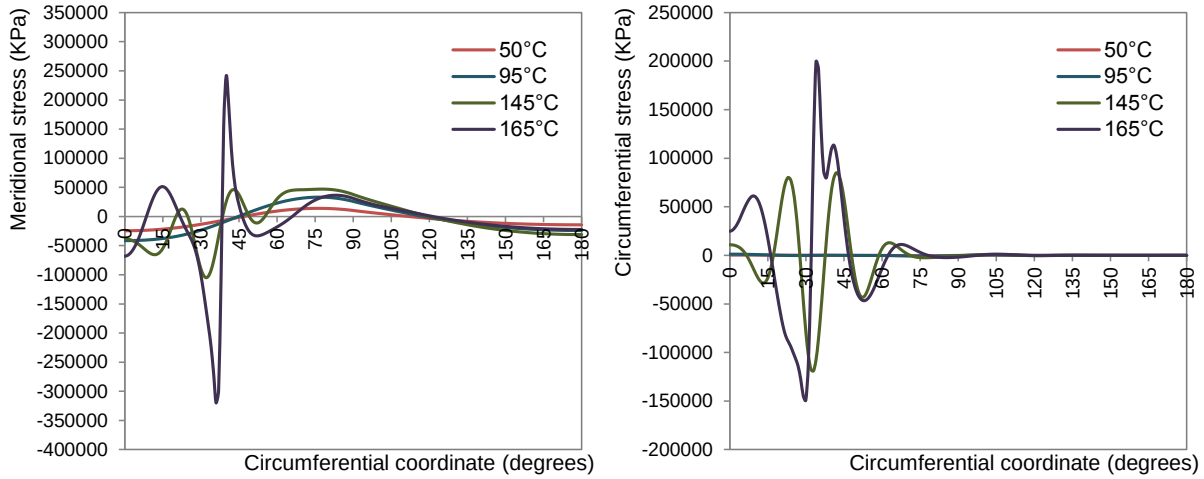

(b) Pre-buckling and post-buckling stage

Figure 6-4: Cauchy stress components around the circumference of cylindrical tank at mid-height (z=10m) for various levels of temperature of most heated generator.

Institutional Repository - Library & Information Centre - University of Thessaly
02/06/2024 20:36:34 EEST - 18.222.76.217

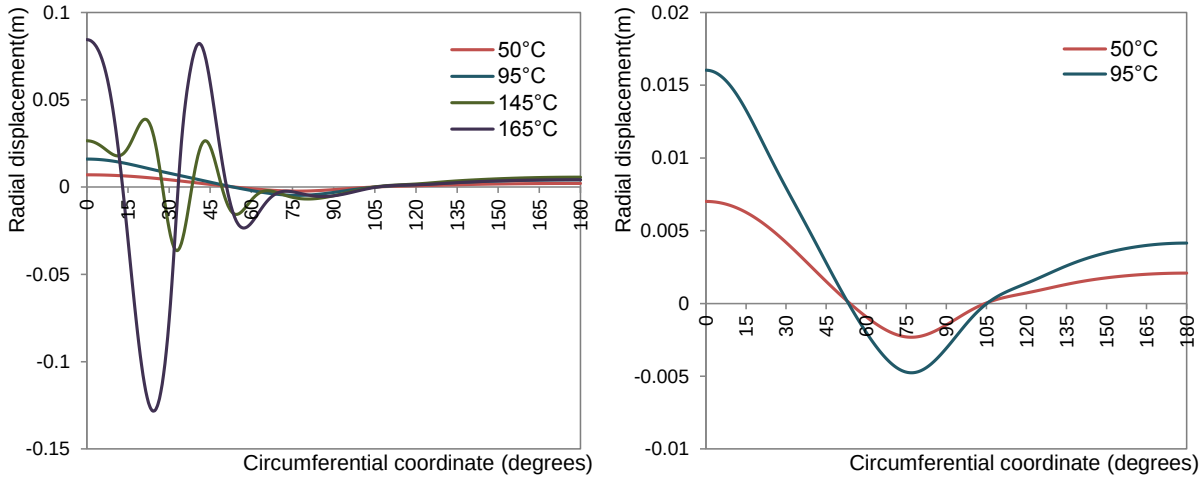

Figure 6-5: Radial displacement around the circumference of cylindrical tank at mid-height (z=10m) for various levels of temperature of most heated generator.

The meridional and circumferential stress patterns around the circumference of the cylindrical tank for different levels of vertical coordinate (z) are depicted in Figure 6-6. During the pre-buckling stage, the meridional stress pattern is the same along the height of the tank. The bigger values are observed in the base (z=2.5m) of the tank due to the restraint of the clamped end and the magnitude of the stresses is reduced away from the base. Moreover, the bigger compression stresses are noted in the most heated generator ($\theta = 0^o$). Near the buckling temperature, the meridional stress pattern around the circumference and along the height of the tank remains the same and the magnitude of the stresses increases as the temperature is escalated. At the post-buckling stage (T=190°C), the stress patterns are more complicated. A detailed description is given in Figure 6-7. The maximum values of compressive meridional stresses appear at z=7.5m and z=15m for $\theta \approx 45^o$ and $\theta \approx 0^o$ respectively. The range of compression and tension zones is continuously modified along the height of the tank. Also it is not that the cold face of the tank ($120^o \le \theta \le 180^o$), remains in compression during the post-buckling stage and the values are relatively small.

The magnitude of circumferential stresses is insignificant during the pre-buckling stage. The bigger compression values are observed near the base of the tank close to the most heated generator, due to the fixed boundary conditions. The stress pattern is altered near the buckling temperature and the stresses become important at the post-buckling stage. Figure 6-8 presents a detailed view of circumferential stress patterns around the circumference of the cylindrical tank at different levels of vertical coordinate (z) for T=190°C. It can be seen that the maximum negative values are reported at z=7.5m. z=12.5 and z=15m for $\theta \approx 45^o$, $\theta \approx 22.5^o$ and $\theta \approx 0^o$ respectively. The most important compression forces take place in the range of $0^o \le \theta \le 60^o$ for all the rings. The circumferential stresses are trivial in the cold face of the tank ($90^o \le \theta \le 180^o$).

Institutional Repository - Library & Information Centre - University of Thessaly
02/06/2024 20:36:34 EEST - 18.222.76.217

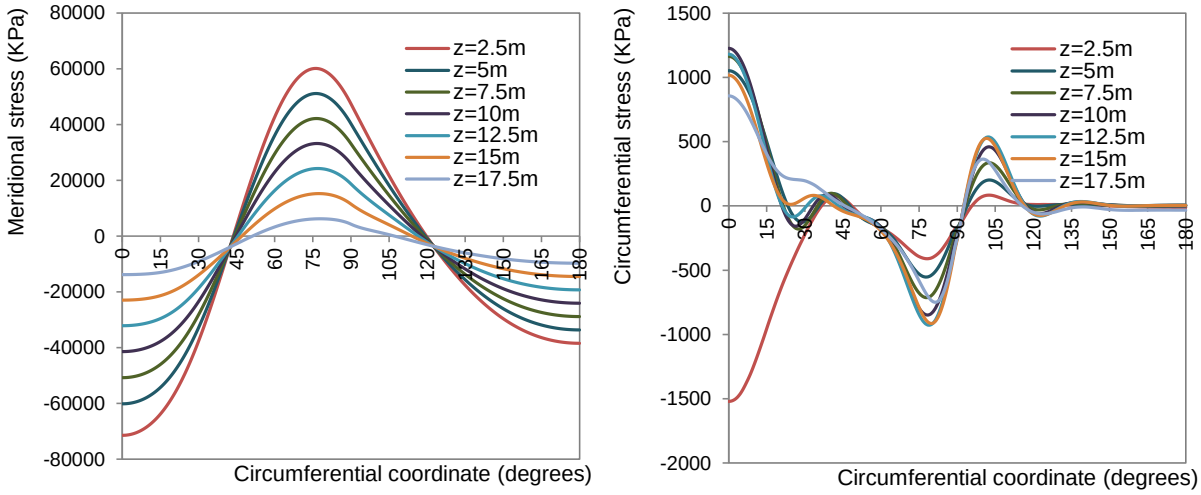

Pre-buckling (T=98°C)

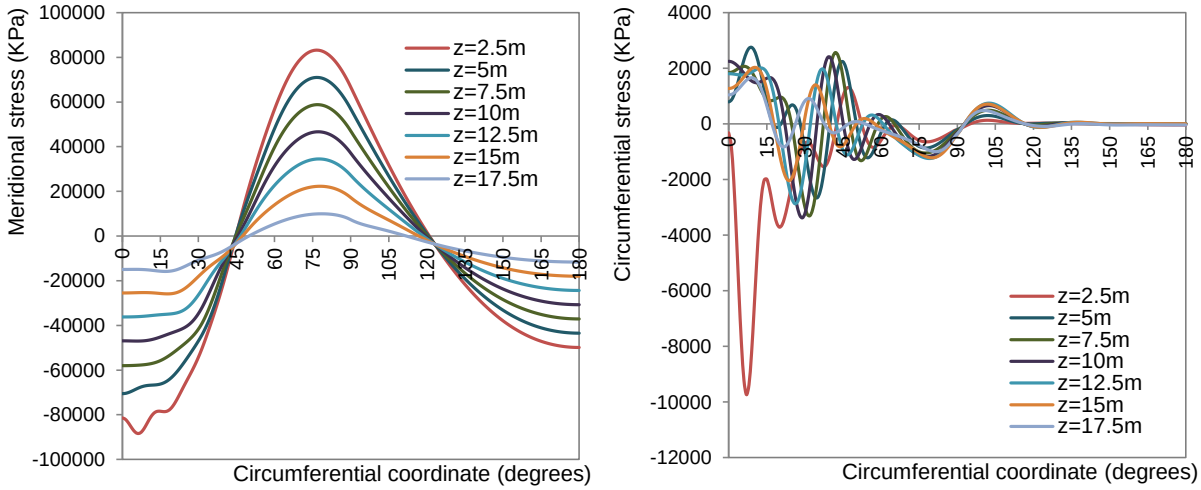

Near-buckling (T=135°C)

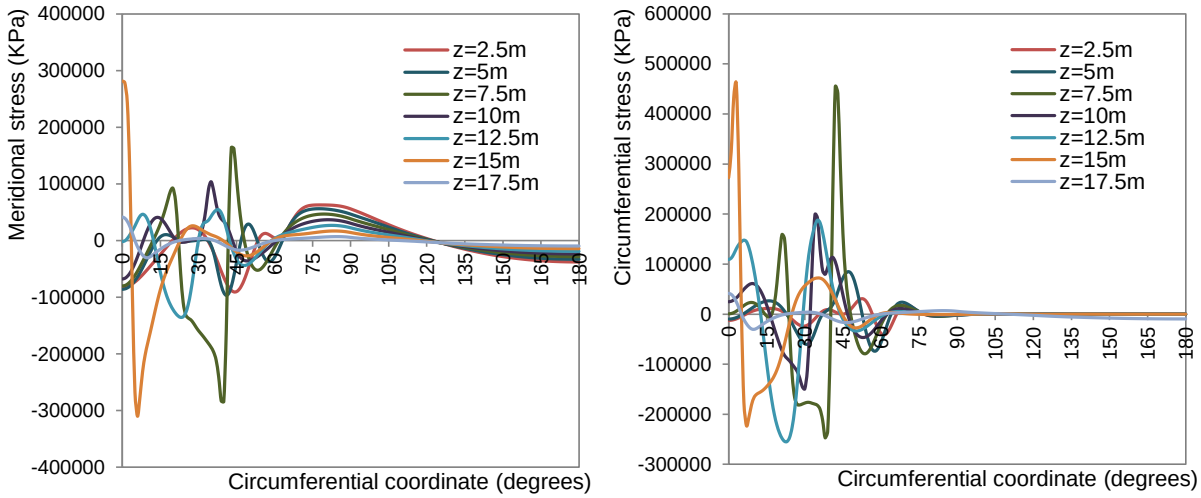

Post-buckling (T=190°C)

Figure 6-6: Stress patterns around the circumference of the cylindrical tank for different levels of vertical coordinate (z).

Institutional Repository - Library & Information Centre - University of Thessaly
02/06/2024 20:36:34 EEST - 18.222.76.217

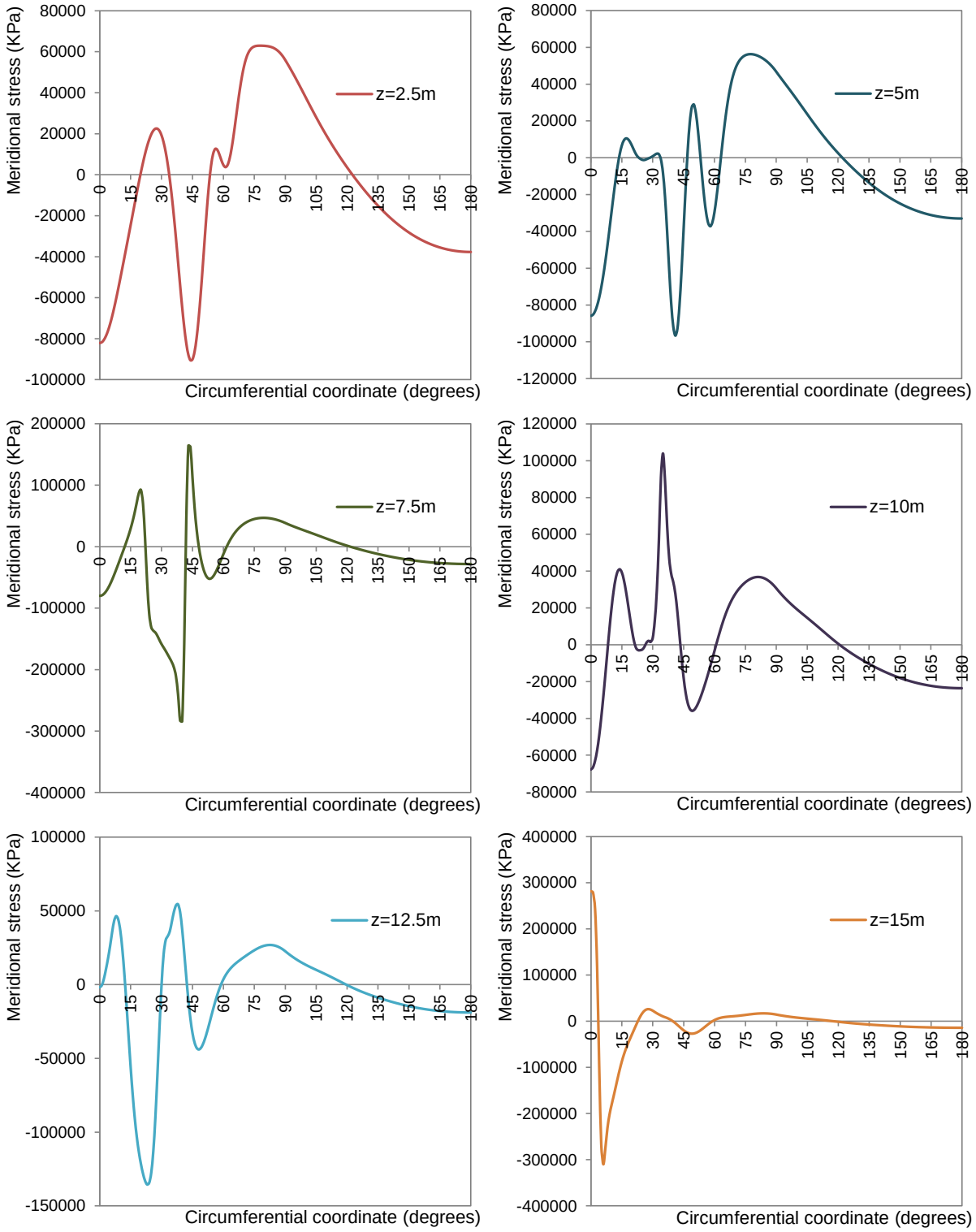

Figure 6-7: Detailed meridional stress patterns around the circumference of the cylindrical tank at different levels of vertical coordinate (z) for T=190°C.

Institutional Repository - Library & Information Centre - University of Thessaly
02/06/2024 20:36:34 EEST - 18.222.76.217

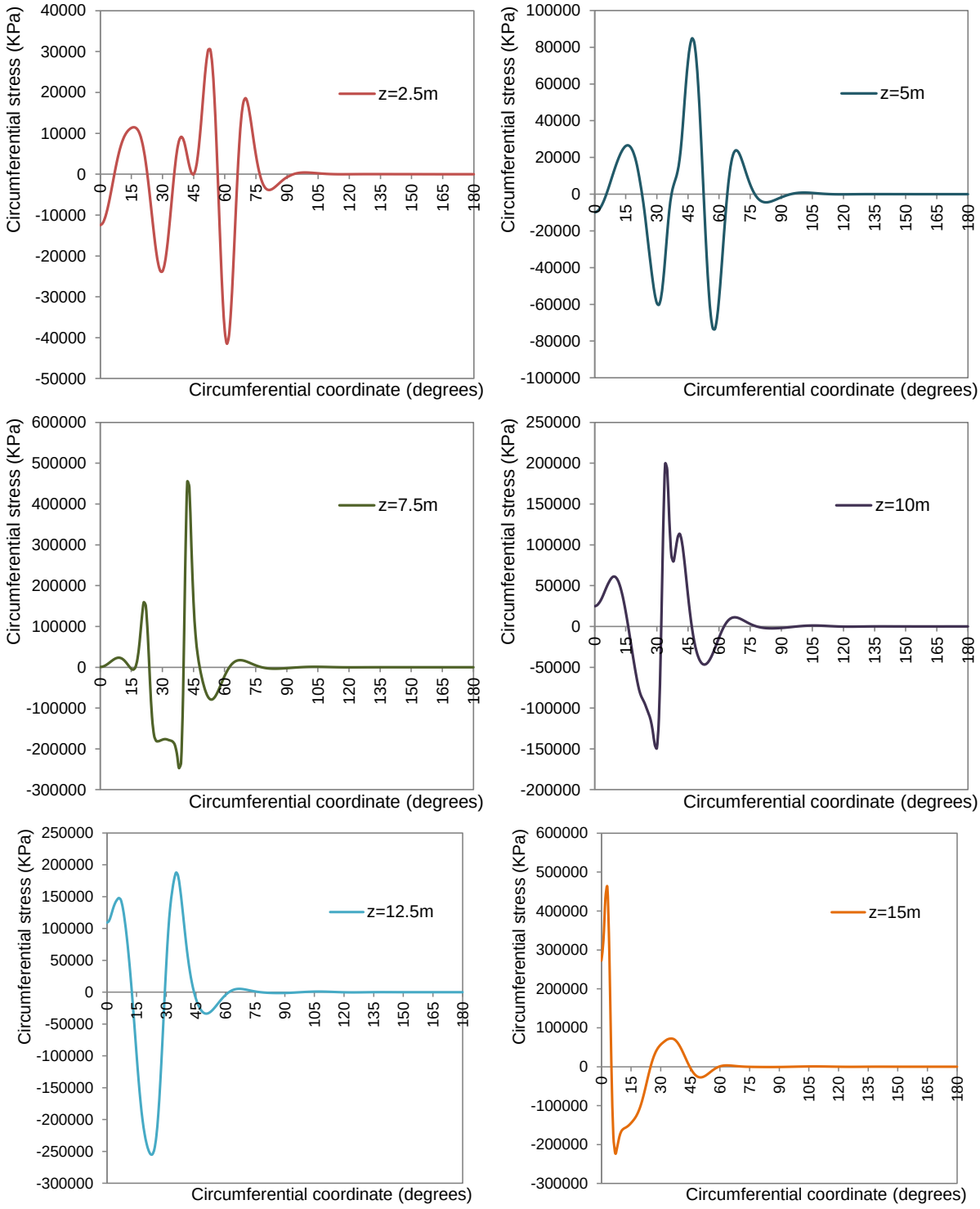

Figure 6-8: Detailed circumferential stress patterns around the circumference of the cylindrical tank at different levels of vertical coordinate (z) for T=190˚C.

The meridional stress pattern along the height of the tank for different heated generators ($\theta = 0^{o}, \theta = 15^{o}, \theta = 30^{o}, \theta = 45^{o}$) of the cylindrical shell and the corresponding distribution of radial displacements are plotted in Figure 6-10. Before buckling and close to the critical temperature, the variation of the meridional stress along the height of the generators is almost linear except the upper and the lower base of the tank. In these zones, large compressive and

Institutional Repository - Library & Information Centre - University of Thessaly
02/06/2024 20:36:34 EEST - 18.222.76.217

tensile stresses are detected locally, due to the constraint provided by the fixed boundary and the roof of the tank respectively. After buckling, the distribution of meridional stresses becomes non-linear and the important compressive forces take place in the body of the cylinder (i.e. far from the upper and lower base of the tank). The maximum values of negative stresses are detected between the generators $\theta = 30^{o}$ and $\theta = 45^{o}$. Regarding the radial displacements, it can be seen that at the post-buckling stage, the maximum values are recorded in a zone upper of the mid-height of the tank for the most heated generator ($\theta = 0^{o}$) and this zone is transferred downwards in the less heated generators i.e. moving from $\theta = 0^{o}$ to $\theta = 45^{o}$.

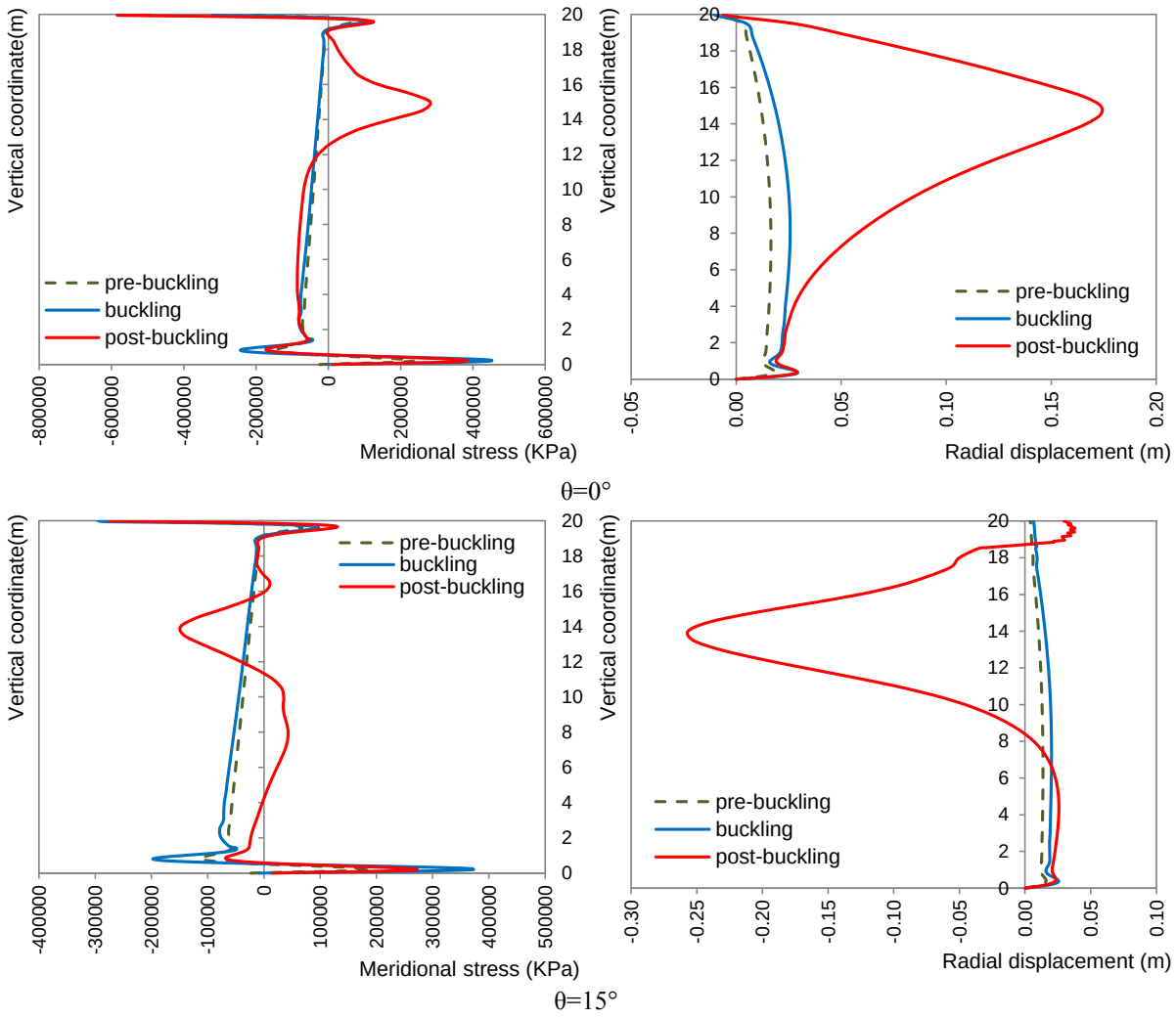

Figure 6-9: Meridional stress and radial displacement along generators of the cylinder in heated zone (θ=0° and 15°).

Institutional Repository - Library & Information Centre - University of Thessaly
02/06/2024 20:36:34 EEST - 18.222.76.217

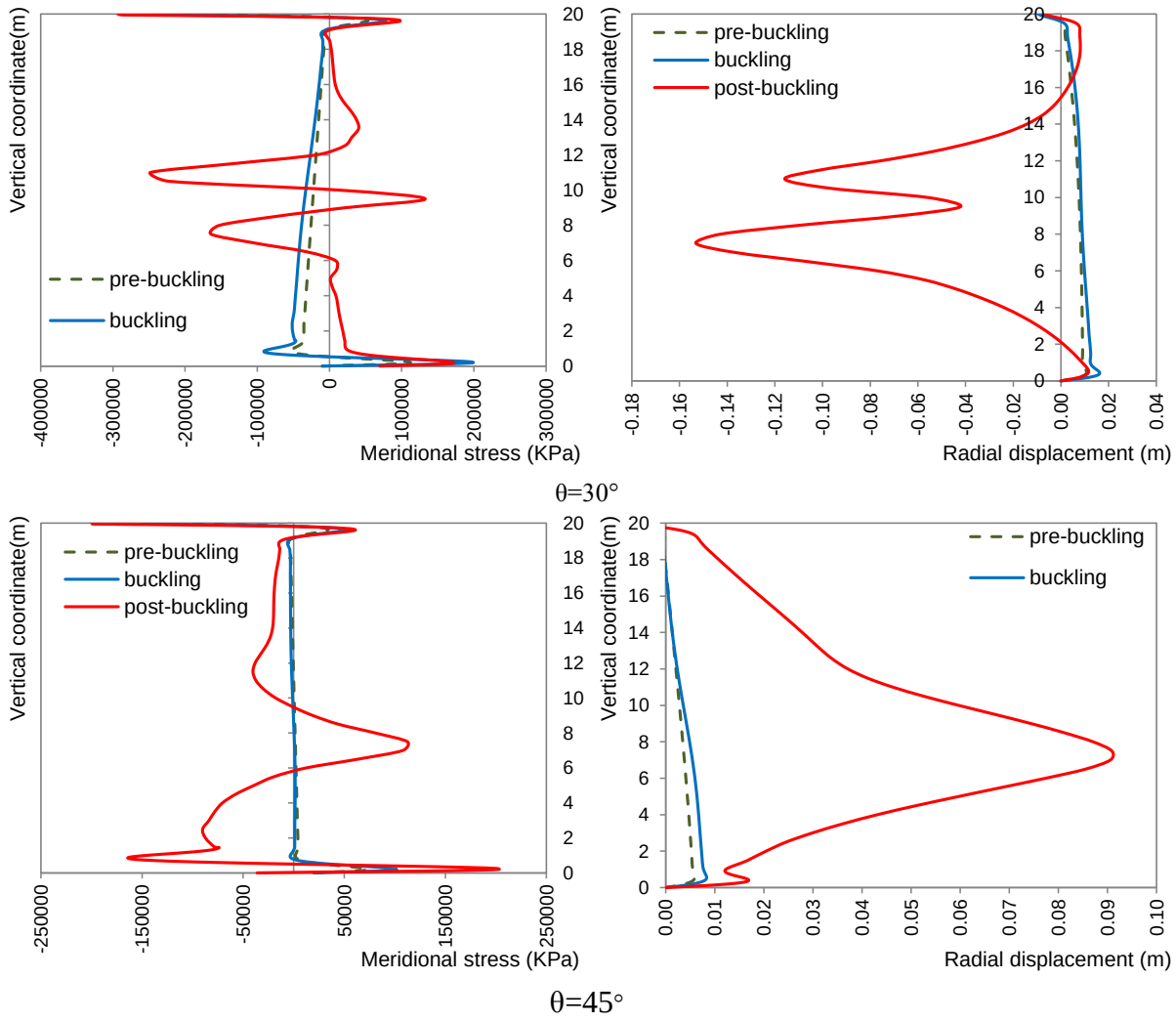

Figure 6-10: Meridional stress and radial displacement along generators of the cylinder in heated zone (θ=30° and 45°).

Figure 6-11 presents the distribution of the shear stress component around the circumference of the cylindrical tank at the mid-height for different levels of temperature of the most heated generator that correspond to the pre-buckling, neat buckling and post-buckling stage. As it can be observed in Figure 6-12 , the distribution of shear stress is almost uniform along the height of the cylinder during at the pre-buckling stage and the maximum values are recorded near the upper and lower base of the cylinder. The shear stresses can be connected to the gradient of temperature around the circumference of the cylinder. The distribution at the mid-height of the tank is antisymmetric with respect to the x-axis, and in half of the heated zone the shear stresses are negative ($0^o \le \theta \le 90^o$) while in the rest zone the values are positive ($270^o \le \theta \le 360^o$). The same holds for the back-clod zone. Considering the heated face, the maximum values are recorded in 45° away from the most heated generator i.e. for $\theta \approx 45^o$ and $\theta \approx -45^o$. It is noted that the shear stresses during the pre-buckling stage are bigger than the respective values of the circumferential stresses and smaller compared with the values of the meridional components. After buckling the shear stress pattern becomes

Institutional Repository - Library & Information Centre - University of Thessaly
02/06/2024 20:36:34 EEST - 18.222.76.217

more complicated as it is depicted in both Figure 6-11 and Figure 6-12.

It can be concluded that the buckling phenomenon can be attributed to both meridional and shear stress that appear in the zone $-45^{o} \le \theta \le +45^{o}$ of the circumference of the cylindrical shell due to restrained thermal expansion at the axial direction and to the gradient of temperature around the circumference of the cylinder. The coexistence of compressive meridional and shear stresses leads to the occurrence of the diagonal buckling mode. The contribution of compressive circumferential stresses seems to be less important.

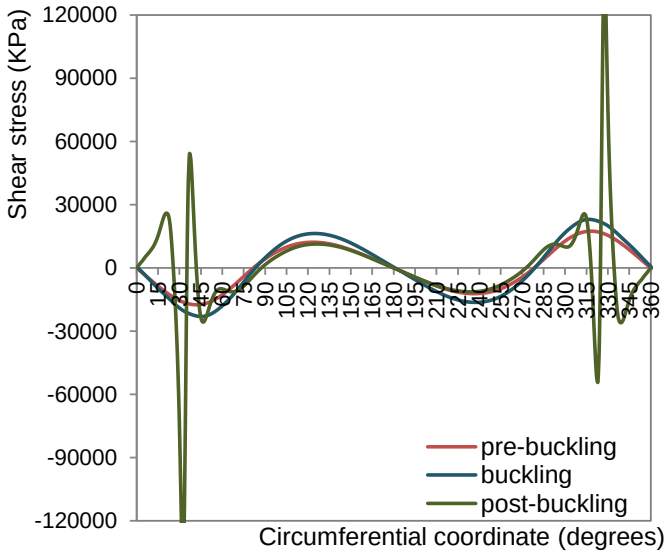

Figure 6-11: Shear stress pattern around the circumference of the cylindrical tank at mid-height (z=10m).

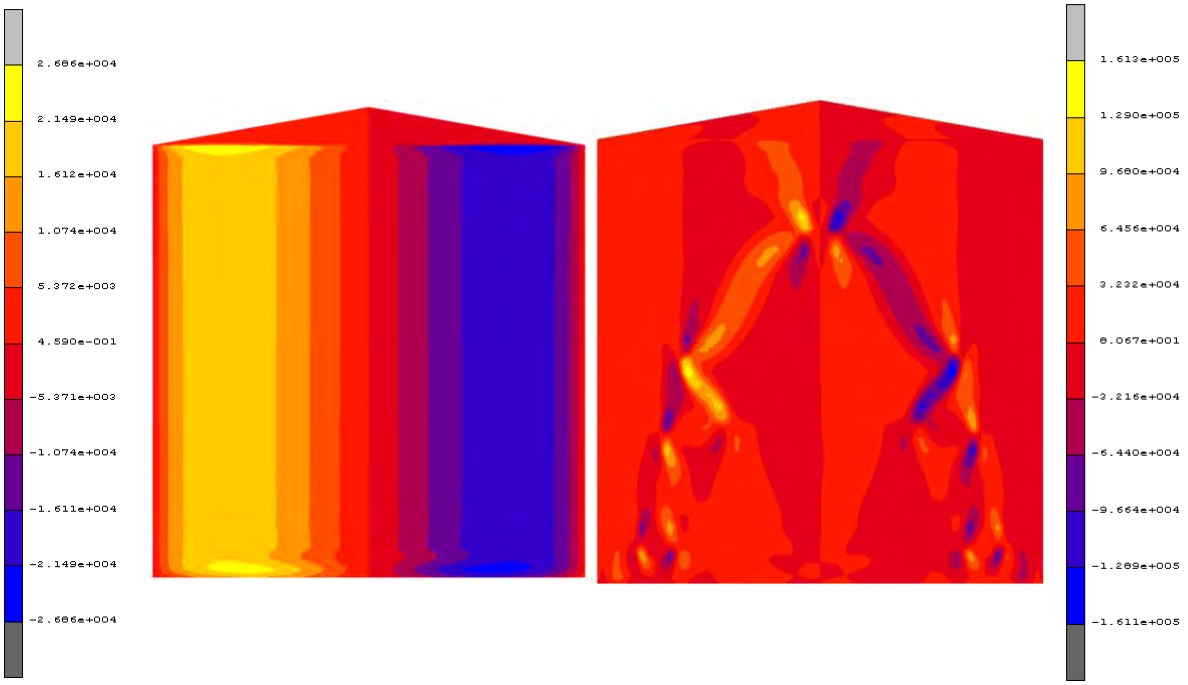

(a) pre- buckling (b) Post-buckling

Figure 6-12: Shear stress distribution in the hated ace of the cylindrical tank.

Institutional Repository - Library & Information Centre - University of Thessaly
02/06/2024 20:36:34 EEST - 18.222.76.217

All, the previous remarks describe in detail the complicated thermal/structural behavior of the cylindrical steel tank and they are in accordance with the deflected configuration of the tank as it is presented in Figure 6-1 and Figure 6-2. Moreover, it is underlined that it is quite difficult to describe the global behavior of the tank due to the multiple local and global buckling phenomena that are detected. The global evaluation of the behavior of the heated tank can be obtained if the artificial damping energy based time stepping scheme is used. Specifically, the evolution of the ratio of artificial damping energy to the total strain energy of the system with the temperature depicts accurately the occurrence of buckling phenomena. Figure 6-13 presents the temperature evolution of the energy dissipation fraction. It can be observed that initially, the value of the fraction is set 0.1 and in the sequel the magnitude of the fraction decreases as the temperature increases, if no instability occurs. For temperature equal to 145°C, a sudden jump takes place and this indicates the occurrence of the global buckling. In the sequel, the magnitude of the fraction is reduced since and this branch corresponds to the post-buckling stage. For T=190°C, a new jump occurs due to the occurrence of the local buckling in zone C as it is illustrated in Figure 6-3. The sequence of buckling phenomena is as they are defined in the curve of the temperature evolution of the energy dissipation fraction (1), (2) and (3) correspond to the deformed configurations of the cylindrical tank as they are illustrated in Figure 6-1a, Figure 6-1b and Figure 6-1c respectively. It is noted that the jump amplitude depends on the range of the buckling area. A global buckling instability corresponds to larger jump comparing with a local bucking phenomenon. For this reason the first jump in the diagram between points 1 and 2 is considerably larger than the second jump. Moreover, it is observed that the fraction of the artificial damping energy of the system presents the vertical braches in the case where the velocities of the nodes are coming important (in the case of static loading the velocities are minor and this is a basic separation between static and dynamic problems). Actually in this mathematical scheme, the nodal velocities are calculated (which may or may not have a physical meaning in the context of the problem being solved) and the artificial damping energy becomes considerable if the magnitude of velocities is important i.e. the buckling is instantaneous. For this reason in the post-buckling branch of the diagram (2 up to 3) although the buckling regions are spreading out, no sudden jumps ae taking place.

Institutional Repository - Library & Information Centre - University of Thessaly
02/06/2024 20:36:34 EEST - 18.222.76.217

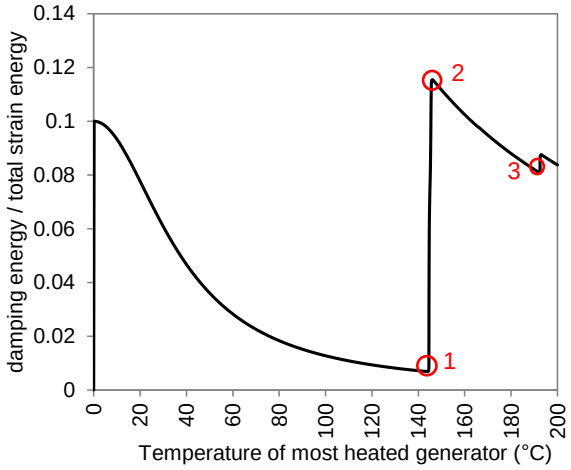

Figure 6-13: Evolution of ratio of artificial damping energy to the total strain energy with temperature ($t_r = 10t_c$).

The advantage of using artificial damping scheme is more obvious in modelling the cases that involve multiple occurrences of buckling along the thermal loading path. Such a situation is typical in the thermal buckling of tanks with slender roof (e.g. $t_r = t_c$) where the tank roof often buckles before the tank wall. This case is presented in Figure 6-14 and the corresponding deformed shapes of the cylindrical tank are illustrated in Figure 6-15. In this case of slender roof, the first instability that occurs is the buckling of the roof (point 1) and the second jump corresponds to the buckling of the cylindrical shell (point 2).

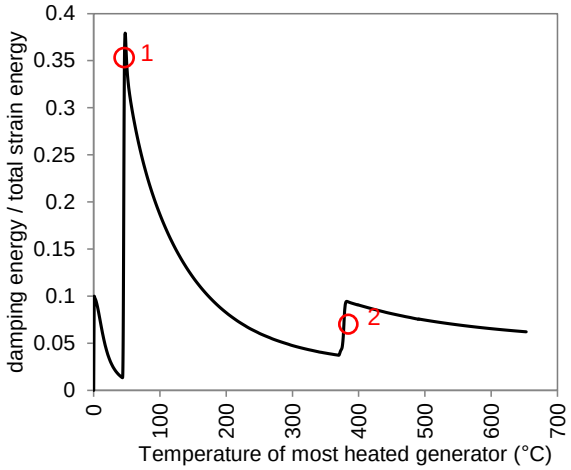

Figure 6-14: Evolution of ratio of artificial damping energy to the total strain energy with temperature ($t_r = t_c$).

(a) Point 1 (b) Point 2

Figure 6-15: The deformed shape of the cylindrical tank at characteristic levels of temperature for the slender roof case ($t_r = t_c$).

Institutional Repository - Library & Information Centre - University of Thessaly
02/06/2024 20:36:34 EEST - 18.222.76.217

Effect of roof stiffness to the structural behavior of fixed roof heated tank

The failure modes of the heated cylindrical tank and the corresponding radial displacement field, for different values of roof thickness, are presented in Figure 6-16, Figure 6-17Figure 6-18. Two different modes are observed. In the case where the roof is slender ($t_r = t_c$ and $t_r = 1.5t_c$), the roof of the tank buckles. This failure mode is altered for thicker roofs ($t_r > 2t_c$) and the buckling of the cylindrical wall takes place. It is observed that the buckling mode of the tank wall is very sensitive to the ration of roof thickness to the tank wall thickness. In case of restively stiff roofs the final mode may be either shear-diagonal global buckling e.g. (Figure 6-16c) or local buckling which occurs near the boundaries where large meridional, circumferential and shear membrane stresses are present (e.g. Figure 6-18).

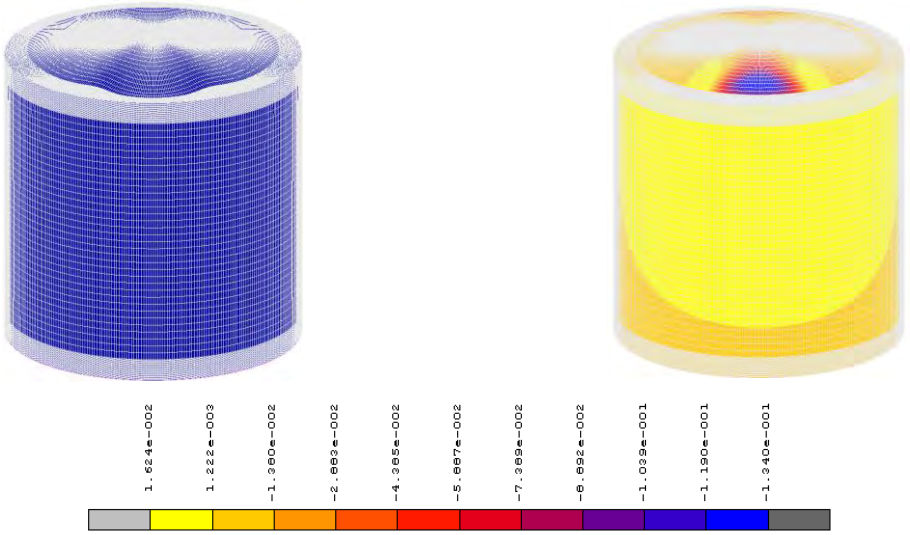

(a) $t_r = t_c$

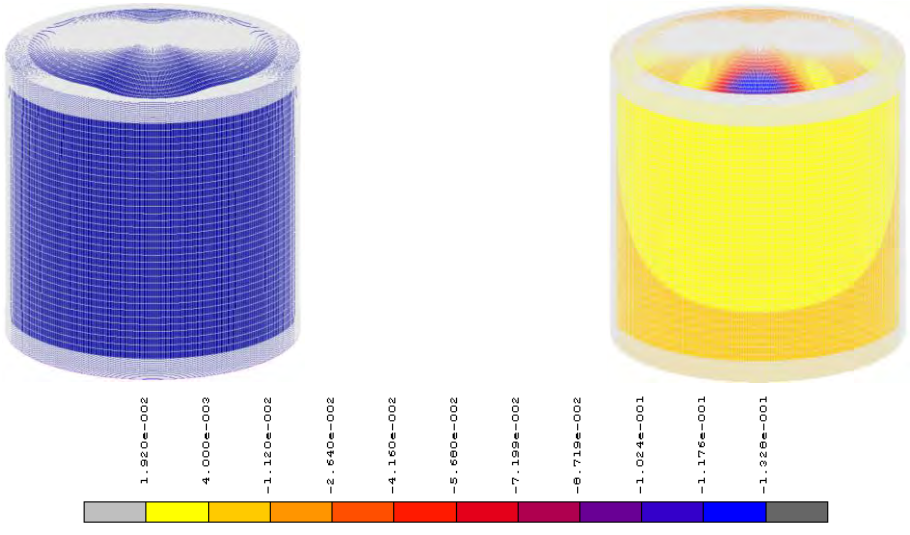

(b) $t_r = 1.5t_c$

Figure 6-16: Failure modes of the heated tank and the corresponding radial displacement field for roof thickness $t_r = t_c$ and $t_r = 1.5t_c$.

Institutional Repository - Library & Information Centre - University of Thessaly
02/06/2024 20:36:34 EEST - 18.222.76.217

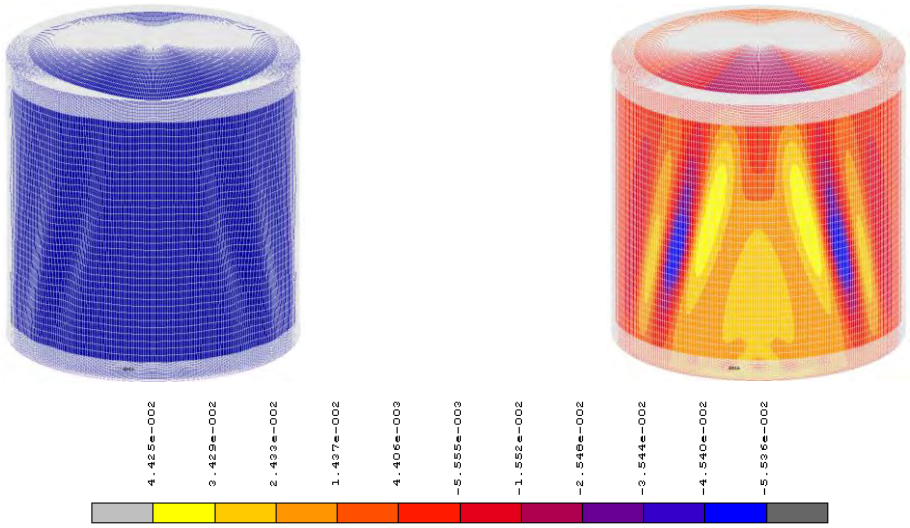

(c) $t_r = 2t_c$

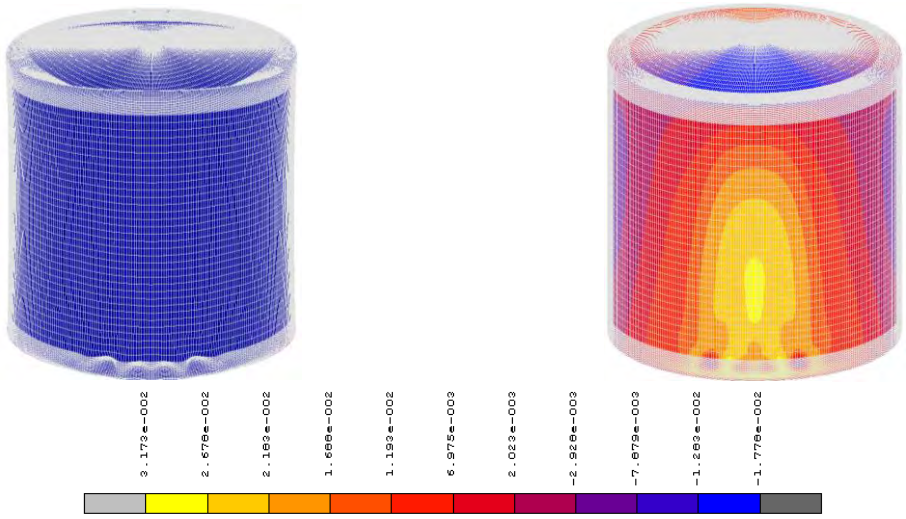

(a) $t_r = 3t_c$

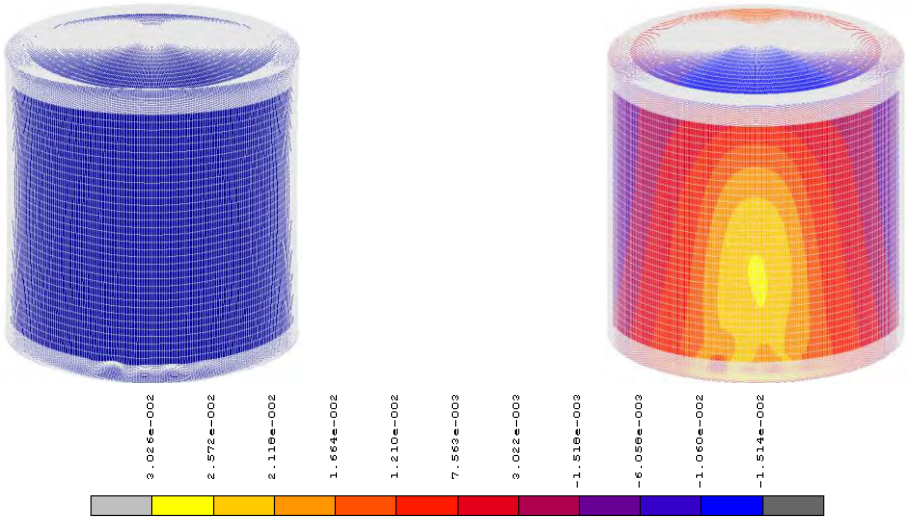

(b) $t_r = 5t_c$

Figure 6-17: Failure modes of the heated tank and the corresponding radial displacement field for roof thickness $t_r = 2t_c$, $t_r = 3t_c$ and $t_r = 5t_c$.

Institutional Repository - Library & Information Centre - University of Thessaly
02/06/2024 20:36:34 EEST - 18.222.76.217

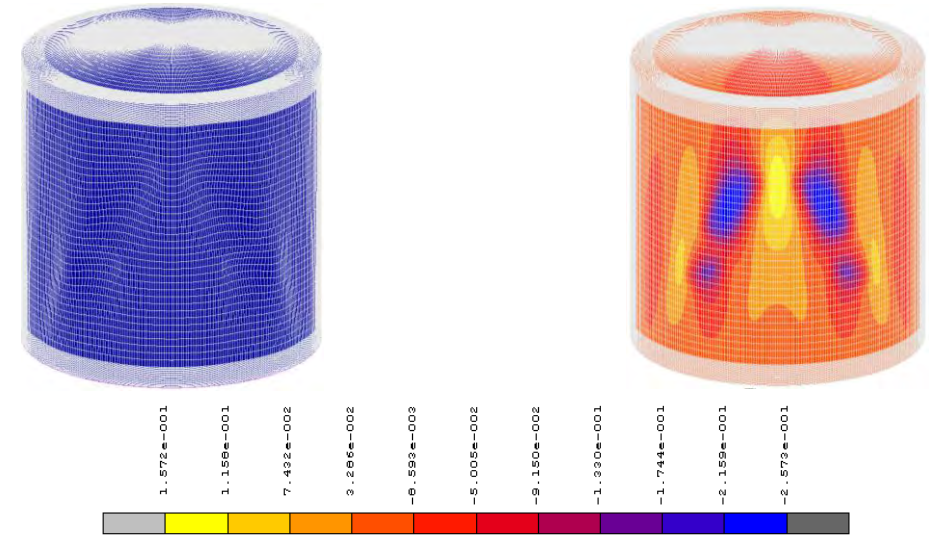

(c) $t_r = 10t_c$

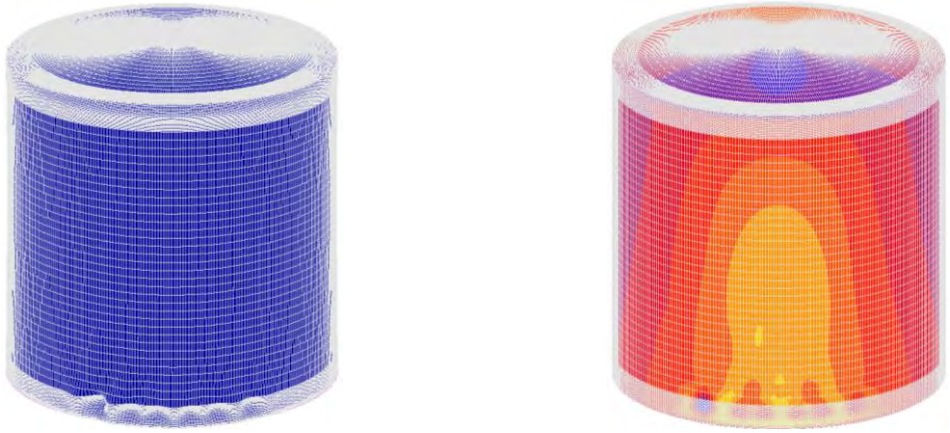

$t_r = 100t_c$

Figure 6-18: Failure modes of the heated tank and the corresponding radial displacement field for roof thickness $t_r = 10t_c$ and $t_r = 100t_c$.

Figure 6-19 presents the evolution of the critical buckling temperature of the heated fixed-roof tank as the ratio of roof thickness to cylindrical shell thickness increases. Two different branches are detected. In the ascending branch, as the thickness of roof increases, the buckling temperature is also accordingly escalated and this holds for $t_c \le t_r \le 2t_c$ i.e. the stiffer roof buckles for higher level of temperature. It is noted that in the case of very slender roofs e.g. $t_r = t_c$ the roof of the tank buckles at extremely low temperature less than 40°C. The peak point is recorded for the case of $t_r = 2t_c$ where the critical buckling temperature is equal to 164°C. In the descending branch $2t_c \le t_r \le 100t_c$, as the thickness of roof increases the buckling temperature is decreased. This can be attributed to the fact that the thicker roof is actually stiffer and subsequently the degree of restraint at the upper base of the tank increases and bigger axial membrane stresses are induced in the cylindrical wall due to the restraint to

Institutional Repository - Library & Information Centre - University of Thessaly
02/06/2024 20:36:34 EEST - 18.222.76.217

differential thermal expansion. The decrease of the critical buckling temperature in the extreme case where $t_r = 100t_c$ is 39% comparing with the pick value that correspond to the case where $t_r = 2t_c$. The previous indicate that the roof stiffness is a crucial parameter for the fire behavior of the cylindrical tank.

Due to the fact that the cylindrical wall buckling is expected to result in more serious consequences during a pool fire, comparing with the roof buckling, the interest in this study is mainly focused on the cases that lie in the descending branch of the curve presented in Figure 6-19. A more detailed view of the problem can be obtained from the stress patterns in the wall of the tank. Figure 6-20 presents the axial and circumferential stress patterns around the circumference of the cylindrical tank in two different rings (z=1m and z=10m) at the pre-buckling stage as the ratio of the roof thickness to the wall thickness increases. Near the base of the tank (z=1m), the magnitude of the meridional stresses is important for all the cases that are studied here. The maximum values appear in the case of $t_r = 100t_c$ .A logical sequence is noted and the magnitude of stresses is escalated as the thickness of the roof increases. During the post-buckling stage, higher values of both membrane stresses occur near the lower base of the tank for all the case studies. Moreover, the circumferential stresses are important at near the fixed end and minor in the body of the tank. The meridional stress distributions along the height of the tank for the most heated generator and for various values of ratio of roof thicknesses to cylinder shell thickness are presented in Figure 6-21. It is observed that in the body of the cylindrical shell ($2.5 \le z \le 17.5$) the most heated generator is in compression, while the significant values of meridional stress (both positive and negative) are recorded at the upper and lower end of the cylindrical shell (Figure 6-22). The stress concentration at the boundaries is a local phenomenon and it is attributed to the restraint due to the clamped end conditions and to the restraints that are induced due to the presence of the fixed roof. Moreover, the magnitude of shear stresses (Figure 6-23) increases as the shell of the roof becomes thicker.

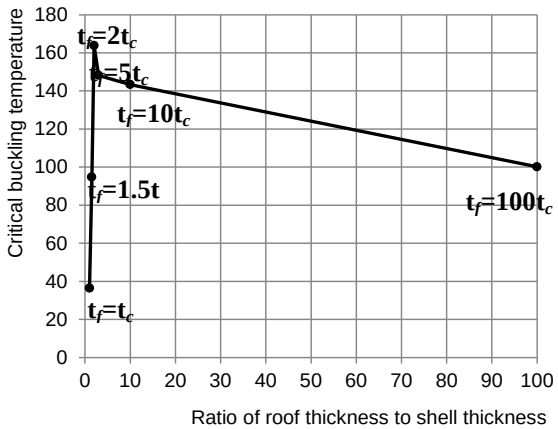

Figure 6-19: Critical buckling temperature for empty fixed-roof cylindrical tank for different roof thickness.

Institutional Repository - Library & Information Centre - University of Thessaly
02/06/2024 20:36:34 EEST - 18.222.76.217

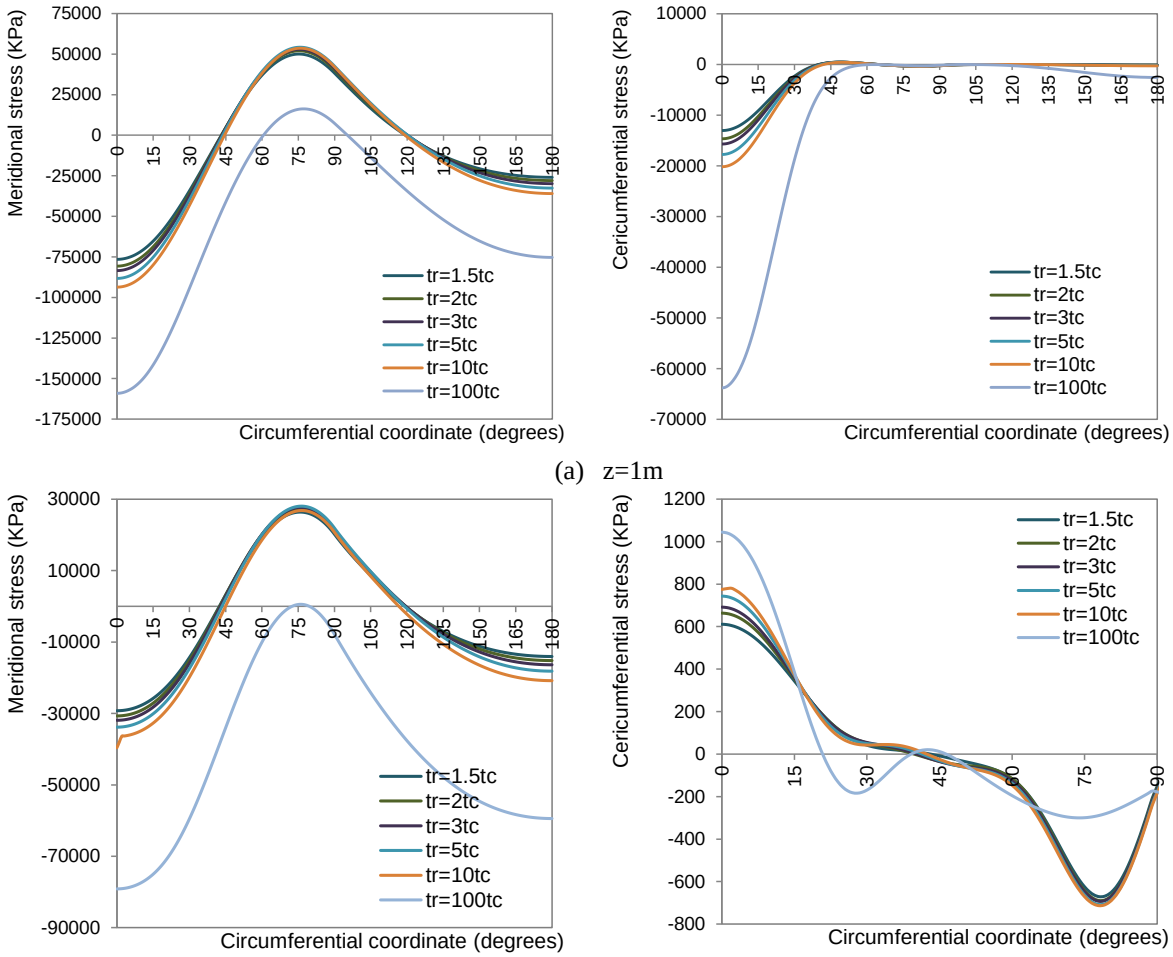

(a) z=1m

(b) z=10m

Figure 6-20: Stress patterns around the circumference of the cylindrical tank before buckling (T=80°C) for various roof thickness.

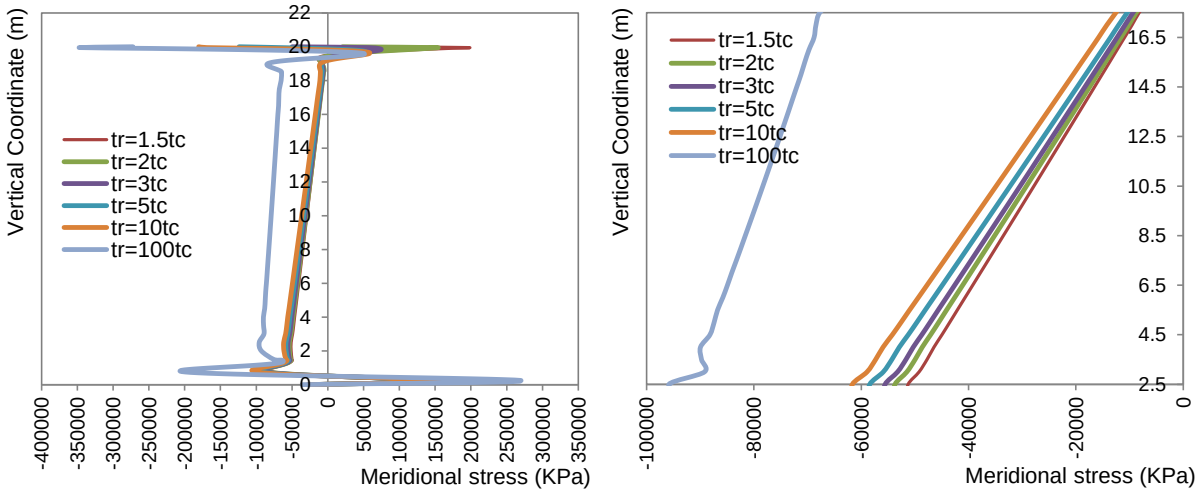

(a) total diagram

(b) detailed diagram for $2.5 \le z \le 17.5$

Figure 6-21: Meridional stress distribution along the height of the cylindrical tank for the most heated generator for various values of roof thickness (pre-buckling stage, T=80°C).

Institutional Repository - Library & Information Centre - University of Thessaly
02/06/2024 20:36:34 EEST - 18.222.76.217

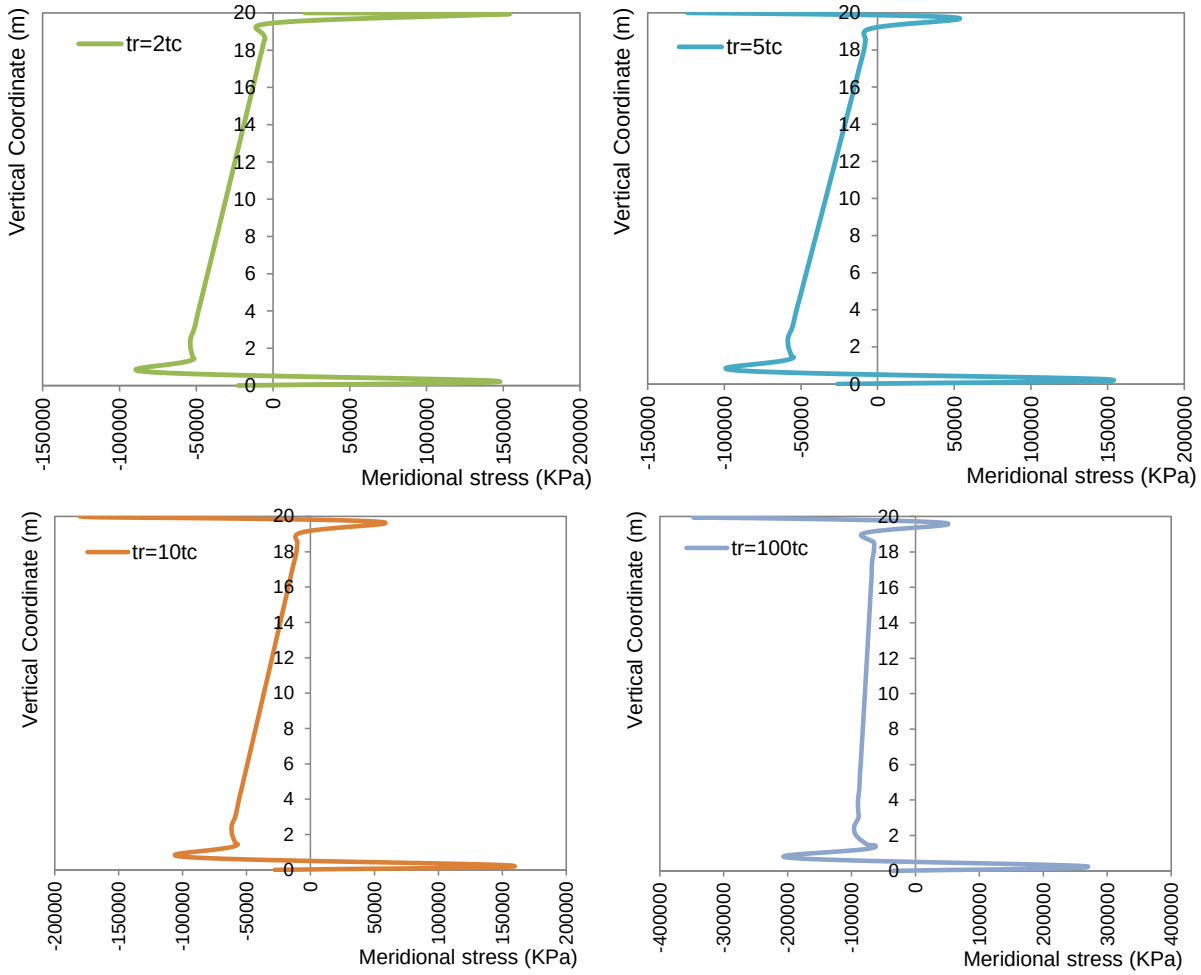

Figure 6-22: Meridional stress distribution along the height of the cylindrical tank for the most heated generator for roof thickness $t_r = 2t_c$, $t_r = 5t_c$, $t_r = 10t_c$ and $t_r = 100t_c$ (pre- buckling stage ,T=80°C).

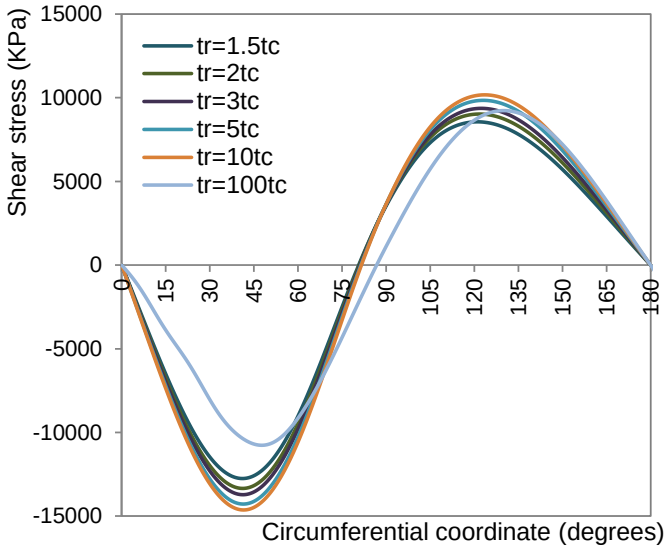

Figure 6-23: Shear stress pattern around the circumference of the cylindrical tank before buckling (T=80°C) for various roof thickness (z=10m).

Institutional Repository - Library & Information Centre - University of Thessaly
02/06/2024 20:36:34 EEST - 18.222.76.217

Effect of thermal roof pattern to the thermal behavior of the fixed roof tank

In the case where the "hot" roof thermal pattern is adopted, the behavior of the tank is similar comparing with the case of the cool roof. Figure 6-24 presents the evolution of the critical buckling temperature as the roof thickness increases, for the case where the "hot" roof is included in the analysis. The results concerning the "cool" roof are also quoted in the same Figure. In can be observed that the critical buckling temperature for the "hot" roof scheme is very close comparing to the case where the "cool" roof is used. Specifically, the buckling temperature for the "hot" roof is slightly increased with respect to the "cool" roof case. Actually, for the same roof thickness, the "hot" roof is less stiff with respect to the "cool" roof since the modulus of elasticity of steel reduces at elevated temperatures. This indicates that the "hot" roof induces lower degree of restraint to the tank, with respect to the cold roof and subsequently the degree of restraint at the upper base of the tank decreases and reduced axial membrane stresses are induced in the cylindrical wall due to the restraint to thermal expansion. The previous indicate that the fire behavior of the cylindrical tank is insensitive to the specific parameter and that the "hot" scheme can be omitted from the numerical analyses.

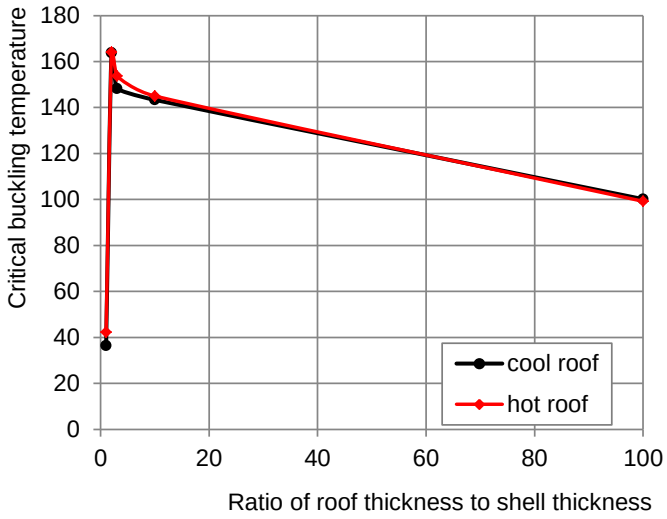

Figure 6-24: Evolution of critical buckling temperature with the ratio of roof thickness to cylindrical shell thickness, for both hot and cool roof schemes.

6.3 Evaluation of the thermal behavior of heated tank through GMNA

In this section, the elastic-plastic material law is implemented in the numerical model. The goal is to reveal the effect of plasticity to the thermal buckling phenomena that arise as the temperature of the tank increases. First, a sensitivity study is conducted, with respect to the roof stiffness i.e. for escalated roof to cylindrical wall thickness considering elastoplastic behavior (S275). In the sequel, the effect of the magnitude of yield strength of steel in studied.

Effect of roof stiffness to the structural behavior of the fixed-roof heated tank

Figure 6-25 presents the evolution of the critical buckling temperature with the ratio of roof to

Institutional Repository - Library & Information Centre - University of Thessaly
02/06/2024 20:36:34 EEST - 18.222.76.217

cylindrical shell thickness. In all cases the "cool" roof pattern is adopted and the tank is supposed to be empty. The results, in terms of critical buckling temperature are compared with the corresponding values for the elastic model and the diagram includes the respective values for the elastic tank. The response of the elastic-plastic heated tank follows the corresponding behavior of the elastic tank, in terms of critical buckling temperature. Two different branches can be detected and the limit point for the elastic-plastic tank is the case of $t_r = 2.5t_c$. In the ascending branch, the failure mode is dominated from the roof buckling values of roof thickness $t_c \le t_r \le 1.5t_c$ while for thicker roofs ($1.5t_c < t_r \le 2.5t_c$) the tank wall buckling takes place. The same failure mode (cylinder wall buckling) is detected also in the descending branch of the curve. The final failure modes are included in Figure 6-26 (T=400°C). Moreover it is observed that for slender roof tanks ($t_c \le\le t_r \le 1.5t_c$) the buckling temperature of the elastoplastic tank is higher than the corresponding values that arise from the GNA analysis. For more stiff roofs ($2.5 \le t_r \le 100t_c$) the phenomenon is reversed and the predicted buckling temperature is lower for the cases where the elastoplastic law of steel is adopted in the analyses. The previous indicate that the elastoplastic material law should be taken into account for the evaluation of the behavior of steel tanks under fire conditions.

The evolution of the dissipated energy fraction with temperature for different escalated values of roof to cylindrical shell thickness is also presented in Figure 6-25. It can be observed that the maximum jump is detected for the case where the roof buckling takes place ($t_r = 1.5t_c$). In this actually a global buckling roof mode is detected, while in the rest cases where the buckling takes place in the wall of the cylinder, the buckling mode is local and it is appears in the base of the tank in the hated face of the tank, for $-30^o \le \theta \le +30^o$ as it is illustrated in Figure 6-27.

Institutional Repository - Library & Information Centre - University of Thessaly
02/06/2024 20:36:34 EEST - 18.222.76.217

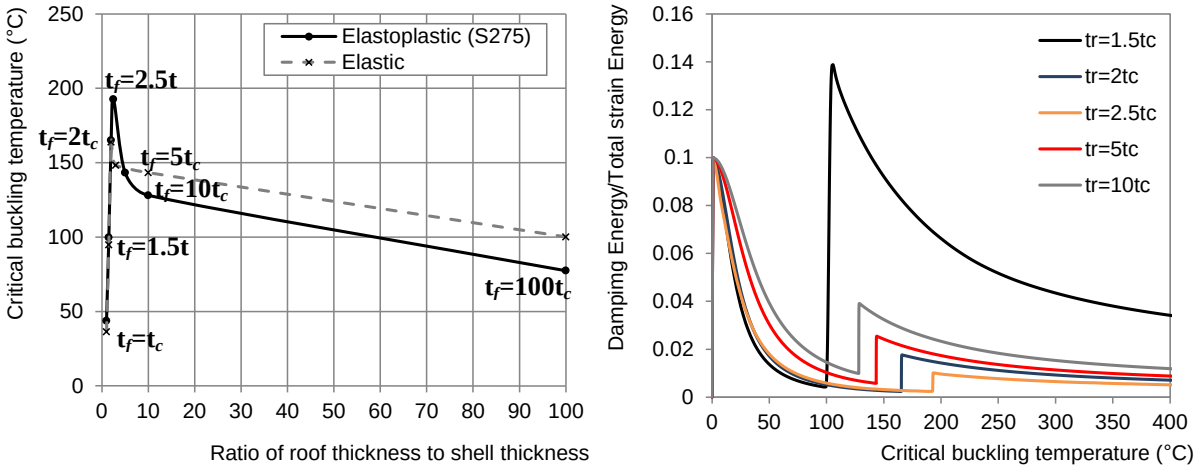

Figure 6-25: Critical buckling temperature for the heated tank for escalated roof stiffness and the corresponding curves of evolution of energy dissipation fraction with the temperature.

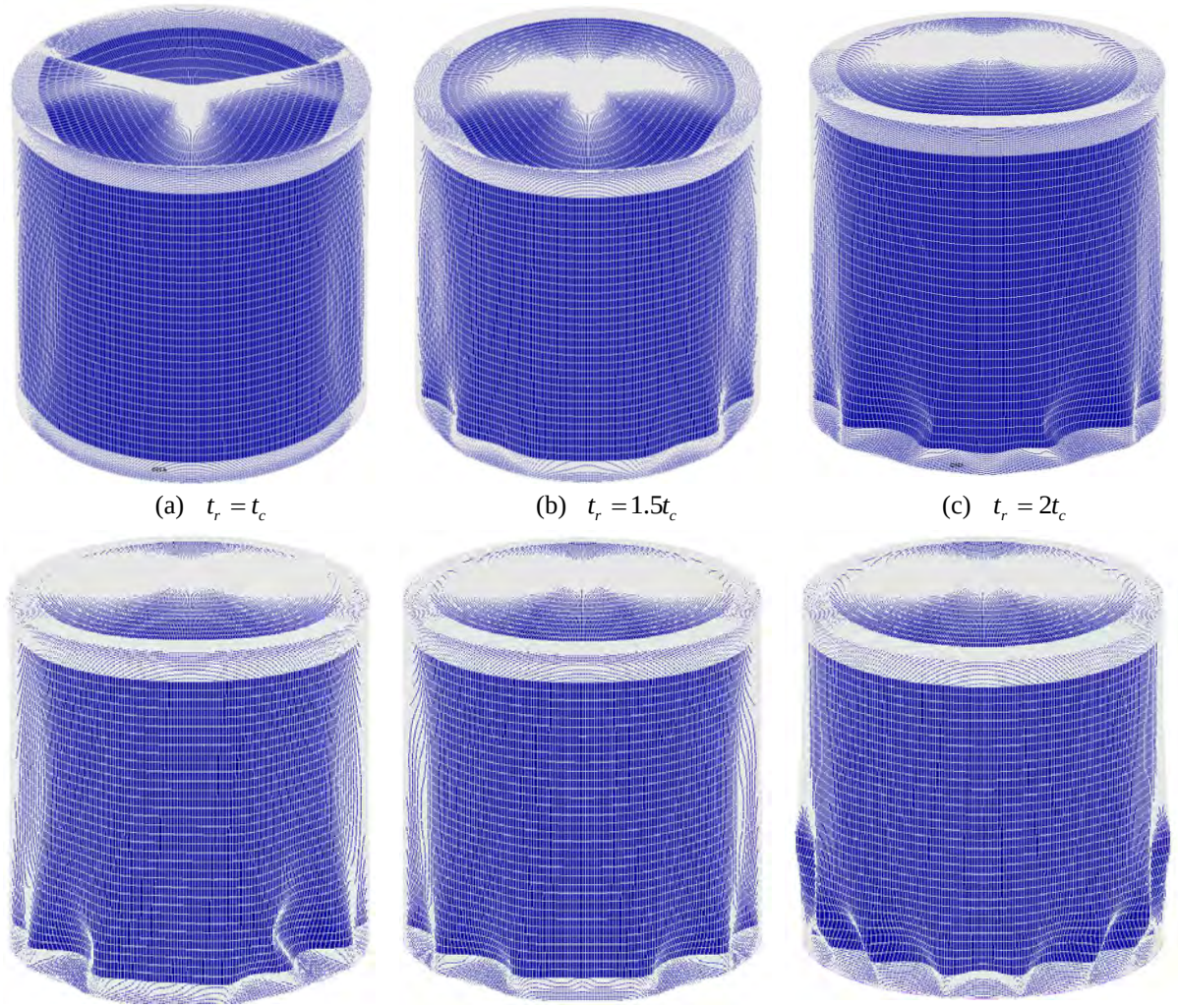

(a) $t_r = t_c$ (b) $t_r = 1.5t_c$ (c) $t_r = 2t_c$

(d) $t_r = 2.5t_c$ (e) $t_r = 10t_c$ (f) $t_r = 100t_c$

Figure 6-26: Deformed shape of the heated tank for escalated values of roof stiffness.

Institutional Repository - Library & Information Centre - University of Thessaly
02/06/2024 20:36:34 EEST - 18.222.76.217

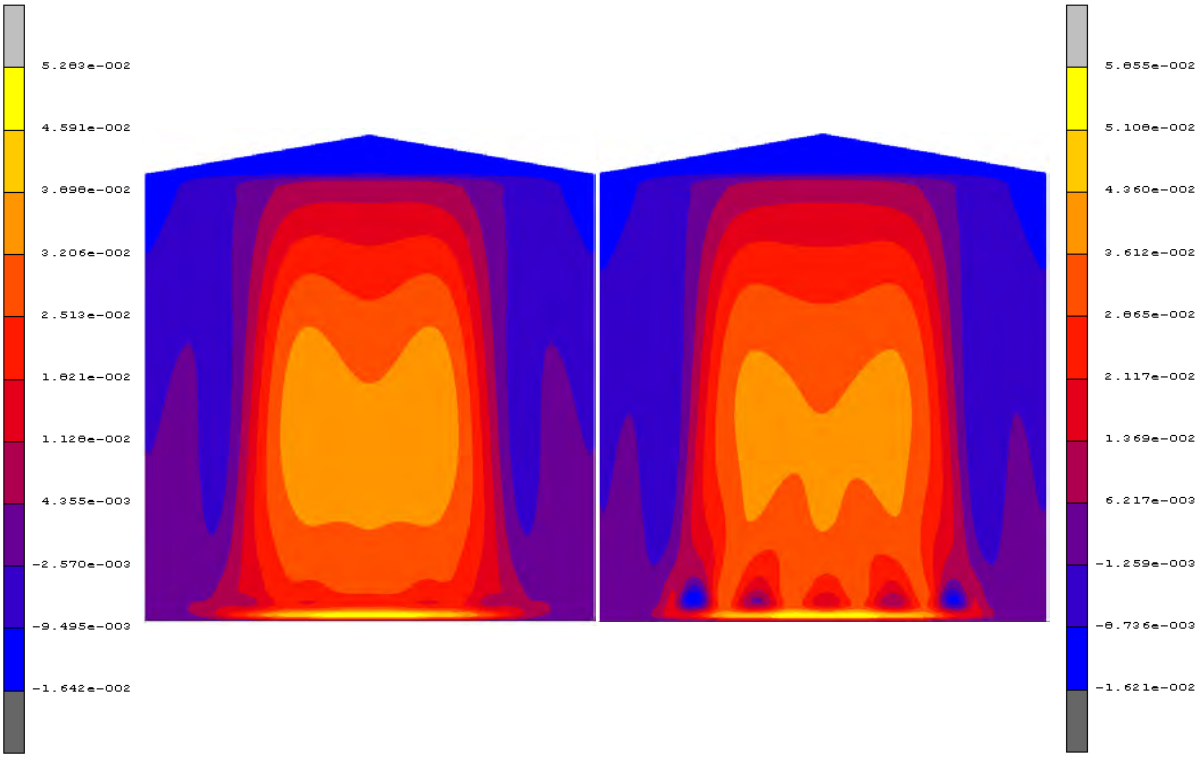

(a) Pre-buckling stage (T= 178°C) (b) Near buckling (T= 193°C)

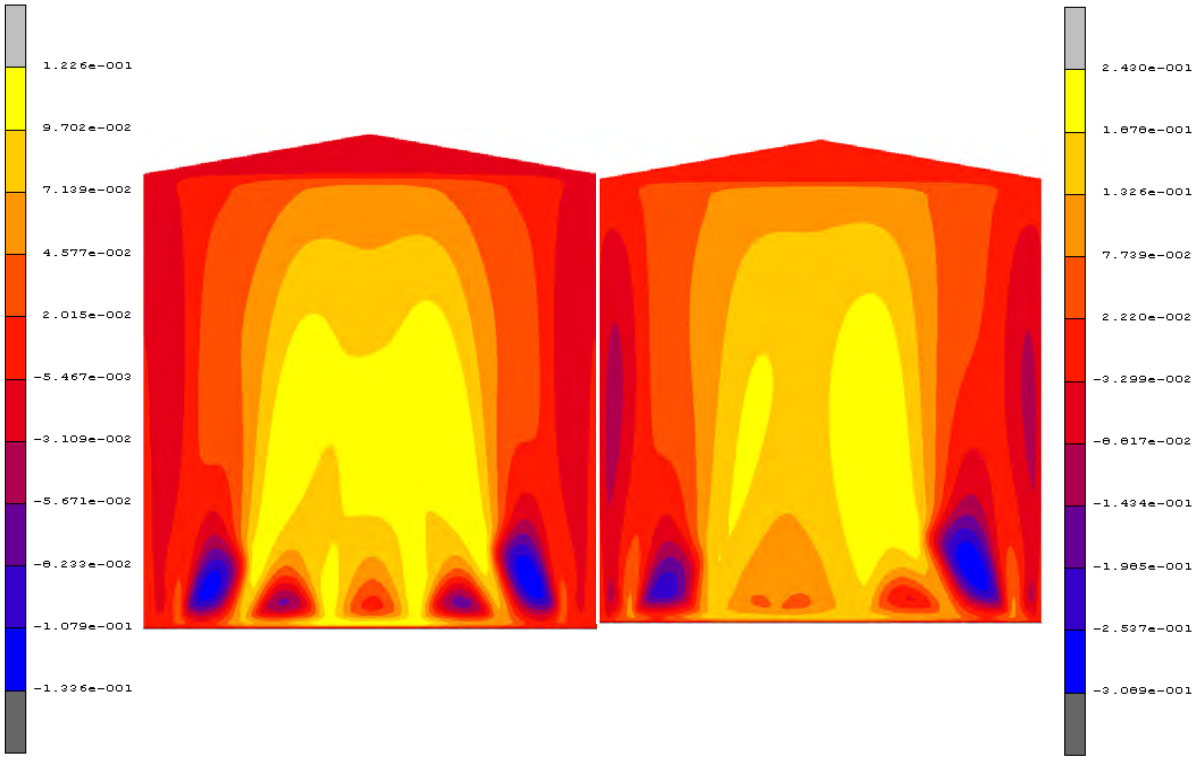

(c) Post-buckling stage (T= 450°C) (d) Post-buckling stage (T= 800°C)

Figure 6-27: Deformed configuration of the tank ($t_r = 2.5t_c$) for different levels of temperature of most heated generator.

The radial displacement fields for various values of roof to cylindrical shell thickness are

Institutional Repository - Library & Information Centre - University of Thessaly
02/06/2024 20:36:34 EEST - 18.222.76.217

presented in Figure 6-28. In all the cases included in this figure the temperature of the most heated generator is T=400°C. It can be observed that as the stiffness of the roof increases, the magnitude of the radial displacements is escalated and furthermore, the buckles near the lower base of the tank are growing and the phenomenon spreads in heated region far away from the most heated generator.

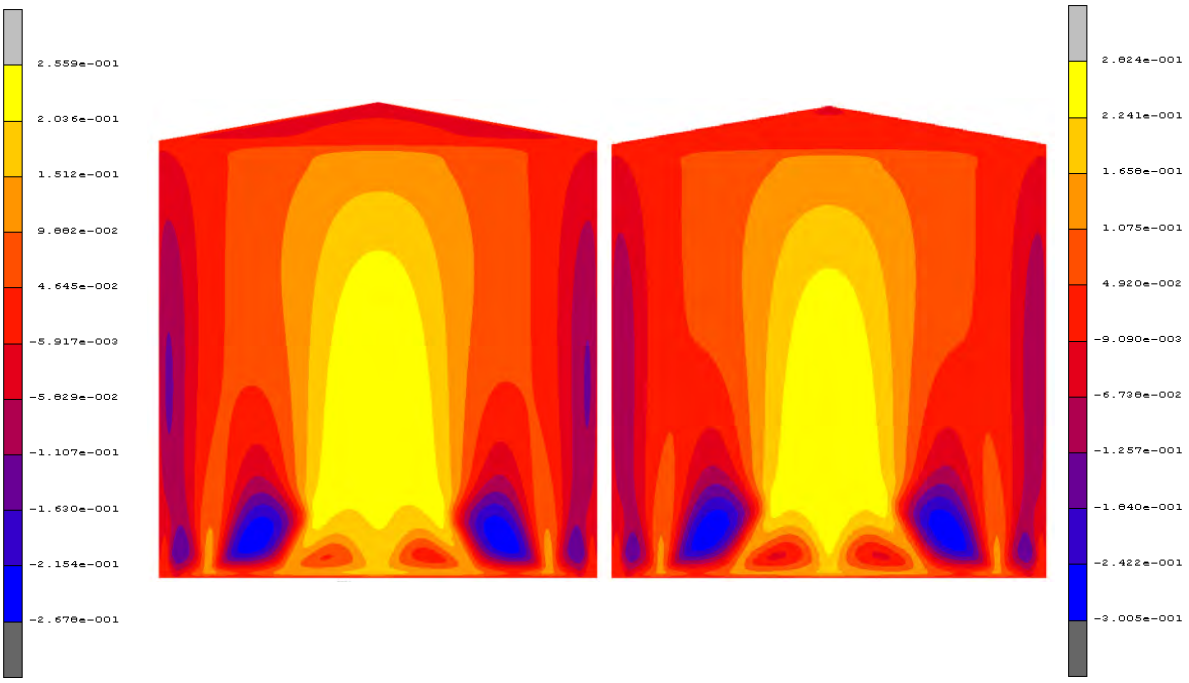

(e) $t_r = 2t_c$ (f) $t_r = 5t_c$

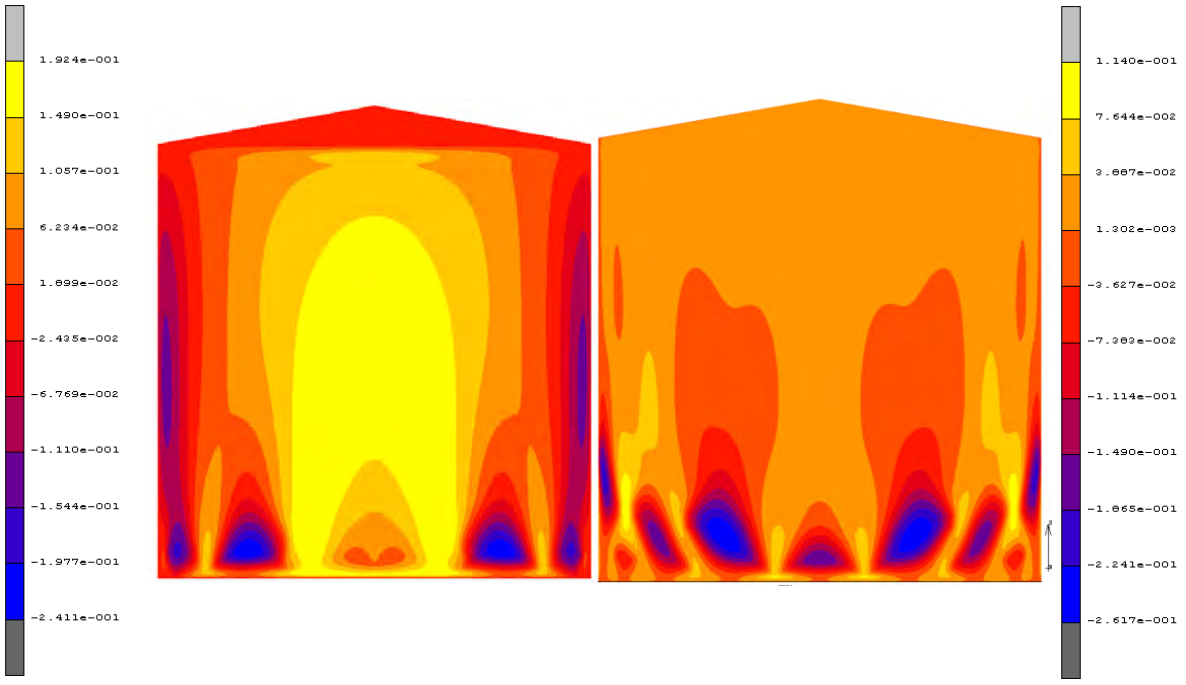

(g) $t_r = 10t_c$ (h) $t_r = 100t_c$

Institutional Repository - Library & Information Centre - University of Thessaly
02/06/2024 20:36:34 EEST - 18.222.76.217

Figure 6-28: Radial displacement field for various values of roof stiffness for the temperature of most heated generator equal to 400°C.

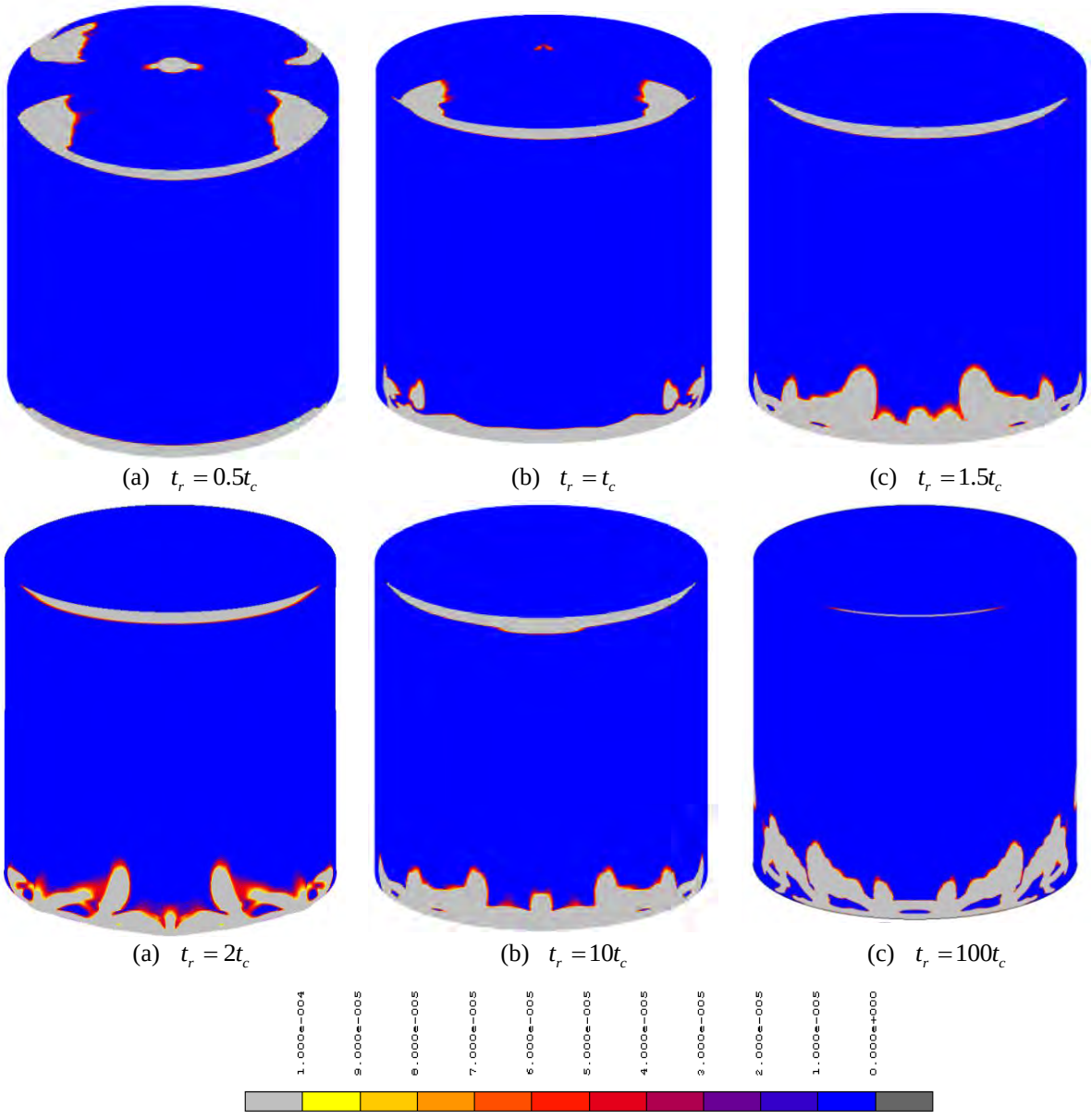

Figure 6-29: Equivalent plastic strain field for escalated roof stiffness.

Effect of yield strength of steel to the structural behavior of the fixed-roof heated tank

Figure 6-30 presents the evolution of the critical buckling temperature of the heated tank as the yield strength of steel increases for two different cases of roof stiffness $t_r = 2t_c$ and $t_r = 10t_c$. Five different cases are studied with respect to the yield strength which are S235, S275, S355, S420 and S460. In all cases the "cool" roof pattern is adopted and the tank is supposed to be empty. The critical buckling temperature that results from the GNA analysis is included. According to the results of the analyses, in the case of low-yield steel (S235), the

Institutional Repository - Library & Information Centre - University of Thessaly
02/06/2024 20:36:34 EEST - 18.222.76.217

elastoplastic material behavior contributes beneficially since the premature occurrence of elastic thermal buckling is prevented. If high-strength steel is adopted, the structural behavior is dominated by the thermal buckling and the plasticity can be omitted during the numerical analysis. Specifically for steel with yield strength up 275MPa, the predicted critical buckling temperature is on almost in the same level with the case where the elastic behavior is adopted in the analyses. For both cases of roof stiffness that are studied, fluctuations are detected around the elastic critical temperature for yield strength $275 \le f_y < 460\,Mpa$. In the case of $f_y = 460MPa$ the critical predicted temperatures that result from GNA and GMNA analyses are almost identical. Figure 6-31, Figure 6-32Figure 6-33 illustrate the Equivalent Von-Mises and Equivalent plastic strain fields in the pre-buckling stage. As it is shown, for low strength steel (S235) the base of the tank on the front side of the heated face is plastified before thermal buckling takes palce. Since the buckling occurs in the same region, it is concluded that the behaviour of the tank is dominated by the elastic-plastic buckling. The limits of the plastification zone near the base of the tank is deriorated as the yield strength increases and in the case of S460 the behaviour of the tank is dominated by the elastic buckling. The previous indicate that, if high-strength steel is adopted, the structural behavior is dominated by the thermal buckling and the plasticity can be omitted during the numerical analysis.

Regarding, the curves that describe the evolution of the fraction of the artificial damping energy to the total strain energy, it can be seen that the jump that specifies the occurrence of buckling is enlarged as the yield strength of steel is escalated. This indicates that the region where the buckling occurs is enlarged for high strength steel. This remark is in accordance with the final deformed configurations of the heated tanks as they are presented in Figure 6-34Figure 6-35.

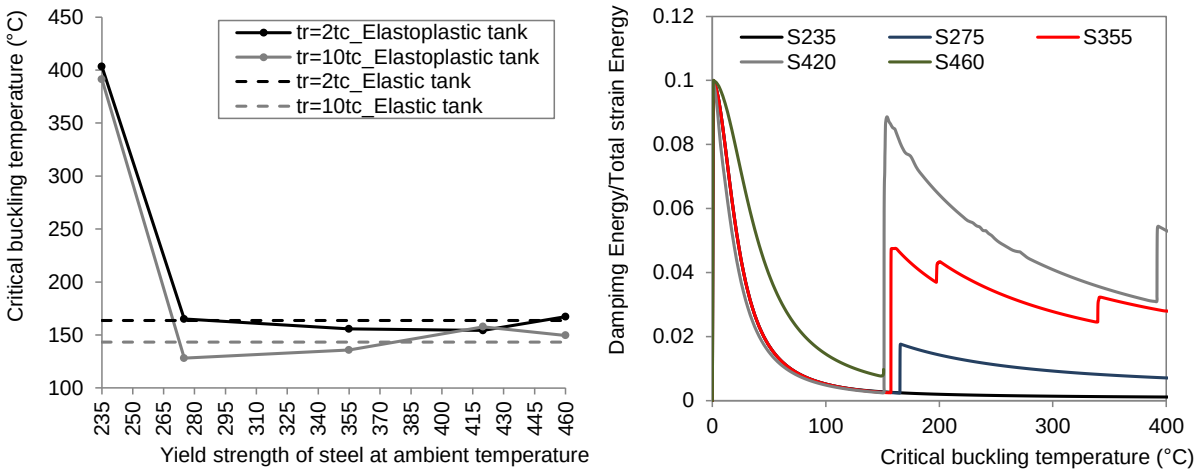

Figure 6-30: Effect of yield strength of steel on critical buckling temperature and the corresponding curves of the evolution of fraction of damping energy with temperature.

Institutional Repository - Library & Information Centre - University of Thessaly
02/06/2024 20:36:34 EEST - 18.222.76.217

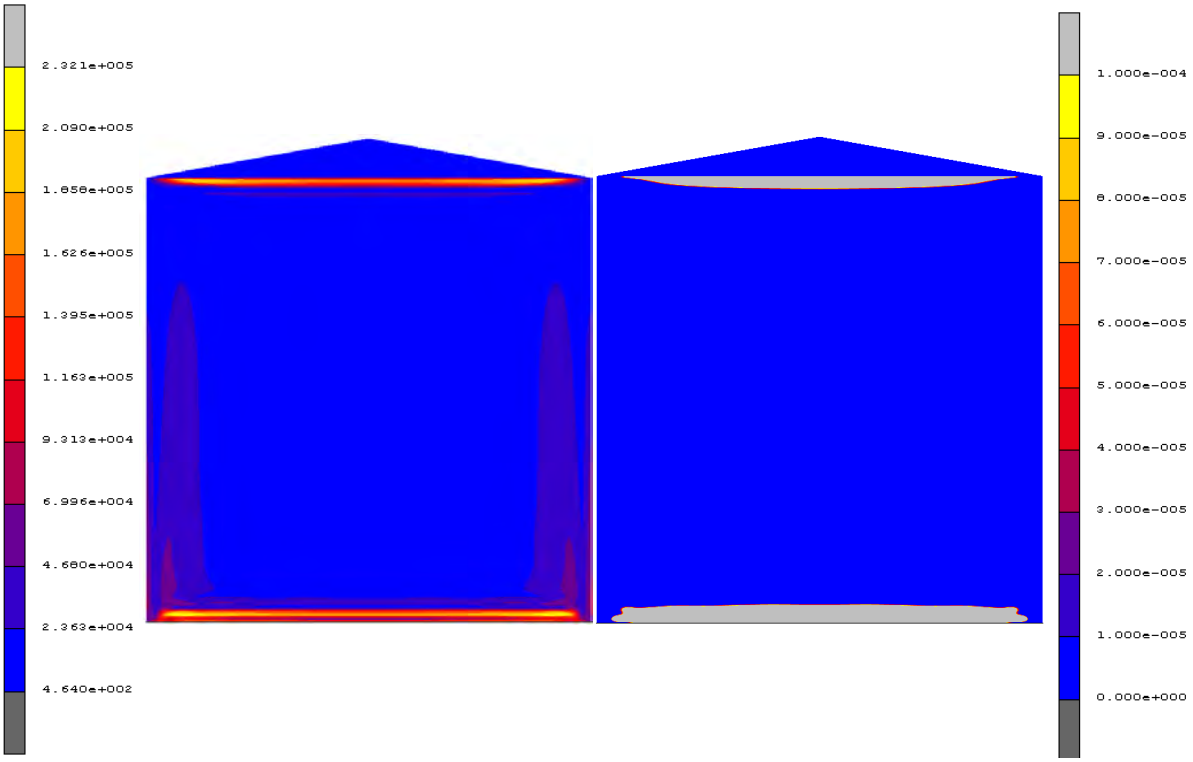

Equivalent Von-Mises stress field Equivalent plastic strain field

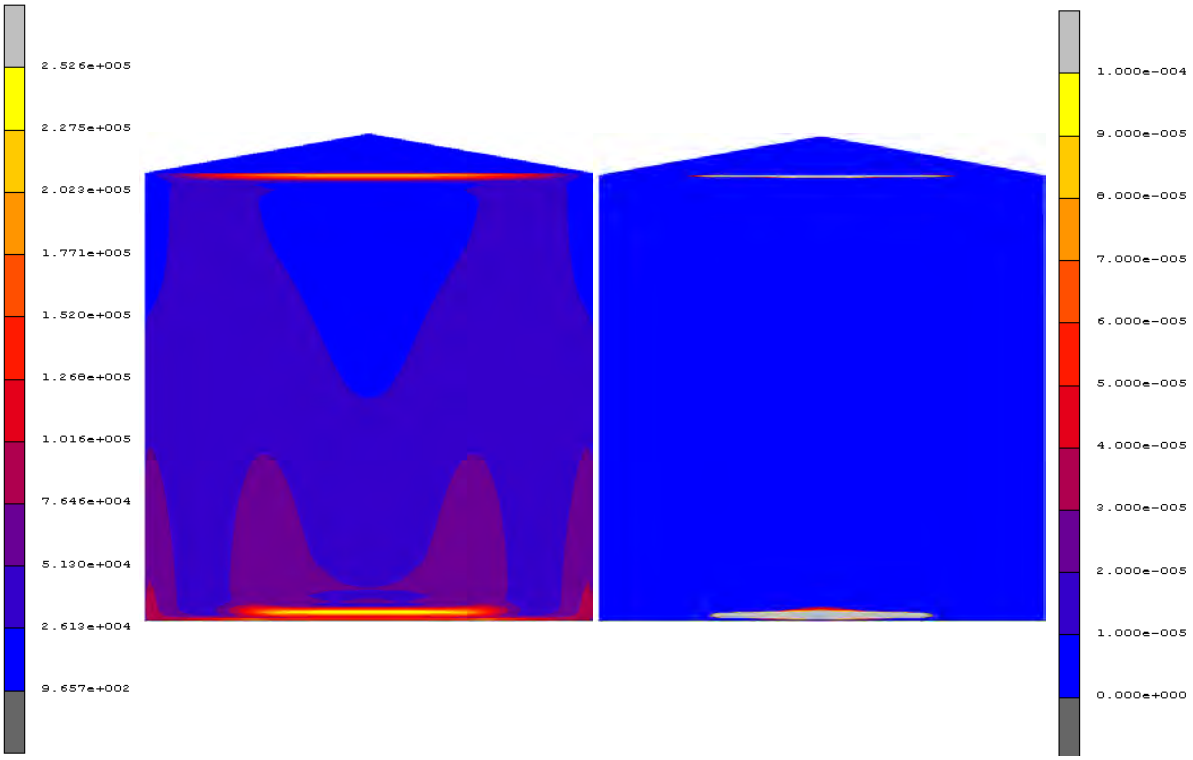

Equivalent Von-Mises stress field Equivalent plastic strain field

(a) S275

Figure 6-31: Equivalent Von-Mises and Equivalent plastic strain fields in the pre-buckling stage for the case of $t_r = 10t_c$ (S235 and S275).

Institutional Repository - Library & Information Centre - University of Thessaly
02/06/2024 20:36:34 EEST - 18.222.76.217

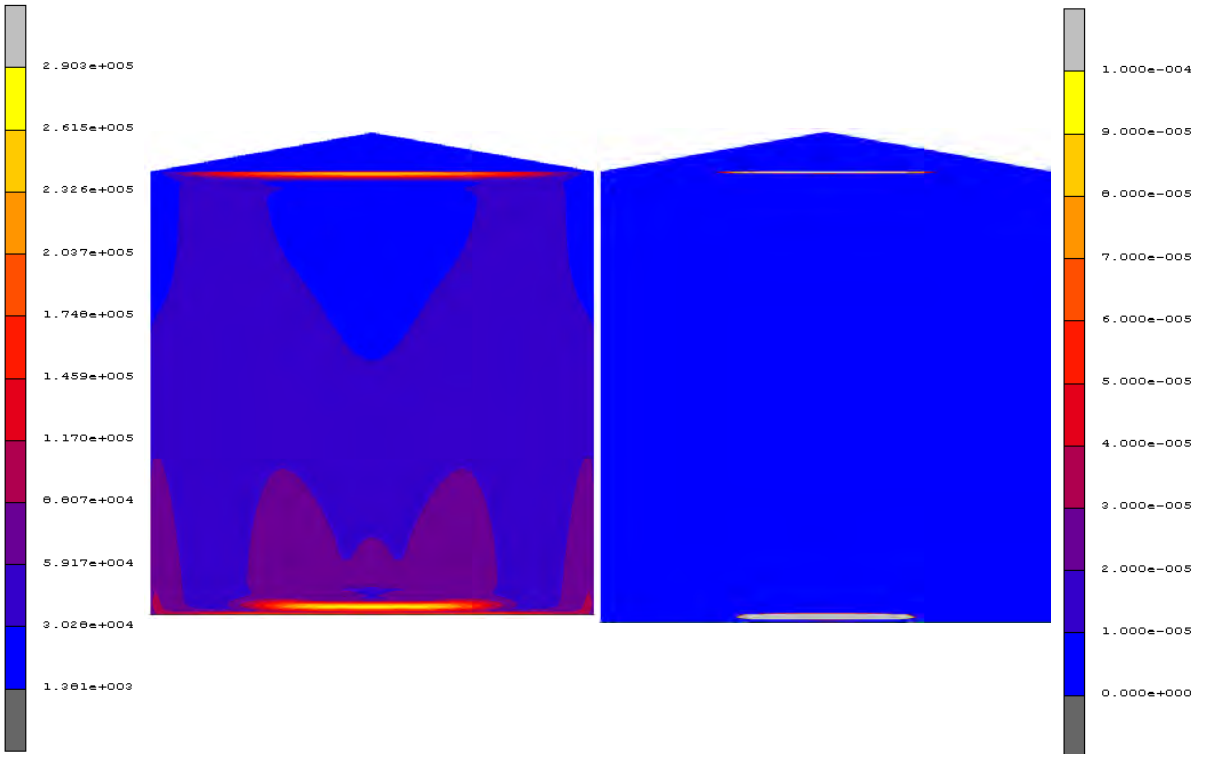

Equivalent Von-Mises stress field Equivalent plastic strain field

S355

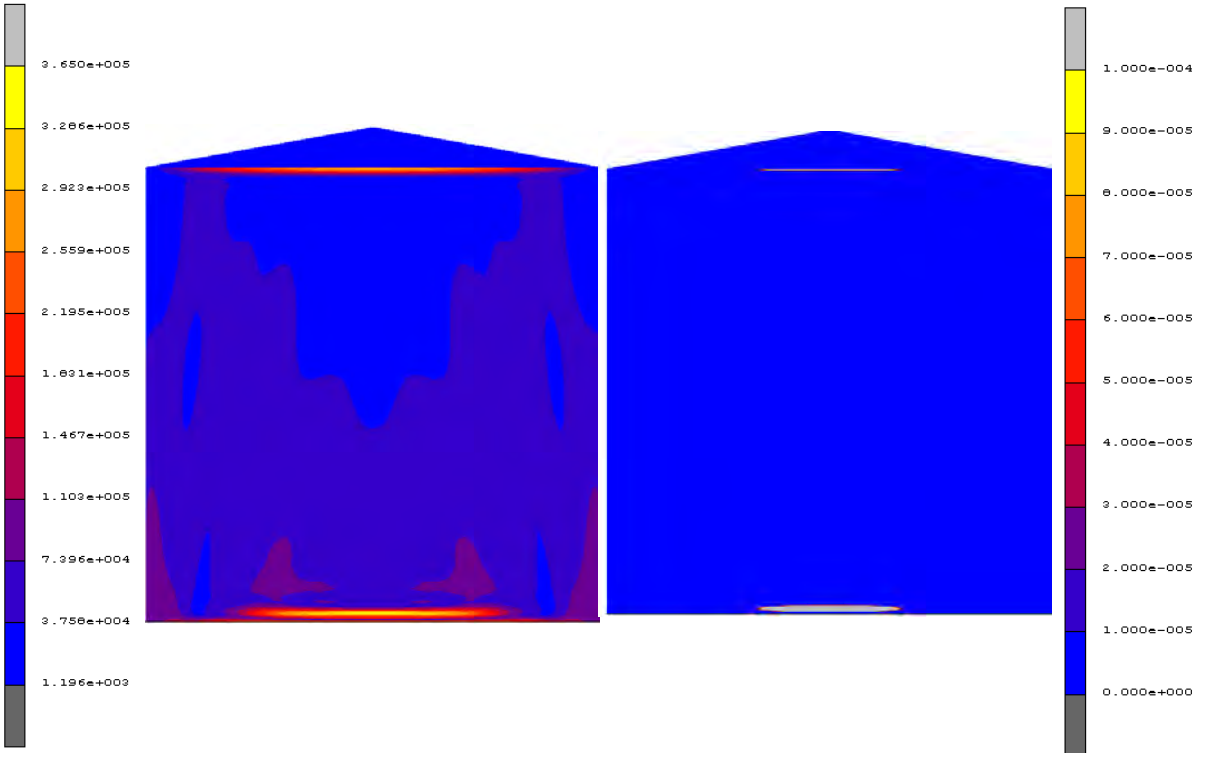

Equivalent Von-Mises stress field Equivalent plastic strain field

S420

Figure 6-32: Equivalent Von-Mises and Equivalent plastic strain fields in the pre-buckling stage for the case of $t_r = 10t_c$ (S355 and S420).

Institutional Repository - Library & Information Centre - University of Thessaly
02/06/2024 20:36:34 EEST - 18.222.76.217

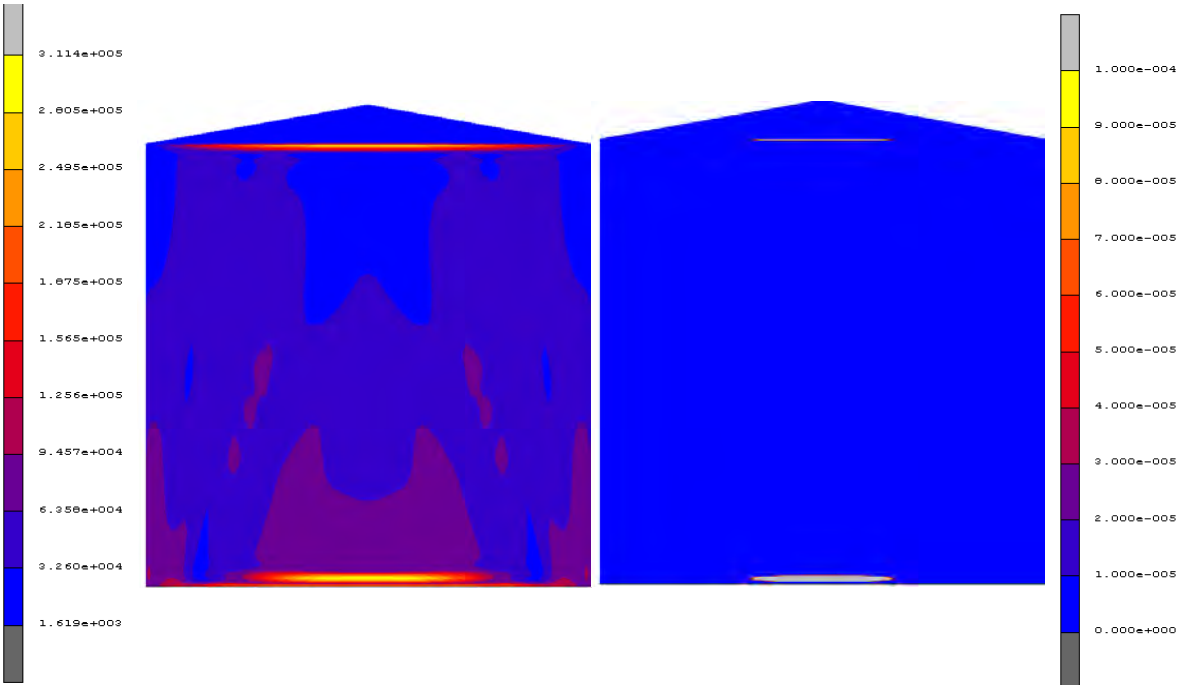

Equivalent Von-Mises stress field Equivalent plastic strain field

S460

Figure 6-33: Equivalent Von-Mises and Equivalent plastic strain fields in the pre-buckling stage for the case of $t_r = 10t_c$ (S460).

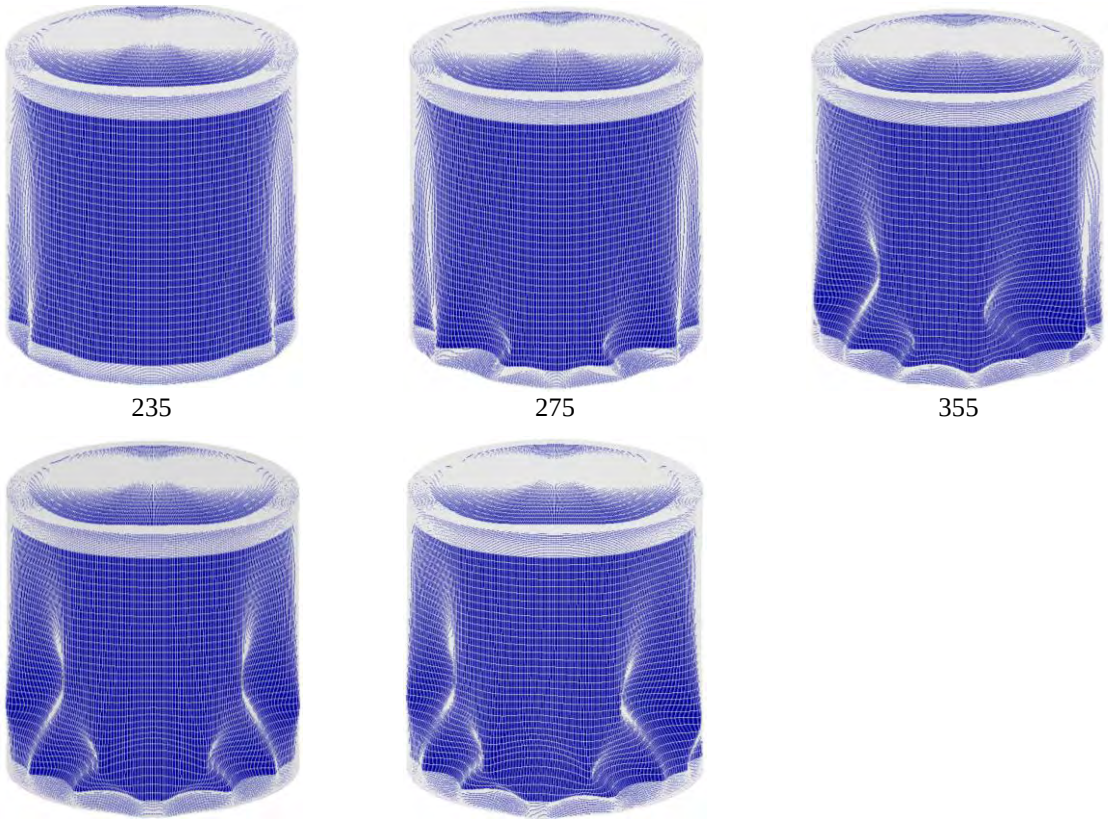

235 275 355

420 460

Figure 6-34: Deformed configuration of the heated tank for different magnitude of yield strength of steel (front view).

Institutional Repository - Library & Information Centre - University of Thessaly
02/06/2024 20:36:34 EEST - 18.222.76.217

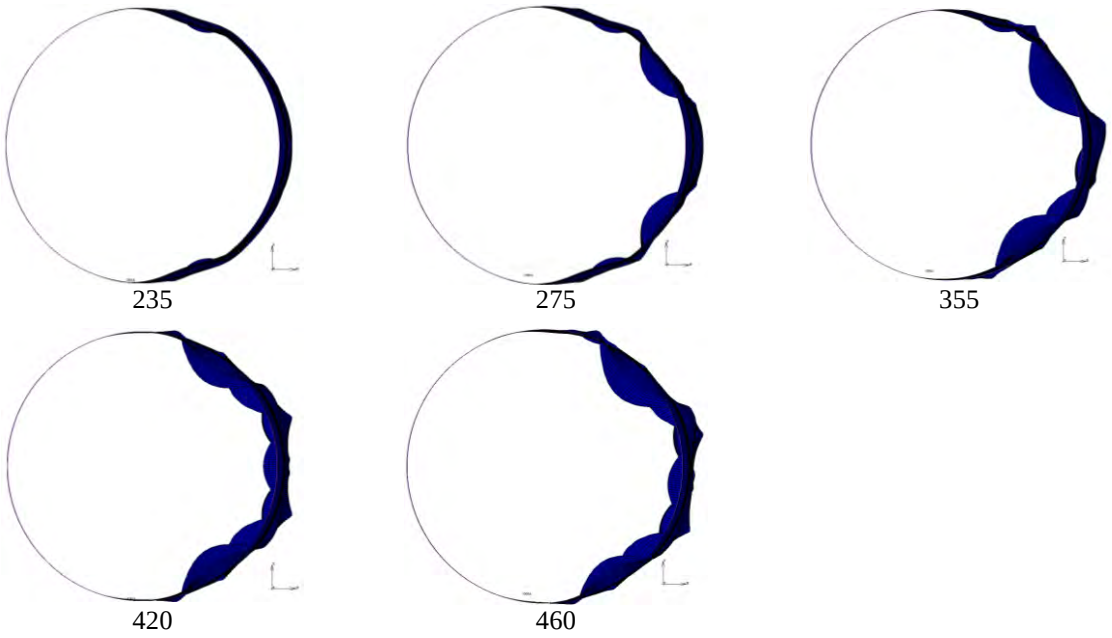

Figure 6-35: Deformed configuration of the heated tank for different magnitude of yield strength of steel (elevation view).

The equivalent plastic strain filed for escalated values of the ratio of roof to cylindrical shell thickness are illustrated in Figure 6-29. For tanks with slender roofs ($t_c \le t_r \le 1.5t_c$) plastic deformations appear in both roof and base of the cylinder while in the case of more slender roofs ($2t_c \le t_r \le 100t_c$) the plastic strain field in limited in the upper and the lower base of the cylinder. It is observed that the equivalent plastic strain field spreads in the base of the cylindrical tank as the roof becomes thicker. In the case of $t_r = 100t_c$, the plastisfication is detected in only in the lower base of the tank.

Finally, Figure 6-36 compares the evolution of the plastic strain energy of the structural system with the temperature of the most heated generator for different values of yield strength of steel. It is concluded that the effect of the plasticity is reduced as the yield strength of steel increases and that the phenomenon approaches the elastic behavior in the case where high strength steel is used.

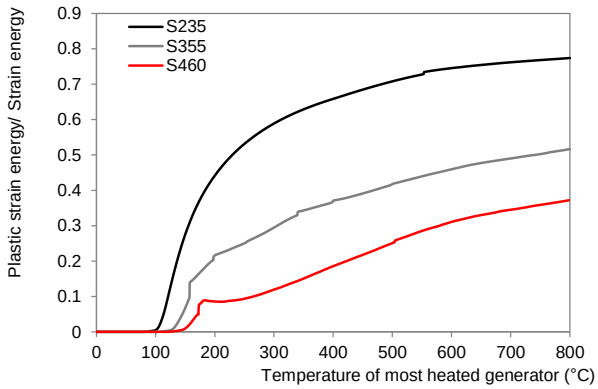

Figure 6-36: Effect of steel yield strength to plastic strain energy of the tank ($t_r = 2t_c$).

Institutional Repository - Library & Information Centre - University of Thessaly
02/06/2024 20:36:34 EEST - 18.222.76.217

Chapter 7. Parametric studies

This Chapter presents parametric studied concerning the basic parameters that may affect the structural behavior of a heated tank during a pool fire event. The parameters that are considered are the geometric initial imperfections, the level of the stores liquid (oil) and the zone of the tank that is affected by the fire.

7.1 Effect of initial imperfections

Initial imperfections are incorporated in the geometry of the steel tank for a more realistic assessment of its behavior. There are many different ways to introduce initial geometric imperfections in structural members. A simple way in the context of finite element analysis is to extract the buckling eigenmodes and introduce them as imperfections with a specific amplitude. More specifically, the normalized buckling mode is multiplied by a scale factor, leading to certain maximum amplitude and the resulting displacements are added to the initial coordinates of the structural member. For the case studied here, the first eigenmode is used as it is defined in Chapter 5. The amplitude of the initial imperfections that is used for the analysis is taken equal to 1mm, 2mm, 5mm and 10mm i.e. the ratio of the amplitude of the initial imperfections to the thickness of the shell is considered equal to 0.1, 0.2, 0.5 and 1 respectively.

The imperfection sensitivity study for three different values of roof to cylindrical shell thickness ratio is presented in Figure 7-1. It is observed the critical buckling temperature is reduced as the amplitude of the geometric initial imperfections is scaled up and this holds for all the cases that are studied. This reduction is more obvious for tanks that use less stiff roofs i.e. for low values of roof to cylindrical shell thickness ratio. Specifically, for the cases of $t_r = 2t_c$ and $t_r = 10t_c$, the reduction of the critical buckling temperature is around 33% comparing with the critical values of temperature that result from the analyses of perfect models i.e. the models with no-initial imperfections. The corresponding reduction is almost 25% when the stiffer roof is used ($t_r = 100t_c$). The final deformed configurations of the tank and the radial displacement fields, are depicted in Figure 7-2 and Figure 7-4 for the cases of $t_r = 2t_c$ and $t_r = 100t_c$ respectively. It is noted that the deformed shape of the cylindrical tank is affected by the amplitude of the initial imperfections that is used. For relatively small amplitude, failure mode is almost local and is detected in the base of the tank in the front face of the most heated region. As the amplitude of the initial imperfection increases, the phenomenon spreads in the body of the tank and becomes global.

Institutional Repository - Library & Information Centre - University of Thessaly
02/06/2024 20:36:34 EEST - 18.222.76.217

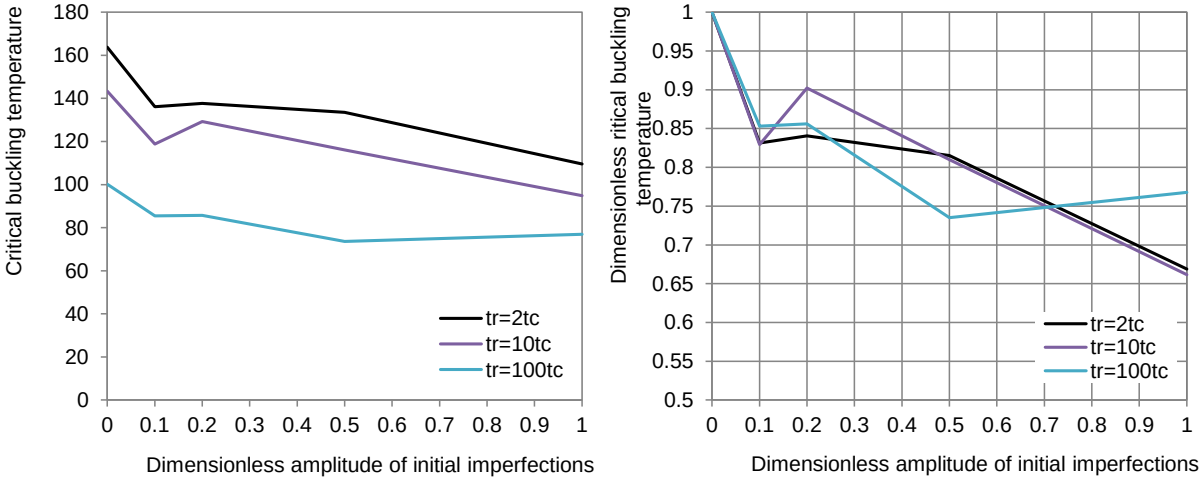

Figure 7-1: Imperfection sensitivity of an empty fixed-roof tank for different roof to cylindrical shell thickness ratio.

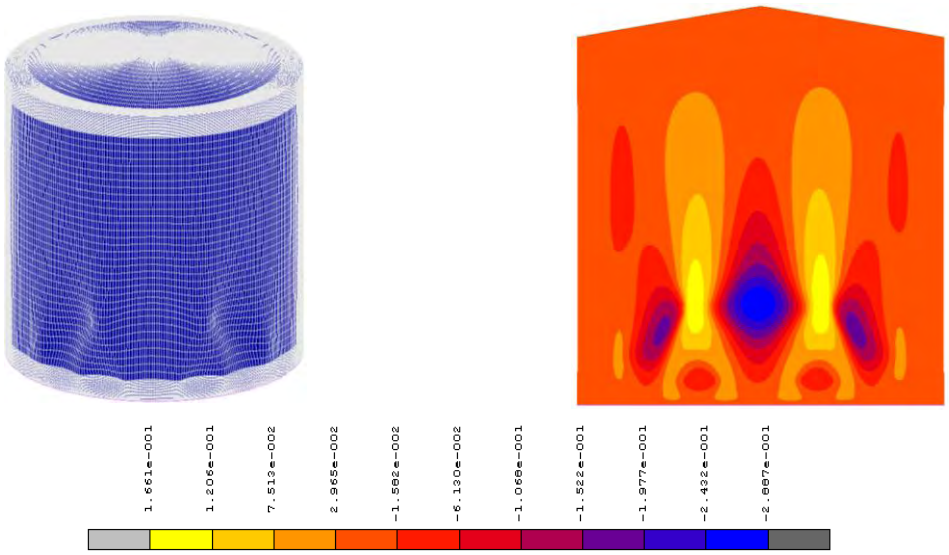

(a) Amplitude of initial imperfections equal to 1mm

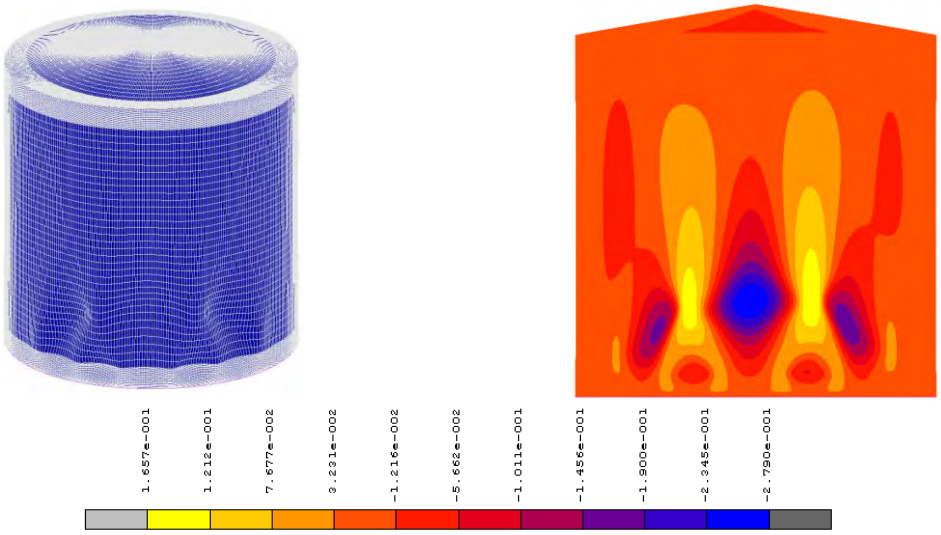

(b) Amplitude of initial imperfections equal to 2mm

Figure 7 2: Final deformed shape and radial displacement field for the case of $t_r = 2t_c$ (continued)

Institutional Repository - Library & Information Centre - University of Thessaly
02/06/2024 20:36:34 EEST - 18.222.76.217

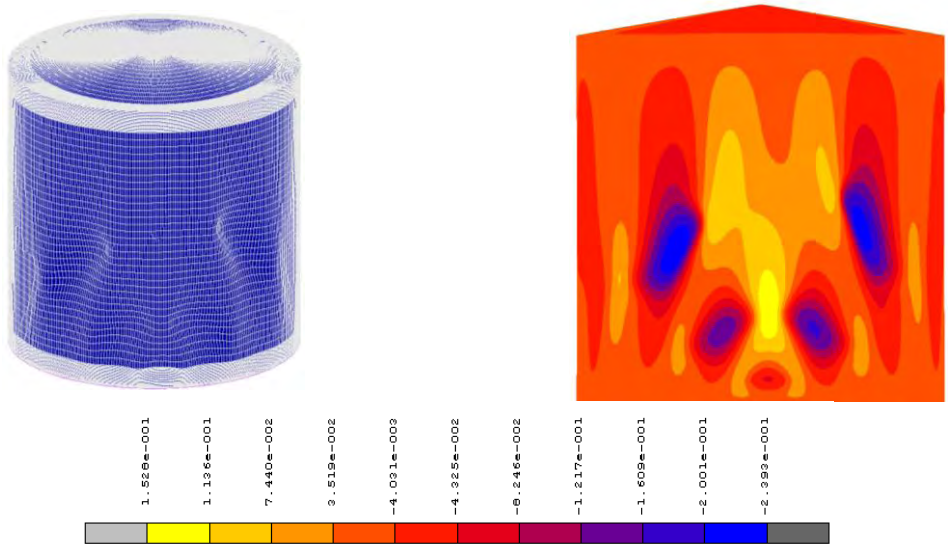

(c) Amplitude of initial imperfections equal to 5mm

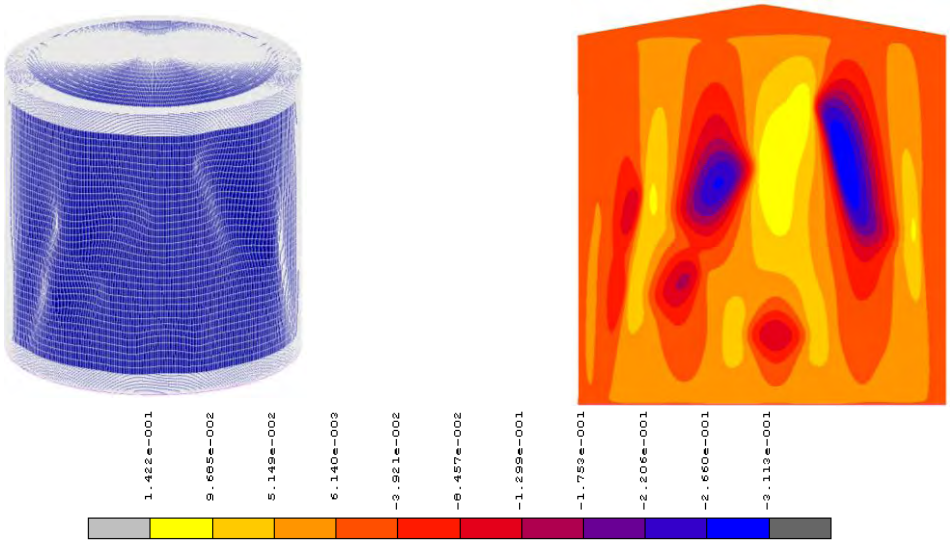

(d) Amplitude of initial imperfections equal to 10mm

Figure 7-2: Final deformed shape and radial displacement field for the case of $t_r = 2t_c$

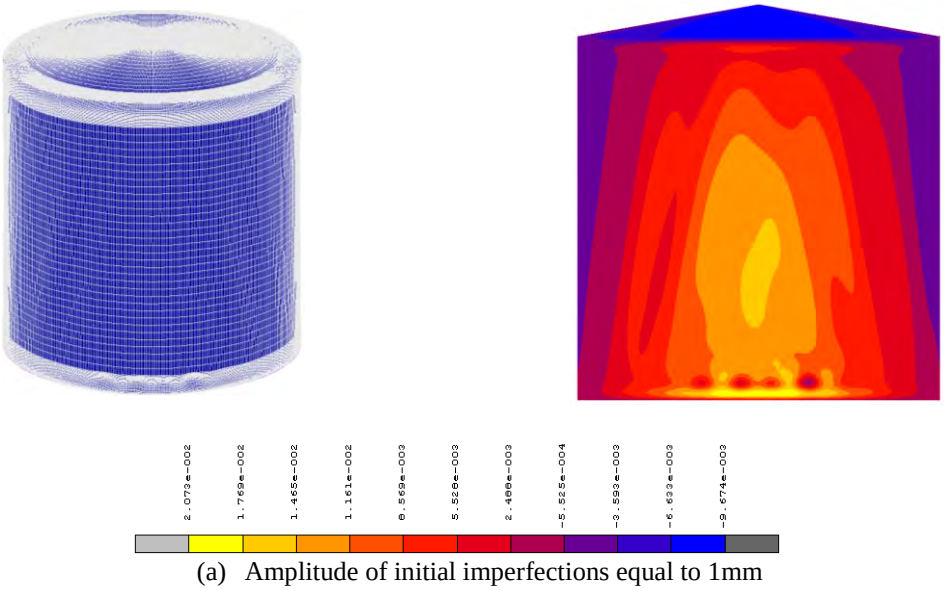

(a) Amplitude of initial imperfections equal to 1mm

Figure 7-3: Final deformed shape and radial displacement field for the case of $t_r = 100t_c$ (continued)

Institutional Repository - Library & Information Centre - University of Thessaly
02/06/2024 20:36:34 EEST - 18.222.76.217

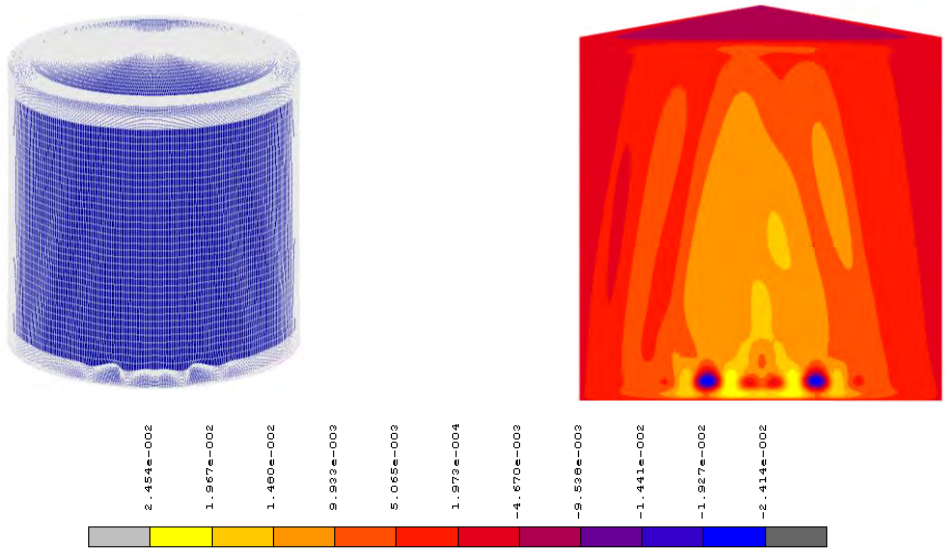

(b) Amplitude of initial imperfections equal to 2mm

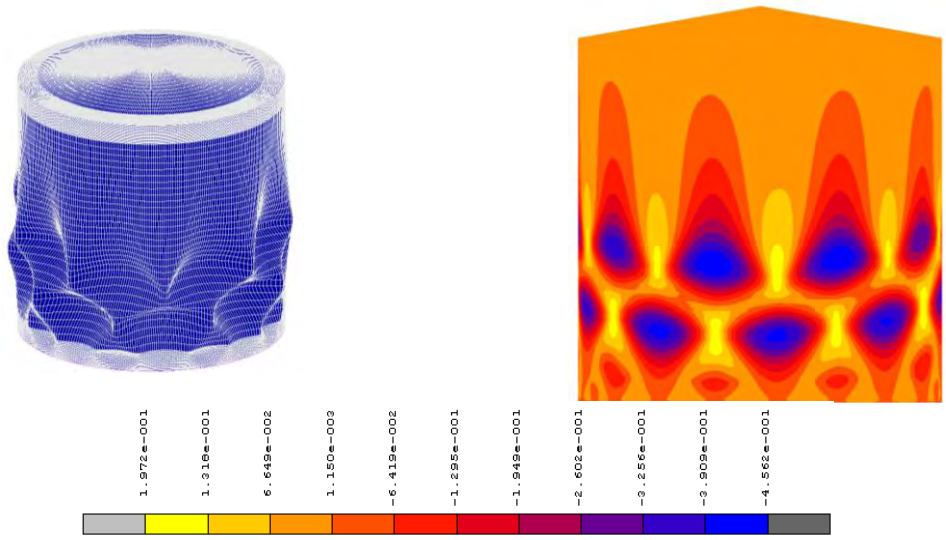

(c) Amplitude of initial imperfections equal to 5mm

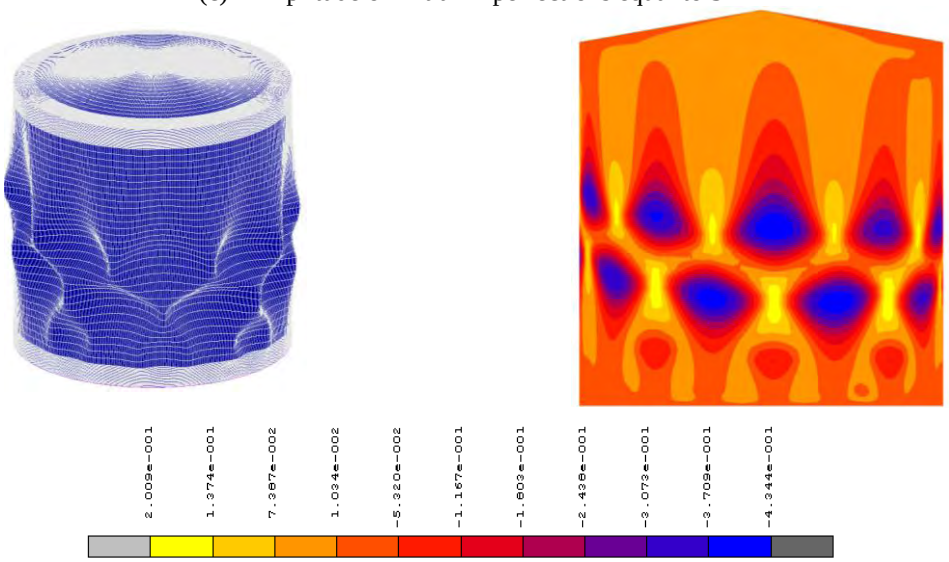

(d) Amplitude of initial imperfections equal to 10mm

Figure 7-4: Final deformed shape and radial displacement field for the case of $t_r = 100t_c$

Institutional Repository - Library & Information Centre - University of Thessaly
02/06/2024 20:36:34 EEST - 18.222.76.217

In order to look thoroughly in the effect of initial imperfection to the buckling behavior of the heated tank, the deformed configuration of the structural system during the fire exposure is depicted in Figure 7-5 ($t_r = 5t_c$) and amplitude of initial imperfections 1mm). It is observed that at the 142nd step of the analysis, the deflected configuration of the tank is mainly affected by the first eigenmode of the modal analysis, while in the next step for minor increase of temperature (0.005°C), the contribution of the first eigenmode is insignificant and the deflected shape in mainly affected the local buckling mode at the base of the tank (9th eigenmode according to LBA). This sudden change indicates that this temperature (T=124.85) consists a bifurcation point for the solution.

During Buckling - Step 142 (T=124.846°C) | During Buckling -Step 143 (T=124.851°C) | Psot-buckling Buckling (T=128°C)

Figure 7-5: Deformed configuration of the tank ($t_r = 5t_c$) for different levels of temperature of most heated generator.

7.2 Effect of level of stored liquid

The stored liquid is included in the numerical analysis through the hydrostatic pressure that is induced and no other fluid/solid interaction is taken into account. The critical buckling temperature variation with the level of stored liquid is depicted in Figure 7-6 for variable roof stiffness ($t_r = 2t_c, t_r = 10t_c$ and $t_r = 100t_c$). The post-buckling deflected shapes are shown in Figure 7-7 Figure 7-8. As the level of the stored liquid increases, the buckling temperature is scaled up. For low levels of stored liquid, the buckling temperature is very close to the value that corresponds to an empty tank. Buckling always occurs near the liquid surface and spreads into the empty part, as shown in Figure 7-7Figure 7-8. Also it is noted that in the case of slender roof ($t_r = 2t_c$), the buckling temperature of the tank is almost constant for liquid level up to the half of the height of the tank. It is concluded that the level of the stored liquid has a significant influence on the buckling behavior of the cylindrical tank.

Institutional Repository - Library & Information Centre - University of Thessaly
02/06/2024 20:36:34 EEST - 18.222.76.217

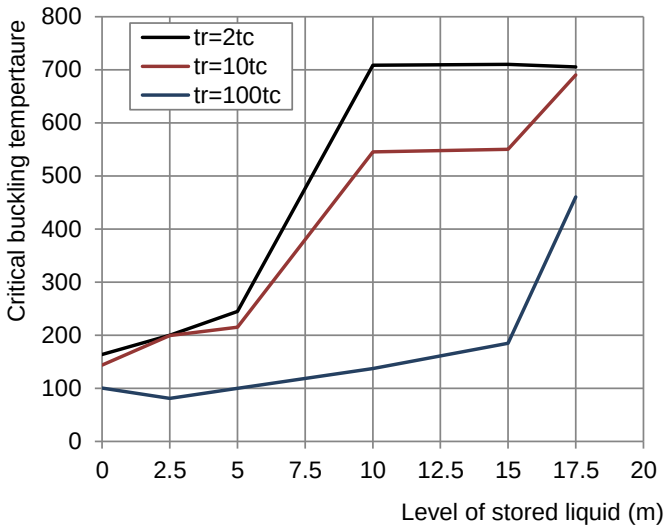

Figure 7-6: Influence of the level of stored liquid to the critical buckling temperature for different roof to cylindrical shell thickness ratios.

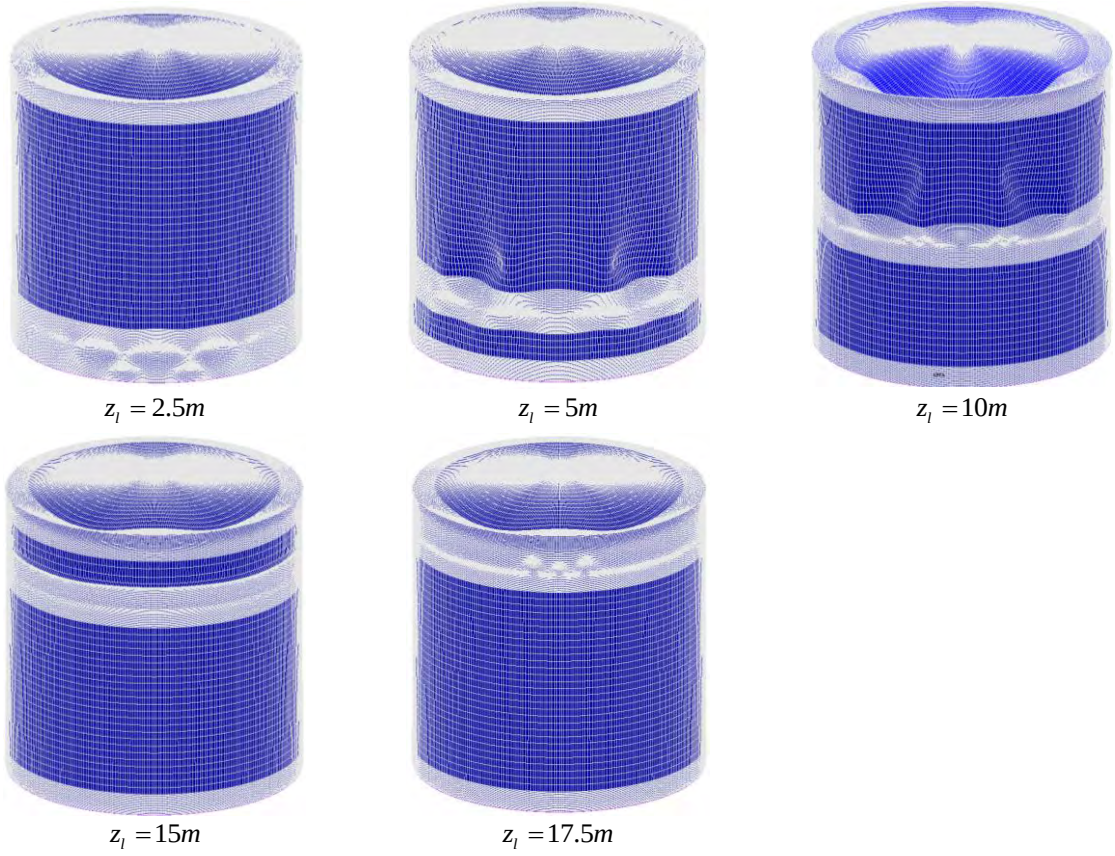

Figure 7-7: Influence of level of liquid to the deformed shape of the tank for $t_r = 2t_c$.

Institutional Repository - Library & Information Centre - University of Thessaly
02/06/2024 20:36:34 EEST - 18.222.76.217

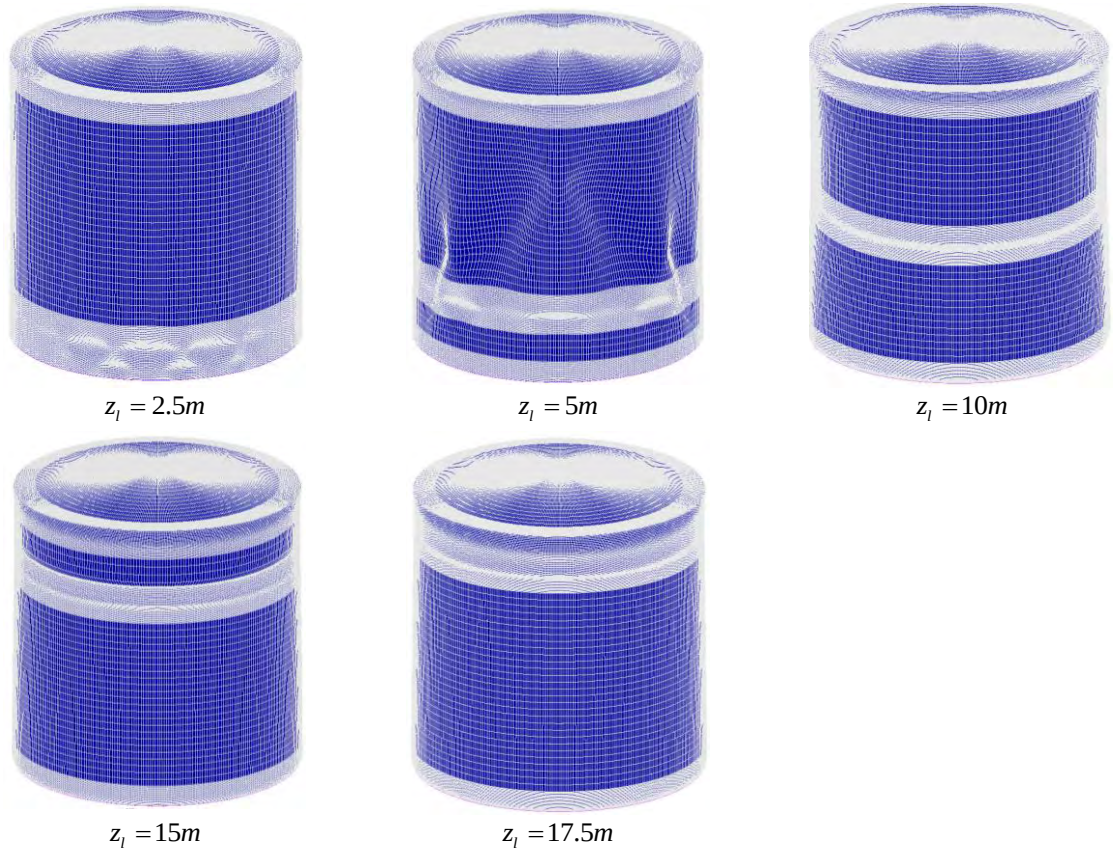

Figure 7-8: Influence of level of liquid to the deformed shape of the tank for $t_r = 10t_c$.

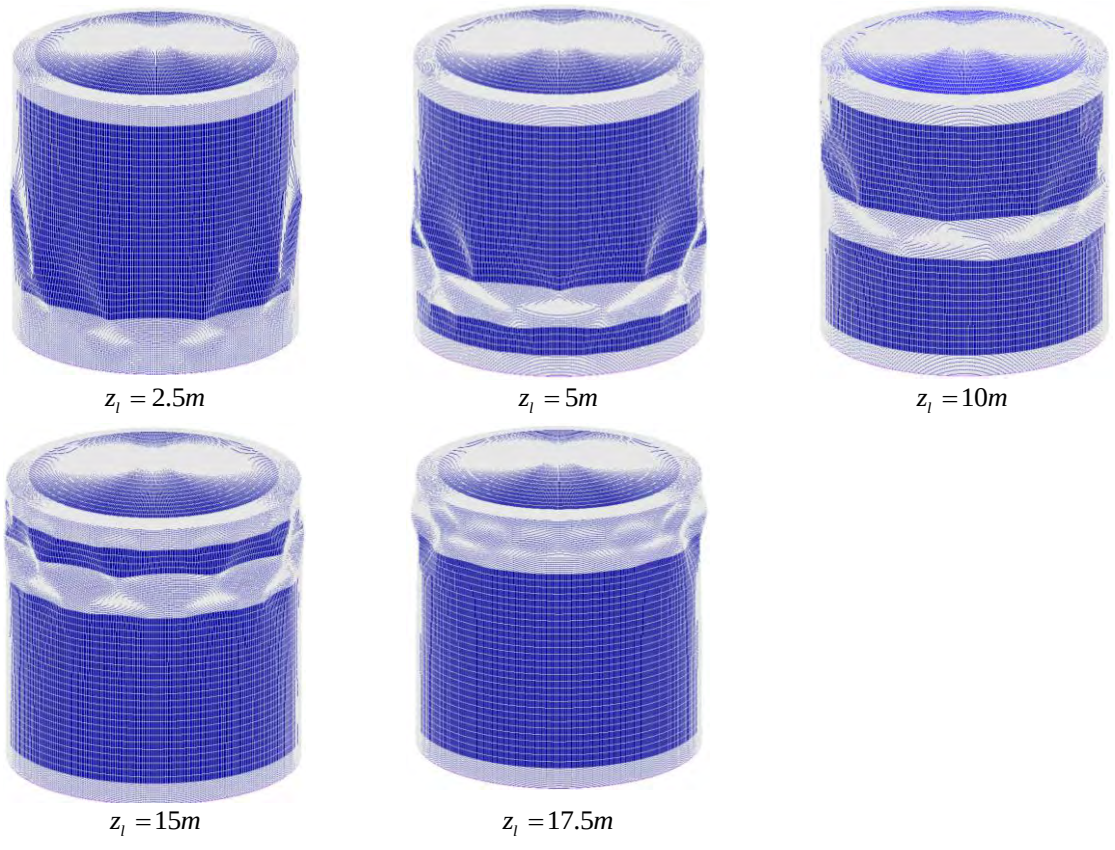

Figure 7-9: Influence of level of liquid to the deformed shape of the tank for $t_r = 100t_c$.

Institutional Repository - Library & Information Centre - University of Thessaly
02/06/2024 20:36:34 EEST - 18.222.76.217

7.3 Effect of size of heated zone

If the size of the adjacent tank fire is changed, the target tank is exposed to heating in a zone of different size. The circumferential range of the heated zone models this effect. Here, characteristic angles θ_0 (*see Eq. 5.1*) of 45°, 120°, 135° and 150° are studied. The buckling temperatures of the empty tanks are shown in Figure 7-10. It is observed that the critical buckling temperature scales up as the heated zone is expanded. When the hated zone of the tank is narrow, buckles concentrate within the zone. When the heated zone is wider (θ_0 =120° and 135°), buckles take place in the cool zone of the tank. This is altered for the case where the heated zone covers almost all the circumference of the tank (θ_0 =150°), where the buckling occurs again in the heated zone and near the bottom boundary.

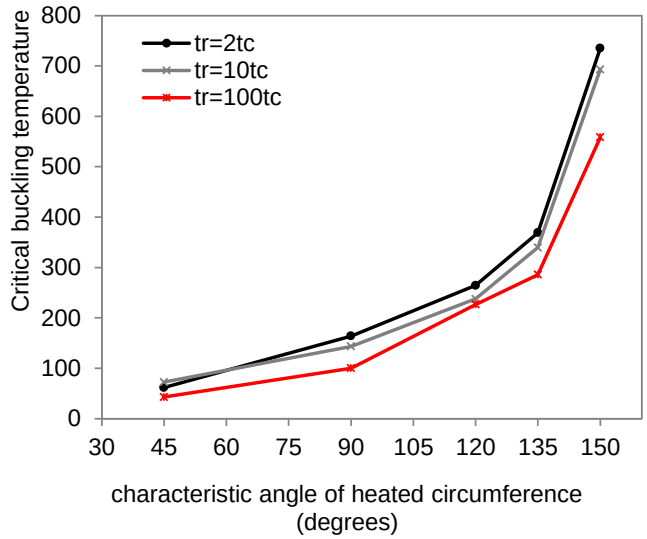

Figure 7-10: Influence of the size of the heated zone to the critical buckling temperature for different roof to cylindrical shell thickness ratios.

Institutional Repository - Library & Information Centre - University of Thessaly
02/06/2024 20:36:34 EEST - 18.222.76.217

$\theta_0 = 45^o$

$\theta_0 = 120^o$

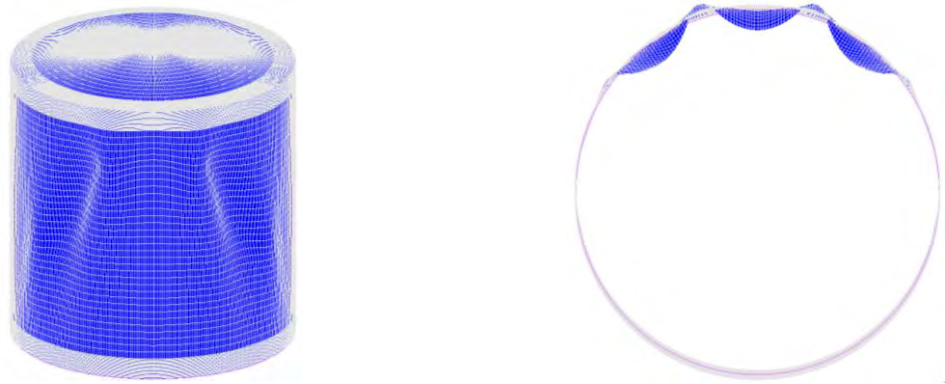

$\theta_0 = 135^o$

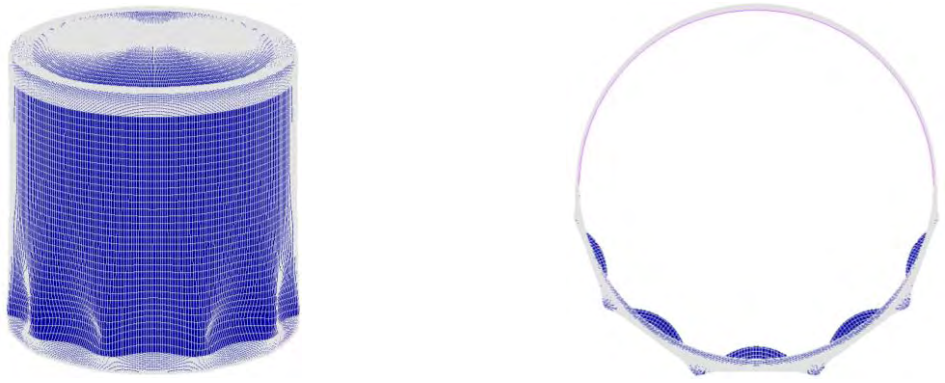

$\theta_0 = 150^o$

Figure 7-11: Influence of the size of the heated zone to the deflected shape of the tank ($t_r = 2t_c$).

Institutional Repository - Library & Information Centre - University of Thessaly
02/06/2024 20:36:34 EEST - 18.222.76.217

Conclusions

The present thesis addresses the problem of the behavior of steel oil-storage cylindrical tanks under thermal loading induced by an adjacent fire-engulfed tank. The study is focused on a fixed-roof tank with radius equal to 10m and 20m high. The problem is handled numerically through the Finite Element methodology. Geometric non-linear analysis is used and the arc-length method is utilized for the evaluation of the equilibrium path of the structural system. Primary results are obtained through LBA. It is concluded that the critical buckling temperature of the storage tanks depends on the roof stiffness which is modified by using different thickness for the roof shell. Moreover it is observed that the thermal pattern of the roof ("cool" or "hot") does not affect the thermal buckling behavior of the tank.

Moreover the thermal buckling of empty cylindrical tanks is studied through GNA. In the case where the elastic material law is adopted in the numerical analyses, the empty tanks buckle for low levels of temperature depending on the roof stiffness. Specifically, the critical buckling temperature of empty tanks lies between 100°C and 170°C for slender and stiff roofs respectively. The failure mode of the tank depends also on the stiffness of the roof. The deflected shape of the tank in the post-buckling stage indicates roof buckling for tanks with very slender roofs and this turns to cylindrical wall buckling as the stiffness of the roof increases. In order to obtain more realistic results, the non-linear elastic plastic law of steel at elevated temperatures is included in the analyses. Once more, it is concluded that the thermal buckling behavior of the tank depends on the roof stiffness and two different buckling modes are distinguished for slender and stiff roofs. The predicted critical buckling temperature for elastoplastic tanks is lower with respect to the values that arise from the elastic tanks if the yield strength of the steel is equal to 275MPa. Furthermore, the results indicate that both the critical buckling temperature and the post-buckling deflected shape of the tank are strongly affected by the yield strength of the steel adopted. For high strength steel the empty tanks buckle earlier compared with the case where low strength steel is used. Specifically, as the yield strength of steel increases the thermal buckling behavior of the tank tends to the case where the elastic material law is used.

The next step was the incorporation of initial geometric imperfections in the numerical model. From that it is concluded that the critical buckling temperature and failure mode of the cylindrical tank are affected by the adopted amplitude of the initial imperfections. This is valid for both slender and stiff roofs and the phenomenon is more significant when the tanks are using slender roofs. In this case, the reduction of the critical buckling temperature is almost 35% with respect to the perfect model. Moreover, the deformed shape of the

Institutional Repository - Library & Information Centre - University of Thessaly
02/06/2024 20:36:34 EEST - 18.222.76.217

cylindrical tank is affected by the amplitude of the initial imperfections used. For relatively small amplitudes, failure mode is almost local and is detected in the base of the tank in the most heated region. As the amplitude of the initial imperfection increases, the phenomenon spreads to the body of the tank and becomes global.

Next, it is proved that another important parameter that strongly influences the thermal buckling behavior of storage tanks is the level of the stored liquid. It is observed that as the level of the stored liquid increases, the buckling temperature is scaled up. For low levels of stored liquid, the buckling temperature is very close to the value that corresponds to an empty tank. Buckling always occurs near the liquid surface and spreads to the empty part. Also it is noted that in the case of slender roofs, the buckling temperature of the tank is almost constant for liquid level up to the half of the height of the tank. Generally, the presence of the liquid in the tank increases the buckling temperature as a result of the beneficial effect of internal pressure which causes circumferential tension.

Finally, parametric study is conducted with respect to the circumferential range of the heated zone. It is concluded that that the critical buckling temperature scales up as the heated zone is expanded. When the heated zone of the tank is narrow, buckles concentrate within the zone. When the heated zone is wider ($\theta 0 = 120°$ and $135°$), buckles take place in the cool zone of the tank. This is altered for the case where the heated zone covers almost all the circumference of the tank ($\theta 0 = 150°$), with buckling occurring again in the heated zone and near the bottom boundary.

Institutional Repository - Library & Information Centre - University of Thessaly
02/06/2024 20:36:34 EEST - 18.222.76.217

Further research

Institutional Repository - Library & Information Centre - University of Thessaly
02/06/2024 20:36:34 EEST - 18.222.76.217

References

Sengupta, A., Gupta, A. K., and Mishra, I. M. (2010). "Engineering layout of fuel tanks in a tank farm." Journal of Loss Prevention in the Process Industries

NFPA-30. (2001). Aboveground tank installation for tank storage. Quincy, Massachusetts: National Fire Protection Association.

SFPE handbook of fire protection engineering. (1995) (2nd ed.). Quincy. Massachusetts: National Fire Protection Association

Daniel, A., Crowl, J., & Louvar, F. (2002). Chemical process safety - Fundamentals with applications. In B. Goodwin (Ed.) (2nd ed.). Prentice Hall international series

Beyler, C. L. (2004b). "Industrial fire protection engineering." Fire Technology, 40(3): 297-298

Fernandada Silva Santos, Alexandre Landesmann (2014) Thermal performance-based analysis of minimum safe distances between fuel storage tanks exposed to fire, FireSafetyJournal69, 57–68

Beyler, C. L. (2004b). "Industrial fire protection engineering." Fire Technology, 40(3): 297-298.

F.M.A.Fontenelle, Thermal Analysis of Ethanol Storage Tanks Under Fire Conditions

(M.Sc.Dissertation),Federal University of Riode Janeiro(COPPE/UFRJ), RiodeJaneiro,RJ,Brazil,2012.

Landucci, G., Gubinellia, G., Antonioni, G., and Cozzani, V. (2009). "The assessment of the damage probability of storage tanks in domino events triggered by fire." Accid. Anal. Prev., 41(6), 1206–1215.

Earl A. Thornton , (1993) Thermal Buckling of Plates and Shells, Appl. Mech. Rev 46(10), 485-506 (Oct 01, 1993)

R. Shahsiah, M. R. Eslami, Thermal buckling of functionally graded cylindrical shell, Journal of Thermal Stresses, 26:277–294, 2003

M. R. Eslami , R. Shahsiah ,thermal buckling of imperfect cylindrical shells Journal of Thermal Stresses, 24:71^89 , 2001

M.R. Eslami, A.R. Ziaii, and A. Ghorbanpour, Thermoelastic Buckling of Thin Cylindrical Shells Based on Improved Donnell Equations, J. Thermal Stresses, vol. 19, pp. 299–316, 1996.

M.R. Eslami and R. Javaheri, Thermal and Mechanical Buckling of Composite Cylindrical Shells, J. Thermal Stresses, vol. 22, no. 6, pp. 527–545, 1999.

M.R. Eslami and M. Shariyat, Elastic, Plastic, and Creep Buckling of Imperfect Cylinders under Mechanical and Thermal Loading, ASME J. Pressure Vessel Tech., vol. 118, November 1996.

L. H. Donnell, Effect of Imperfection on Buckling of Thin Cylinders and Columns under Axial Compression, ASME J. Appl. Mech., vol. 17, pp. 73^83, 1950.

L. H. Donnell, Effect of Imperfection on Buckling of Thin Cylinders under External Pressure, ASME J. Appl. Mech., vol. 23, p. 569, 1956.

L. H. Donnell, Effect of Imperfection on Buckling of Thin Cylinders with Fixed Edges under External Pressure, ASME J. Appl. Mech., vol. 28, p. 305, 1958.

Abir, D, and Nardo, SV (1959). Thermal Buckling of Circular Cylindrical Shells under Circumferential Temperature Gradients. J Aero Sci, 26, 803-808.

Anderson, MS, and Card. MF (1962). Buckling of Ring-Stiffened Cylinders under a Pure Bending Moment and a Nonuniform Temperature Distribution. (NASA TN D-1513).

Anderson, MS (1962a). Combinations of Temperature and Axial Compression Required for Buckling of a Ring-Stiffened Cylinder. (NASA TND-1224).

Anderson, MS (1962b). Thermal Buckling of Cylinders. Collected Papers on Instability of Shell Struclures-1962. (NASA TN D-1510).

Institutional Repository - Library & Information Centre - University of Thessaly
02/06/2024 20:36:34 EEST - 18.222.76.217

Ari-Gur, J, Baruch, M, and Singer, J (1979). Buckling of Cylindrical Shells under Combined Axial Preload, Non-uniform Healing and Torque. Exp Mech, 19, 406-410.

Belov, VK (1978). Experimental Study of Shell Stability under Healing and Loading. Soviet Aeronaut, 21(1), 1-3.

Bijlaard, PP, and Gallagher, RH (1960). Elastic Instability of a Cylindrical Shell under Arbitrary Circumferential Variation of Axial Stress. J Aeronaut Sci, 27(11), 854-859.

Birman, V (1990). Thermal Dynamic Problems of Reinforced Composite Cylinders. J Appl Mech, 57, 941-947.

Bushnell, D (1971a). Analysis of Ring-Stiffened Shells of Revolution Under Combined Thermal and Mechanical Loading. AlAA .1 9(3), 401-410.

Chang, LK, and Card, MF (1970). Thermal Buckling in Stiffened Cylindrical Shells. AIAAIASME lllh Structures, Structural Dynamics, and Materials Conference, (pp 260-272). New York: AlAA.

Chang, LK., and Card, MF (1971). Thermal Buckling Analysis for Stiffened Orthotopic Cylindrical Shells. (NASA TN D-6332).

Frum, Y, and Baruch, M (1976). Buckling of Cylindrical Shells Heated Along Two Opposite Generators Combined with Axial Compression. Exp Mech, 16(4), 133-139.

Gellatly, RA, Bijlaard, PP, and Gallagher, RH (1965). Thermal Stress and Instability of Sandwich Cylinders on Rigid Supports. J Aircraft, 2(1), 44-48.

Gossard. ML, Seide, P. and Roberts, WM (1952). Thermal Buckling of Plates. (NACATN2771).

Gupta, SD., and Wang, I (1973). Thermal Buckling of Orthotropic Cylindrical Shells. Fibre Sci and Tech, 6, 9-45.

Hill. DW (1959). Buckling of a Thin Circular Cylindrical Shell Heated Along an Axial Strip. (AFOSR-TN-59-1250).

Hoff. NJ (1957b). Buckling of Thin Cylindrical Shell Under Hoop Stresses Varying in Axial Direction. J Appl Mech, 24(3), 405-412.

Hoff, NJ, Chao, C, and Madsen, WA (1964). Buckling of a Thin-Walled Circular Cylindrical Shell Heated Along an Axial Strip. J Appl Mech, 31(2), 253-258.

Hoff, NJ, and Ross, B (1967). A New Solution of the Buckling Problem of Thin Circular Cylindrical Shells Heated Along an Axial Strip. B

Johns, DJ (1959). Comments on 'Thermal Buckling of Clamped Cylindrical Shells'. J Aeronaut Sci (Reader's Forum). 26(1), 59.

Johns, D. J. (1962). Local Circumferential Buckling of Thin Circular Cylindrical Shells. Collected Papers on Instability of Shell Structures-1062. (NASA TN D-1510).

Johns, DJ (1965). Thermal Stress Analysis. London: Pergamon.

Radhamohan, SK, and Venkataramana, J (1975). Thermal Buckling of Ortholropic Cylindrical Shells. AIAA J, 13(3), 397-399.

Ross, B, Mayers, J, and Jaworski, A (1965). Buckling of Thin Cylindrical Shells Heated Along an Axial Strip. Exp Mech, 5(8), 247-256.

Ross, B, Hoff, NJ, and Horton, WH (1966). The Buckling Behavior of Uniformly Heated Thin Circular Cylindrical Shells. Exp Mech, 6(11), 529-537.

Sunakawa. M (1962). Deformation and Buckling of Cylindrical Shells Subjected to Heating. Univ. Tokyo: Aero. Res. Inst. (Rep. 370).

Thangaratnam, RK, Palaninathan, R, and Ramachandran, J (1990). Thermal Buckling of Laminated Composite Shells. AIAA J, 28(5), 859-860.

Timoshenko, S, and Gere, JS (1961). Theory of Elastic Stability (Second Edition).: McGraw-Hill.

Wilcox, MW" and Ma, S (1989). Thermal Buckling of Antisymmetric Angle-Ply Composite Circular Cylindrical Shells. 30lh AIAA/ASME/ASCE/AHS/ASC Structures, Structural DVllamics and Malerials Conference Vol AIAA Paper No 89-11 n-cp;, 1989, April 3 (pp 113-120). Also Ma. S-F and Wilcox.MW,

Institutional Repository - Library & Information Centre - University of Thessaly
02/06/2024 20:36:34 EEST - 18.222.76.217

"Thermal Buckling of Antisymmetric Angle-Ply Laminated Cylindrical Shells," ComposileEng, Vol 1. No 3,1991, pp 183-192.

Zuk. W (1957). Thermal Buckling of Clamped Cylindrical Shells. J Aeronoul Sci, 24{5), 389 (Reader's Forum).

Society of Fire Protection Engineers (SFPE), Bethesda, Maryland. Engineering Guide for Assessing Flame Radiation to External Targets from Pool Fires, June 1999

Hamins A., Kashiwagi T., Burch R., (1995), Characteristics of Pool Fire Burning, Fire resistance of Industrial Fluids, ASTM STP 1284, G.E. Totten ans J. Reicel, Eds Americal Society for Testing and Materials, Phladelphia

Cowley, L. T. and Johnson, A. D., 1992. Oil and Gas Fires: Characteristics and Impact. Chester: Shell Research Limited.

Shokri, M., and Beyler, C. L., "Radiation from Large Pool Fires," Journal of Fire Protection Engineering 1(4):141–149;1989.

K.S. Mudan and P.A. Croce. SFPE Handbook, chapter Fire Hazard Calculations for Large Open Hydrocarbon Fires. National Fire Protection Association, Quincy, Massachusetts, 2nd edition, 1995.

N. Takahashi, H. Koseki, and T. Hirano. Temporal and Spatial Characteristics of Radiation from Large Pool Fires. Bulletin of Japanese Association of Fire Science and Engineering, 49(1):27–33, 1999.

V. Babrauskas. SFPE Handbook, chapter Burning Rates. National Fire Protection Association, Quincy, Massachusetts, 2nd edition, 1995.

Fire Protection Handbook. National Fire Protection Association, Quincy, Massachusetts, 18th edition, 1997.

Kevin B. McGrattan, Howard R. Baum, Anthony Hamins (2000), Thermal Radiation from Large Pool Fires, National Institute of Standards and Technology (NIST)

Biao Sun, Kaihua Guo, Vishnu K. Pareek, 2015, Dynamic simulation of hazard analysis of radiations from LNG pool fire, Journal of Loss Prevention in the Process Industries 35 (2015) 200-210

Benjamin D. Ditch, John L. de Ris , Thomas K. Blanchat, Marcos Chaos , Robert G. Bill Jr., Sergey B. Dorofeev, Pool fires – An empirical correlation, Combustion and Flame 160 (2013) 2964–2974

S. Vasanth, S.M. Tauseef, Tasneem Abbasi, S.A. Abbasi, Multiple pool fires: Occurrence, simulation, modeling and management, Journal of Loss Prevention in the Process Industries 29 (2014) 103-121

Biao Sun , Kaihua Guo , Vishnu K. Pareek, Dynamic simulation of hazard analysis of radiations from LNG pool fire, Journal of Loss Prevention in the Process Industries 35 (2015) 200-210

Khalid Abusaieda Mansour, (2012) Fires in large atmospheric storage tanks and their effect on adjacent tanks, Ph. D Dissertation, Loughborough University Institutional Repository

S. Vasanth , S.M. Tauseef , Tasneem Abbasi , A.S. Rangwala , S.A. Abbasi, Assessment of the effect of pool size on burning rates of multiple pool fires using CFD, Journal of Loss Prevention in the Process Industries 30 (2014) 86-94

Cowley, LT, Johnson, AD, Oil and gas fires — Characteristics and impact. Report HSE-OTI–92–596, Offshore Technology Information, Health and Safety Executive, London, 1992.

MSC Software Corporation, MSC Marc, Volume A: Theory and User Information, Version 2011.

Institutional Repository - Library & Information Centre - University of Thessaly
02/06/2024 20:36:34 EEST - 18.222.76.217

Institutional Repository - Library & Information Centre - University of Thessaly
02/06/2024 20:36:34 EEST - 18.222.76.217